CD4+ T cells cooperate with myeloid cells to remotely control immune-evasive tumours

Thesis

for the degree of

doctor rerum naturalium (Dr. rer. nat.)

approved by the Faculty of Natural Sciences of Otto von Guericke University Magdeburg

by M.Sc. Bastian Kruse

born on 03.01.1990 in Hamburg

Examiner: Prof. Dr. Thomas Tüting
Prof. Dr. Tim Lämmermann

submitted on: 25.08.2023

defended on: 23.02.2024

Table of contents

Summary

Current clinically applied cancer immunotherapies mainly focus on augmenting cytotoxic effector functions of CD8$^+$ T cells. However, tumours can evade direct immune control by loss of MHC expression or by becoming unresponsive to interferons (IFN). In recent years, the ability of CD4$^+$ T cells to eliminate even such "immune-evasive" tumours has been increasingly studied. The extent, to which CD4$^+$ T cell effector cells contribute to anti-tumour immunity, and the development of strategies to unleash their full potential remain to be substantiated.

The aim of this work was to further investigate the mechanisms how CD4$^+$ effector T cells control tumours independent of CD8$^+$ T cells in an experimental melanoma inoculation mouse model using adoptively transferred melanoma-specific CD4$^+$ or CD8$^+$ T cell receptor transgenic T cells. Initial experiments showed that a small number of CD4$^+$ T cells can control tumours as efficiently as a much larger number of CD8$^+$ T cells. Strikingly, CD4$^+$ T cells were able to also eliminate MHC-deficient and IFN-insensitive tumour cell variants that escape CD8$^+$ T cell control.

Sophisticated fluorescence microscopic methods were established to further investigate the mechanisms how CD4$^+$ T cells indirectly control tumours independent of cytotoxic CD8$^+$ T cells. Histological and intravital microscopic studies revealed fundamental differences in the spatial distribution and the temporal dynamics of tumour-specific CD4$^+$ T cells and CD8$^+$ T cells in tumour tissues. While CD8$^+$ T cells infiltrated deep into tumour tissue in large numbers in a MHC-I molecule-dependent manner, CD4$^+$ T cells mostly interacted with MHC-II$^+$ antigen-presenting cells at the invasive tumour margin. Subsequent molecular pathological and flow cytometric studies showed that the CD4$^+$ T-cell-based therapy induced a recruitment of inflammatory monocytes into tumour tissue. Under the influence of IFNs, monocytes differentiated into both antigen-presenting and tumouricidal iNOS$^+$ myeloid immune cells.

In summary, very few CD4$^+$ T cells reprogrammed the network of tumour-infiltrating myeloid cells. Together, they were able to indirectly and remotely eradicate even "immune-evasive" tumours. These data demonstrate the potential for clinical use of CD4$^+$ T cells in cancer immunotherapy.

Zusammenfassung

Die derzeit klinisch angewandten Krebsimmuntherapien fokussieren sich auf die Verstärkung der direkten Zytotoxizität von CD8$^+$ T-Zellen. Allerdings können Tumore Therapieresistenzen entwickeln, indem sie ihre MHC-Expression verlieren oder nicht mehr auf Interferone (IFN) ansprechen. In den letzten Jahren ist die Fähigkeit von CD4$^+$ T-Zellen, auch solche „immun-evasiven" Tumoren zu eliminieren, verstärkt untersucht worden. Ziel dieser Arbeit war es, die Mechanismen der CD8$^+$ T-Zell-unabhängigen Tumorkontrolle durch CD4$^+$ Effektor T-Zellen in einem experimentellen Melanom-Inokulations-Mausmodell mit adoptiv transferierten, Melanom-spezifischen CD4$^+$ oder CD8$^+$ T-Zell-Rezeptor transgenen T-Zellen näher zu untersuchen. Dabei zeigte sich zunächst, dass eine kleine Anzahl von CD4$^+$ T-Zellen Tumore ebenso effizient kontrollieren kann wie eine viel größere Anzahl an CD8$^+$ T-Zellen. Besonders eindrücklich war die Tatsache, dass CD4$^+$ T-Zellen auch MHC-defiziente und IFN-unempfindliche Tumorzell-Varianten eliminieren, die der Kontrolle durch CD8$^+$ T-Zellen entkommen.

Um den Mechanismus der indirekten, von zytotoxischen CD8$^+$ T-Zellen unabhängigen Tumorkontrolle durch CD4$^+$ T-Zellen direkt *in vivo* zu untersuchen, wurden anspruchsvolle fluoreszenzmikroskopischen Methoden etabliert. Histologische und intravitalmikroskopische Untersuchungen ergaben grundlegende Unterschiede in der räumlichen Verteilung und der Bewegungsdynamik von tumorspezifischen CD4$^+$ T-Zellen und CD8$^+$ T-Zellen im Tumorgewebe. Während CD8$^+$ T-Zellen in großer Anzahl das Tumorgewebe erreichen und in einer von MHC-I Molekülen abhängigen Weise infiltrierten, interagierten CD4$^+$ T-Zellen am invasiven Tumorrandbereich mit MHC-II$^+$ antigen-präsentierenden Zellen. Weiterführende molekularpathologische und durchflusszytometrische Untersuchungen ergaben, dass die CD4$^+$ T-Zell-basierte Therapie eine Rekrutierung von inflammatorischen Monozyten in das Tumorgewebe induziert, die unter dem Einfluss von IFN-Signalen sowohl zu antigen-präsentierenden als auch zu tumoriziden iNOS$^+$ myeloiden Immunzellen ausdifferenzieren.

Zusammengefasst waren sehr wenige CD4$^+$ T-Zellen in der Lage, durch eine Reprogrammierung des Netzwerkes tumor-infiltrierender myeloider Zellen auch „immun-evasive" Tumoren indirekt und aus der Ferne zu beseitigen. Diese Daten zeigen das Potential für die klinische Nutzung von CD4$^+$ T-Zellen in der Krebsimmuntherapie auf.

1. Introduction

1.1 Development of cancer immunotherapy

1.1.1 Early successes of immunotherapies

The earliest beginnings of cancer immunotherapy date back to 1891, when the American surgeon William B. Coley observed that sarcoma patients experienced tumour regression in association with bacterial infections. He hypothesised that the stimulation of the immune system led to those regressions and developed a therapy using a mixture of heat-inactivated *Streptococcus pyogenes* and *Serratia marcescens* bacteria, which were coined Coley's toxins[1]. However, due to a lack of mechanistic explanation for his findings, his approach was not appreciated by his peers and instead, surgery and radiotherapy emerged as standard care for cancer patients for the following decades. Today, Coley's work is appreciated as the first cancer immunotherapy and he is now considered the "Father of Cancer Immunotherapy"[1].

In 1969, a ground breaking result was published, which showed that immunotherapy using the cytokine IFNα inhibits tumour growth in mice[2]. These findings paved the way for IFNα to be the first FDA approved immunotherapy for clinical use in cancer in 1986. Around the same time, Steven A. Rosenberg pioneered the use of tumour-infiltrating lymphocytes (TILs) to treat melanoma patients[3,4]. The use of IL-2 in combination with TILs was particularly important, as it demonstrated the importance of the adaptive immunity to achieve durable anti-tumour responses[5]. This adoptive cell therapy (ACT) protocol was further improved by combination with a preparative lymphodepletion, using cyclophosphamide, to achieve complete tumour regressions in mouse[6] and man[7,8]. Additionally, in the early 1990s, parallel discoveries of the first melanoma-associated antigen (MAGE) and gp100 enabled the development of cancer vaccines against melanoma[9,10]. However, therapy responses were limited by regulatory mechanisms, such as by surface receptors inhibiting T cell responses.

1.1.2 Breakthrough with immune checkpoint inhibition

In 1987 and 1992, respectively, the T cell co-receptors CTLA-4 and PD-1 were discovered and found to be associated with T cell activation[11,12]. It was not until 1996 however, that

in a pioneering study led by James P. Allison, CTLA-4 was described as the first immune checkpoint, evidenced by tumour regression in mice upon receiving antibody-mediated CTLA-4 blockade[13]. Shortly after, PD-1 was found to be another immune checkpoint, also showing durable tumour regression in mice upon antibody-mediated inhibition[14,15]. In terms of their anti-tumour mechanism, CTLA-4 and PD-1 differ fundamentally. While CTLA-4 competes with the T cell co-stimulator CD28 to bind their shared ligands B7-1 or B7-2, the PD-1 signalling cascade is induced upon binding of its distinct ligands PD-L1 and PD-L2. Clinical development for immune checkpoint blockade (ICB) therapy started in June 2000 and, over a decade later, in 2011, the anti-CTLA-4 antibody ipilimumab was the first ICB that was FDA approved for clinical use against melanoma, which was followed by numerous approvals of checkpoint inhibitors for different cancer entities from 2014 onwards[5]. This ultimately led to the Nobel Prize in Medicine and Physiology being awarded to James P. Allison and Tasuku Honjo in 2018 for their discovery of the immune checkpoints CTLA-4 and PD-1. Despite its successes, response to ICB is limited by a number of factors including low immunogenicity of tumours, active T cell exclusion, a stem-like or mesenchymal tumour phenotype as well as additional immune checkpoints[16–18].

1.2 Regulation of T cell effector functions in the tumour microenvironment

1.2.1 CD8^{+} T cells in anti-tumour immunity

While immune checkpoints are expressed on both CD8^{+} and CD4^{+} T cells, ICB and other therapeutic strategies such as ACT and vaccination approaches are primarily thought to unleash the ability of CD8^{+} cytotoxic T lymphocytes (CTLs) to directly kill tumour cells. During the priming process, CD8^{+} T cells require initial recognition of their cognate antigen bound to MHC-I molecules of professional antigen-presenting cells (APCs) in the lymph node, most notably cDC1 cells. CD8^{+} T cells then differentiate into effectors, clonally expand and subsequently enter the circulation. Primed CD8^{+} T cells upregulate the chemokine receptor CXCR3, which enables CD8^{+} T cell extravasation at the site of inflammation guided by the chemokines CXCL9, CXCL10 and CXCL11, where the T cells require a second activation in order to exert their effector functions[19]. The secondary activation of CD8^{+} T cells largely depends on direct recognition of the specific CD8^{+} T cell antigen being bound to MHC-I molecules on their malignant target cells. Following the

TCR-MHC dependent interaction, the most critical anti-tumour effector functions of CD8^{+} CTLs are the release of cytotoxic granules containing perforin and granzymes as well as FasL-induced activation of cell death domains[20]. Additionally, the release of pro-inflammatory cytokines such as IFNγ and TNFα can directly act on cancer cells or promote anti-tumour functions of other cells in the TME such as macrophages or endothelial cells[21].

1.2.2 Tumour immune escape mechanisms

Currently applied CD8^{+} T cell-focused cancer immunotherapies are counteracted by the occurrence of immune-evasive tumours, which leads to many cancer patients not showing durable responses[22–24]. The emergence of therapy resistant tumours is a dynamic and highly individual process as tumours are constantly evolving. Nevertheless, therapy resistance can be categorised into primary, adaptive and acquired resistances[16]. Primary and adaptive resistance factors are typically present before therapy or can be quickly gained by the majority of the tumour cells upon therapeutic intervention, whereas acquired resistance typically occurs after an initial response to the therapy due to a selection process of resistant clones. Additionally, factors of therapy resistance can be categorised into tumour-intrinsic and -extrinsic.

Tumour-intrinsic factors, such as genetic or epigenetic alterations within the tumour cells, which lead to primary resistance, involve lack of antigenic mutations, loss of HLA expression, alterations in the antigen processing machinery or constitutive PD-L1 expression[16,25,26]. Furthermore, alterations in signalling pathways of tumour cells can lead to an active T cell exclusion, as shown for constitutive WNT signalling in melanoma[27]. For acquired resistance, IFN-signalling pathways have emerged as key regulators, as a number of studies found that becoming unresponsive to IFN can result in therapy resistance due to impaired CD8^{+} T cell control[28–32]. Additionally, the downregulation of MHC-I expression[33–35] and de-differentiation[36] are well described tumour-intrinsic mechanisms to evade CD8^{+} T cell recognition.

Tumour-extrinsic factors of therapy resistance are mechanisms mediated by components other than tumour cells within the tumour microenvironment (TME) that contribute to tumour progression or immune regulation[16]. The TME consists of many different types of immune cells, a variety of non-hematopoietic cells and the extracellular matrix. A frequent

tumour-extrinsic resistance factor is the absence of T cells with tumour antigen-specific TCRs, likely caused by lack of either antigen availability, co-stimulatory signals or T cell help, resulting in an immune-deserted TME[37]. Additionally, many human tumours are infiltrated by regulatory T cells (Tregs)[38–40]. Tregs are known to inhibit immune responses through secretion of cytokines such as TGFβ and IL-10 or by direct cell contact[41] and multiple experimental studies show that the depletion of Tregs improves anti-tumour immunity[42,43].

Myeloid cells are highly abundant in the TME of many tumours and can exert a variety of pro- or anti-tumour functions. Most notably, tumour associated macrophages (TAM) are associated with poor prognosis in cancer[44,45]. Historically, TAMs were subdivided into M1 and M2 macrophages, which exhibit dichotomous roles in cancer pathogenesis[46]. While this concept is becoming outdated since it is too general to describe the complexity of macrophage biology in an inflammatory *in vivo* situation, it is well established that macrophages can promote tumour progression with proangiogenic and immunoregulatory effects, but also exert anti-tumour functions[45,46]. In mouse models, depletion of M2-like macrophages results in reduced tumour growth in cutaneous T cell lymphoma[47], breast cancer[48] and melanoma[49,50]. Neutrophils are another myeloid cell subset that is associated with poor clinical prognosis[51,52]. In experimental melanoma and breast cancer models, it has been shown that hampering neutrophils by targeting c-MET[53] or CXCL1[54] can boost T cell-mediated therapy responses against cancer.

The common denominator of the many aforementioned tumour-intrinsic and -extrinsic resistances is the resulting impairment of CD8+ T cell immune responses, albeit by different mechanisms. Hence, new strategies to either overcome or circumvent CD8+ T cell therapy resistance need to be developed.

1.2.3 CD4+ T cells in anti-tumour immunity

CD4+ T cells show a broad range of effector functions during anti-tumour immune responses and thus recently gained more attention as cellular targets to complement current immunotherapies. Upon initial MHC-II-bound antigen recognition in lymph nodes, naïve CD4+ T cell can differentiate into different helper subsets such as Th1, Th2, Th9, Th17, Tfh as well Tregs, guided by distinct polarizing cytokines[55]. Of those subsets, only

Th1 cells are widely accepted to act anti-tumoural, whereas Tregs are their pro-tumoural counterpart[56]. The Th2, Th9, Th17 and Tfh subsets are less common to be associated with tumour immunotherapy and both beneficial and unfavourable effector functions have been reported[55].

To induce a potent CD4+ T cell-mediated anti-tumour response, adequate priming of the T cells in the lymph node is critical and depends on APCs of the immune system, who engulf and present extracellular antigens to CD4+ T cells[57]. The type of APC to present MHC-II-bound antigen plays a deciding role in this process, as conventional type 2 dendritic cells (cDC2) are essential for CD4+ T cell activation and proliferation[58,59]. More so, CD4+ T cells are key helper cells for the licensing of DCs in order to prime anti-tumour CD8+ T cells[58]. This notion has recently been reinstated by Ferris and colleagues, who found cross-presenting conventional type 1 dendritic cells (cDC1) to be indispensable for CD4+ T cell help towards cytotoxic CD8+ T cell anti-tumour responses[60].

After initial activation in the lymph nodes, the recruitment of CD4+ T cells to the TME depends on chemokines, especially CXCL9, CXCL10 and CCL5, as well as adhesion molecules such as LFA-1[61]. Within the TME, a large variety of CD4+ T cell effector functions are reported, which depend on the type of APC that reactivates the CD4+ T cells, as well as co-stimulatory signals and other environmental factors. Multiple studies showed that, in similarity to CD8+ T cells, CD4+ T cells can release cytotoxic granules to directly kill MHC-II+ cancer cells[62–64]. However, contrary to the ubiquitously expressed MHC-I, the expression of MHC-II is rare in most cancer types with the exception of leukaemia[65] and thus often restricted to APCs of the immune system. Accordingly, CD4+ T cells have been found to engage and control tumours independent of tumour-intrinsic MHC-II expression by interacting with APCs that ingest and present tumour-derived antigen to the CD4+ T cells[66–68]. Once activated, effector CD4+ T cells are able to drive tumour cells into senescence via secretion of the inflammatory cytokines IFNγ and TNFα[69]. In addition to direct effects on the tumour cells, CD4+ T cells have shown potential to modulate and convert the immunosuppressive TME towards an inflammatory state by acting in an anti-angiogenic manner[70] or by partnering with NK cells[71,72] as well as macrophages[73,74]. The extent however, to which these different CD4+ T cell-mediated effector functions contribute to anti-tumour immunity is incompletely understood. Furthermore, their phenotypic

multiplicity and plasticity provide reason that a careful evaluation is required to comprehend and exploit CD4^{+} T cell functions in tumours.

1.3 Experimental mouse models

Mouse models represent a unique opportunity to understand basic concepts of immunology, but also distinct mechanisms of immunity tailored to a specific disease. Throughout history, understanding mechanisms of immunity in mice paved the way for the development of effective therapeutic strategies for human patients. The generation and use of transgenic mouse models to study functions of specific genes is especially worthwhile, since such mechanistic tools are neither feasible nor ethical to employ in humans or closely related primates.

1.3.1 Adoptive cell therapy model against melanoma

To study specific CD8^{+} and CD4^{+} T cell responses against cancer, the laboratory of Nicholas P. Restifo developed two T cell receptor-transgenic (TCRtg) mouse models to experimentally treat melanomas. Firstly, the Pmel-1 mouse harbours CD8^{+} T cells with a TCR that specifically recognises the melanocytic differentiation antigen gp100/Pmel[75]. The Tüting laboratory acquired these mice and used them in an ACT protocol that combines chemotherapeutic preconditioning with cyclophosphamide one day before adenoviral vaccination and intravenous injection of naïve Pmel-1-specific TCRtg T cells, followed by intratumoural injections of immunostimulatory nucleic acids polyI:C and CpG[6]. This therapy protocol was able to eradicate established B16 melanomas due to the activation of both the innate and the adaptive arm of the immune system. Later, this ACT protocol was applied to the melanoma cell line HCmel12, which derived from a serial transplant of a DMBA-induced primary melanoma of a female Hgf-Cdk4^{R24C} mouse[76]. Subsequently, the TCRtg TRP-1 mouse, which harbours CD4^{+} T cells with a TCR that specifically recognises tyrosinase related protein 1 (TRP-1)[77], was substituted for Pmel-1 CD8^{+} T cells in the combined ACT protocol to further our understanding of CD4^{+} T cell-mediated tumour control[78]. The use of these T cell models offer an exquisite opportunity to study CD4^{+} T cell-mediated anti-tumour responses in direct comparison to CD8^{+} T cells in a controlled, experimental environment.

1.3.2 Intravital 2-photon microscopy

Intravital microscopy presents a unique opportunity to obtain spatiotemporal information of cellular interactions in living tissues. The use of microscopic imaging to understand natural immunity was already pioneered in the 1880s by Élie Metchnikoff, who first described phagocytosis and cell-mediated immunity[79]. A century later, intravital microscopy to study the immune system was developed and brought crucial new insights[80]. In particular, the migratory behaviour of innate immune cells such as neutrophils[81] and their intercellular crosstalk[82] were unravelled on the basis of intravital 2-photon microscopy (IV-2PM). Moreover, the understanding of adaptive immunity, in particular the initiation of T cell responses in lymph nodes, was vastly accelerated through the use of IV-2PM. This includes the discovery of the three distinct T cell priming phases in lymph nodes[83] as well as the identification of crucial antigen-presenting cDC types for specific T cell responses in infection and cancer[84].

The use of IV-2PM contributed significantly to our understanding of immune cell migration and cellular interactions in tumour tissues, e.g. in the process of T cell immune-surveillance[85] or the cross-presentation of tumour-derived antigen by cDCs[86]. Furthermore, reporter systems investigating molecular mechanisms such as phagocytosis, apoptosis, calcium signalling, cytokine signalling or subclonal organisation of tumour cells have been effectively used[87,88]. Using these systems, the dynamics of $CD8^+$ T cell-mediated cytotoxic killing[89] and of IFNγ-dependent bystander killing[90,91] as well as the immunosuppressive effects of $CD4^+$ Tregs and their abilities to reduce granule exocytosis of CTLs[92] and to decrease the expression of co-stimulatory receptors such as CD80/CD86 on APCs[93] were shown. However, despite the availability of the aforementioned model systems, the spatiotemporal dynamics of effector $CD4^+$ T cells in tumour tissues have not been extensively addressed and require further attention.

2. Aims of this thesis

Current clinically applied cancer immunotherapies mostly focus on harnessing cytotoxic CD8^{+} T cell functions. These approaches are counteracted by the emergence of MHC-deficient and IFN-unresponsive tumour cells. CD4^{+} T cell effector functions have shown a lot of promise to improve cancer immunotherapies experimentally and clinically. In particular, the variety of CD4^{+} effector functions and their abilities to exert indirect and CD8^{+} T cell-independent anti-tumour functions renders CD4^{+} T cells a promising cellular target to improve immunotherapies. Moreover, uncovering the spatiotemporal organisation of anti-tumour CD4^{+} T cells is needed to understand the requirements for CD4^{+} T cell-mediated tumour eradication.

The overarching hypothesis of this thesis is that effector CD4^{+} T cells are able to eradicate MHC-deficient and IFN-resistant tumour cell variants that escape CD8^{+} T cell control. This could be due to the ability of CD4^{+} T cells to interact with MHC-II^{+} antigen-presenting cells, allowing them to indirectly recognise and destroy tumour cells. Consequently, CD4^{+} T cells should exhibit a fundamentally different distribution and behaviour in the TME when compared to CD8^{+} T cells, which rely on MHC-I expression on tumour cells for their effector functions. To address this hypothesis, the following specified aims were formulated for this thesis.

1. Compare anti-tumour CD4^{+} and CD8^{+} T cells, specifically against immune-evasive tumour variants

2. Characterize the spatial and temporal organisation of anti-tumour CD4^{+} T cells in direct comparison to cytotoxic CD8^{+} T cells

3. Identify critical interaction partners of CD4^{+} T cells within the tumour microenvironment

4. Unravel mechanisms that contribute to CD4^{+} T cell-mediated eradication of immune-evasive tumours.

3. Materials and methods

3.1 Materials

3.1.1 Reagents and chemicals

Reagent	Manufacturer	Order number
β-Mercaptoethanol	Sigma-Aldrich	M-6250
2-Methylbutane	Roth	3923.1
Acepromazine (1%)	Ceva (Vetranquil)	n.a.
Acetone	Roth	9780.1
Agarose NEEO	Roth	2267.4
Ampicillin sodium salt	Sigma-Aldrich	A0166-5G
Bovine serum albumin (BSA)	Sigma-Aldrich	A7030
Bpil (BbsI)	Thermo Scientific	FD1014
Butanol	Roth	7171.2
Calcium chloride	Roth	5239.1
Cyclophosphamide	Baxter (Endoxan)	6035903.00.01
Cytosine-phosphatidyl-Guanosine 1826 (CpG)	InvivoGen (ODN 1826)	tlrl-1826
DNase	Roche	10104159001
DNase-free water	InvitroGen	10977-035
Dimethyl sulfoxide (DMSO)	Sigma-Aldrich	D8418-100ml
dNTPs	Fermentas	00030191
Ethanol	Merck	1.009.831.011
Ethylenediaminetetraacetic acid (EDTA)	Roth	8043.2
Fast Digest Green buffer	Thermo Scientific	00200201
Fetal bovine serum (FBS)	Bio&Sell	FBS.S0615
Fugene HD transfection reagent	Promega	E2311
Gene Ruler 100bp Plus DNA Ladder	Fermentas	SM0322
HEPES	Sigma-Aldrich	H3375
Isoflurane	cp-Pharma	1214
Isopropanol (2-Propanol)	Th.Geyer	1136-1L
Ketamine (10%)	WDT	n.a.
L-Lysine	Sigma	5626-500G

N6-(1-iminoethyl)-L-lysine (L-NIL)	Cayman Chemical	80310
Non-essential amino acids (NEAA)	Gibco	11140-035
Orange G	Sigma-Aldrich	O-3756
Paraformaldehyde (PFA)	Roth	0335.1
Penicillin-Streptomycin	Gibco	15140122
Phosphate buffered saline (PBS)	Life Technologies	14190-094
Phusion HF buffer	Biolabs	B0518S
Phusion HD polymerase	New England Biolabs	M0530S
polyinosinic:polycytidylic acid (Poly(I:C))	InvivoGen	tlrl-pic-5
Puromycine	PanReac Applichem	A2856.0010
Sodium chloride	Roth	9265.1
Sodium pyruvate	ThermoFisher Scientific	11360-088
Sucrose	Sigma-Aldrich	S-7903
Trypan blue solution (0.4%)	ThermoFisher	T8154-10ml
Xylazine (2%)	Bayer (Rompun)	n.a.

3.1.2 Solutions and buffers

Solution/buffer	Ingredients
Annealing buffer	100 nM NaCl, 50 mM HEPES; pH 7.4
Freezing medium	90% (v/v) Cell culture medium, 10%
LB medium (1 L)	5 g yeast extract, 10 g peptone from casein 10 g sodium chloride, (12 g agar-agar)
Transfection mix (CRISPR)	2 µg plasmid, 100 µl OptiMEM, 7 µl Fugene HD
Transfection mix (Retrovirus production)	2 µg pRP-tagBFP, 2 µg gag-pol, 220 ng VSV-G 200 µl HBS, 10 µl 2.5 M $CaCl_2$
FACS buffer	2 ml 50 mM EDTA, 1% FCS in 500 ml of PBS
HBS	HEPES buffered saline, pH 7.1
Mouse anaesthesia solution	20 µl 10% ketamine, 10 µl 2% xylazine, 70 µl PBS

3.1.3 Cell culture media and reagents

Medium/reagent	Ingredients, Manufacturer, Order number
DPBS	Dulbecco's Phosphate-Buffered Saline, Gibco, 14190136

RPMI 1640 + L-Glutamine	Roswell Park Memorial Institute 1640, Gibco, 21875091
DMEM	Dulbecco's Modified Eagle Medium, Gibco, 41965-039
Trypsin-EDTA	0.25% Trypsin-EDTA Phenol Red, Gibco, 25200056
OptiMEM serum-free medium	L-Glutamin, Gibco, 11058021

3.1.4 Commercially available kits and substances

Name of the kit/substance	Manufacturer	Order number
Express STD Vinyl Polysiloxane Registration Material	3M ESPE	6160J
CD45 MicroBeads	Miltenyi Biotec	130-052-301
NucleoBond Xtra Midi kit	Macherey-Nagel	740410.50
NucleoSpin Tissue kit	Macherey-Nagel	740952.50
NucleoSpin Gel and PCR cleanup kit	Macherey-Nagel	740609.250
Vidisic transparent eye gel	Bausch+Lomb	3099559
TissueTek cryomold (OCT compound)	Sakura Finetek	4583
10x Red blood cell lysis buffer	Biolegend	420301
10x Permeabilization buffer	Biolegend	421002
Fixation buffer	Biolegend	420801
Vectashield anti-fade mounting medium	Vector Laboratories	H-1000-10

3.1.5 Flow cytometry antibodies

Antigen	Fluorophore	Clone	Dilution	Manufacturer
anti-mouse CD16/32	none	93	1:300	Biolegend
anti-mouse CD8a	APC/Fire 750	53-6.7	1:1600	BD Biosciences
anti-mouse CD8a	PE	53-6.7	1:800	BD Biosciences
anti-mouse CD45	APC/Fire 750	30-F11	1:1600	Biolegend
anti-mouse CD45	BV 711	30-F11	1:200	Biolegend
anti-mouse CD11c	APC	N418	1:200	Biolegend
anti-mouse CD11c	APC/Fire 750	N418	1:100	Biolegend
anti-mouse F4/80	PE	BM8	1:300	ThermoFisher
anti-mouse CD11b	BV 711	M1/70	1:200	Biolegend
anti-mouse CD11b	PE/Cy7	M1/70	1:2000	Biolegend

anti-mouse Ly6C	PE/Cy7	HK1.4	1:2000	Biolegend
anti-mouse Ly6G	PE	1A8	1:800	BD Biosciences
anti-mouse Ly6G	PE/eFluor610	1A8	1:1600	ThermoFisher
anti-mouse CD3	BV 421	17A2	1:400	Biolegend
anti-mouse CD3	BV 711	145-2C11	1:100	Biolegend
anti-mouse CD3	FITC	145-2C11	1:100	Biolegend
anti-mouse CD4	BV 605	RM4-5	1:500	BD Biosciences
anti-mouse CD4	PE	GK1.5	1:1600	ThermoFisher
anti-mouse CD45	FITC	30-F11	1:1000	BD Biosciences
anti-mouse F4/80	APC	BM8	1:200	Biolegend
anti-mouse Ly6C	BV 421	HK1.4	1:800	Biolegend
anti-mouse iNOS	PE	CXNFT	1:300	ThermoFisher
anti-mouse I-A/I-E	BV 510	M5/114.15.2	1:800	Biolegend
anti-mouse I-A/I-E	APC	M5/114.15.2	1:2000	Biolegend
anti-mouse H2-kb	PE	AF6-88.5	1:500	Biolegend
anti-mouse CD335	APC	29A1.4	1:100	Biolegend

3.1.6 Immunofluorescence antibodies

Antigen	Isotype	Clone	Dilution	Manufacturer
anti-mouse I-A/I-E	rat IgG2a,λ	M5/114.15.2	1:50	BD Biosciences
anti-rat IgG (H+L)	Donkey IgG	polyclonal	1:100	Jackson ImmunoResearch

3.1.7 *In vivo* antibodies

Antigen	Clone	Concentration	Manufacturer
anti-mouse NK1.1	PK136	200 µg per 100 µl; i.p.	BioXCell
anti-mouse MHC-II	Y3P	500 µg per 100 µl; i.v.	BioXCell
anti-mouse IFNγ	XMG1.2	500 µg per 100 µl; i.p.	BioXCell

3.1.8 Hashtag antibodies (scRNA-seq)

Antigen	Clones	Dilution	Manufacturer
anti-mouse TotalSeq™-B0301	M1/42; 30-F11	1:300	Biolegend
anti-mouse TotalSeq™-B0302	M1/42; 30-F11	1:300	Biolegend
anti-mouse TotalSeq™-B0303	M1/42; 30-F11	1:300	Biolegend
anti-mouse TotalSeq™-B0304	M1/42; 30-F11	1:300	Biolegend
anti-mouse TotalSeq™-B0305	M1/42; 30-F11	1:300	Biolegend
anti-mouse TotalSeq™-B0306	M1/42; 30-F11	1:300	Biolegend
anti-mouse TotalSeq™-B0307	M1/42; 30-F11	1:300	Biolegend
anti-mouse TotalSeq™-B0308	M1/42; 30-F11	1:300	Biolegend
anti-mouse TotalSeq™-B0309	M1/42; 30-F11	1:300	Biolegend
anti-mouse TotalSeq™-B0310	M1/42; 30-F11	1:300	Biolegend

3.1.9 NGS primers

Tyrosinase sgRNA primers (adapter sequences for the binding of barcode primers underlined)

Name	Sequence
mTyr fwd	<u>ACACTCTTTCCCTACACGACGCTCTTCCGATCT</u>GGCTGTTTTGTATTGCCTT
mTyr rev	<u>GTGACTGGAGTTCAGACGTGTGCTCTTCCGATC</u>TCCAGATGGTGCACTGGA

Barcode primers forward (individual barcode sequence underlined)

Name	Sequence
D501_long	AATGATACGGCGACCACCGAGATCTACAC<u>TATAGCCT</u>ACACTCTTTCCCTACACGACGCT
D502_long	AATGATACGGCGACCACCGAGATCTACAC<u>ATAGAGGC</u>ACACTCTTTCCCTACACGACGCT
D503_long	AATGATACGGCGACCACCGAGATCTACAC<u>CCTATCCT</u>ACACTCTTTCCCTACACGACGCT
D504_long	AATGATACGGCGACCACCGAGATCTACAC<u>GGCTCTGA</u>ACACTCTTTCCCTACACGACGCT
D505_long	AATGATACGGCGACCACCGAGATCTACAC<u>AGGCGAAG</u>ACACTCTTTCCCTACACGACGCT
D506_long	AATGATACGGCGACCACCGAGATCTACAC<u>TAATCTTA</u>ACACTCTTTCCCTACACGACGCT
D507_long	AATGATACGGCGACCACCGAGATCTACAC<u>CAGGACGT</u>ACACTCTTTCCCTACACGACGCT
D508_long	AATGATACGGCGACCACCGAGATCTACAC<u>GTACTGAC</u>ACACTCTTTCCCTACACGACGCT

Barcode primers reverse (barcode sequence underlined)

Name	Sequence
DS701_long	CAAGCAGAAGACGGCATACGAGAT<u>CGAGTAAT</u>GTGACTGGAGTTCAGACGTGTGCT
DS702_long	CAAGCAGAAGACGGCATACGAGAT<u>TCTCCGGA</u>GTGACTGGAGTTCAGACGTGTGCT
DS703_long	CAAGCAGAAGACGGCATACGAGAT<u>AATGAGCG</u>GTGACTGGAGTTCAGACGTGTGCT
DS704_long	CAAGCAGAAGACGGCATACGAGAT<u>GGAATCTC</u>GTGACTGGAGTTCAGACGTGTGCT
DS705_long	CAAGCAGAAGACGGCATACGAGAT<u>TTCTGAAT</u>GTGACTGGAGTTCAGACGTGTGCT
DS706_long	CAAGCAGAAGACGGCATACGAGAT<u>ACGAATTC</u>GTGACTGGAGTTCAGACGTGTGCT
DS707_long	CAAGCAGAAGACGGCATACGAGAT<u>AGCTTCAG</u>GTGACTGGAGTTCAGACGTGTGCT
DS708_long	CAAGCAGAAGACGGCATACGAGAT<u>GCGCATTA</u>GTGACTGGAGTTCAGACGTGTGCT
DS709_long	CAAGCAGAAGACGGCATACGAGAT<u>CATAGCCG</u>GTGACTGGAGTTCAGACGTGTGCT
DS710_long	CAAGCAGAAGACGGCATACGAGAT<u>TTCGCGGA</u>GTGACTGGAGTTCAGACGTGTGCT
DS711_long	CAAGCAGAAGACGGCATACGAGAT<u>GCGCGAGA</u>GTGACTGGAGTTCAGACGTGTGCT
DS712_long	CAAGCAGAAGACGGCATACGAGAT<u>CTATCGCT</u>GTGACTGGAGTTCAGACGTGTGCT

3.2 Methods

3.2.1 Generation of tyrosinase sgRNA CRISPR/Cas9 plasmids

For molecular cloning of a CRISPR/Cas9 plasmid targeting the mouse tyrosinase gene, the pSpCas9(BB)-2A-GFP plasmid (further referred to as pX458), expressing a single guide RNA to target the first exon of mouse tyrosinase, was used (sgRNA target sequence GAATGCTGCCCACCATGGAT) for transfection of melanoma cells. The sgRNA was modified by adding overhangs for the BpiI restriction site, i.e. for the top strand 5´-3´ CACC and for the complementary bottom strand 5´-3´ AAAC was added. The pX458 plasmid was linearized with BpiI restriction enzyme (Thermo Scientific) in Fast Digest Green Buffer (Thermo Scientific) and purified with a Nucleospin Gel and PCR cleanup kit (Macherey-Nagel). DNA oligonucleotides (Microsynth), representing the sgRNAs targeting the mouse *Tyr* locus, were reconstituted as 100 µM stocks. For both top and bottom strand oligonucleotides, 1 µl of the stock solution was mixed with annealing buffer in 50 µl total volume and annealed for 4 minutes at 90 °C, followed by 10 minutes at 70 °C. The annealed oligonucleotides were allowed to cool down to 10° C. Then, 2 µl of the annealed oligonucleotides were ligated into 50 ng linearized pX458 plasmid and transformed into

DH10ß chemo-competent *E. coli* bacteria for propagation and purification. To this end, one bacteria colony of a 100 μg/ml ampicillin-containing LB agar plate was picked and expanded in 200 ml liquid LB medium overnight. Then, plasmid DNA was isolated using the NucleoBond Xtra Midi kit (Macherey-Nagel) according to the standard manufacturer's protocol.

3.2.2 Generation of tyrosinase-knockout cell lines

CRISPR/Cas9 genome editing was prepared by seeding $5x10^5$ target cells per well in a 6-well cell culture plate overnight. A transfection mix containing 2 μg pX458-mTyr plasmid, 7 μl Fugene HD transfection reagent (Promega) and 100 μl OptiMEM serum-free medium (Gibco) was prepared and incubated for 15 minutes at room temperature. 100 μl of the reaction mix per well was added to the 6-well plate and gently distributed. Transfection efficacy was monitored with a fluorescence microscope. After 48 hours, eGFP$^+$ cells were sorted using the Aria III (BD) of the core facility in the Institute of Molecular and Clinical Immunology (IMKI) in Magdeburg. 96 clones were seeded in a 96-well-plate containing 200 μl of complete RPMI medium. Remaining cells were collected and expanded as a polyclonal cell line. One week after single-cell seeding, wells were monitored for single colonies and 20 monoclones were selected, expanded and verified via Next Generation Sequencing (Illumina MiSeq platform).

3.2.3 Next generation sequencing

Genomic DNA from $1x10^7$ cells per monoclonal cell line was isolated with the NucleoSpin Tissue kit (Macherey-Nagel) according to the manufacturer's protocol and eluted in 50 μl DNAse free water. Two consecutive PCR's were performed to amplify the target region of the *mTyr* gene. First, gene-specific primers linked to the additional adapter sequences P5 and P7 were used to amplify the genomic region of interest. Amplification was performed with 2 μl of the genomic DNA template, a Phusion HD polymerase (New England Biolabs) over 18 cycles in a 12.5 μl reaction mix. Secondly, universal Illumina barcode primers complementary to the adapter sequences P5 and P7 were used. The second PCR was performed over 18 cycles with the Phusion HD polymerase in a 25 μl reaction mix. All sequencing primers are listed in the primers table of the material section. Next generation sequencing was performed with the MiSeq Gene & Small Genome Sequencer (Illumina)

at the Institute for Human Genetics in Magdeburg according to manufacturer's standard protocols.

3.2.4 Insertion or deletion (indel) detection

Sequenced PCR amplicons were retrieved in form of FASTQ files and analysed with the online tool OutKnocker (v1.31)[94]. As a reference sequence of the first mouse *Tyr* exon, obtained from NCBI, was used. The Indel Threshold was set to 2% and the Phred Score Threshold to 27. Three individual clones with a single frameshift indel detected in >90% of the sequencing reads were selected for the functional validation of the gene knockout.

3.2.5 Retroviral transduction

To generate tagBFP expressing cell lines, retroviruses were produced by transfecting HEK293T cells with the retroviral plasmid pRp-tagBFP and the retroviral packaging constructs pCMV-gag-pol and pMD.2G (expressing VSVg) with a calcium-phosphate transfection protocol. To this end, $1x10^6$ HEK293T cells were seeded in a 6-well-plate and allowed to adhere for 5 hours. Then, plasmid DNA was diluted in 200 µl HBS and vortexed briefly. 10 µl of 2.5 M $CaCl_2$ were added and the mixture was vortexed for 5 seconds before a 15 minute incubation at RT. Next, the transfection mixture was added dropwise to the adherent HEK293T cells. After 48 hours, the retrovirus-containing cell culture supernatant was harvested, filtered with a 45 µm filter and added to the HCmel12 target cells. Antibiotic selection of the transduced target cells was initiated 48 hours after transduction using 10 µg/ml Puromycin and was maintained for at least one week.

3.2.6 Cell culture

The mouse melanoma cell line HCmel12 and all its derivates were cultured in complete RPMI medium, i.e. RPMI 1640 (Gibco) supplemented with 10% heat inactivated FCS (Biochrome), 100 IU/ml penicillin, 100 µg/ml streptomycin (Invitrogen), 10 mM non-essential amino acids, 1 mM sodium pyruvate, 20 µM beta-mercaptoethanol and 0.1 mM HEPES. Cells were passaged 1:10-1:40 every 48 to 72 hours, depending on the microscopically observed confluency of the culture flask. The human embryonic retinoblasts 911 cell line and the human embryonic kidney 293T cell line were cultured in complete DMEM medium, supplemented with 10% heat inactivated FCS, 1 mM sodium pyruvate, 100 IU/ml penicillin and 100 µg/ml streptomycin. Cell stocks were generated

with 10% DMSO (Sigma-Aldrich) in complete medium. 1 ml of cell suspension containing 1 to 5×10^6 cells was transferred to a cryotube and placed inside a 2-propanol filled container (Mr. Frosty). Cells were stored in a -80 °C freezer for short-term or a -150 °C freezer for long-term storage. Frozen cell suspensions were revived by thawing the cells in a 37 °C water bath until only a small block of ice remains. Then, 15 ml cold complete medium was added and the cells were allowed to attach to the cell culture flask surface for 2 hours. Residual DMSO was washed away with DPBS and fresh complete medium was provided.

3.2.7 Virus production

The adenoviral vaccine Ad-PT (originally termed Ad-GTY) was generated previously in the Tüting laboratory with the help of Dr. Di Yu and Prof. Magnus Essand, in the Department of Immunology, Genetics and Pathology, University of Uppsala, Sweden. For adenovirus expansion, HER-911 cells were cultured in ten T-175 cell culture flasks until they reached around 80% confluency. Then, culture medium was replaced and Ad-PT was added with a multiplicity of infection (MOI) 1. After 36 hours, when cytopathic effects were observed, both detached and adherent cells were collected in the culture medium, washed once in 30 ml DPBS, pooled in 8 ml DPBS and freeze-thawed three times. Lysates were cleared by centrifuging at 7,000 g for x minutes. The virus titre in FFU/ml was determined according to the $TCID_{50}$ method described by Hierholzer and Killington, Virology Methods Manual.

3.2.8 Mice

All mouse experiments were carried out in male mice of C57BL/6J background. Mice were housed in the central animal laboratory (ZTL) of house 65, University clinic Magdeburg in individually ventilated cages (IVC) containing bedding material, tissues for nesting and enrichment. Wild type mice were ordered from Janvier or Charles River. T cell receptor transgenic RAG1$^-$ B^W TRP-1 TCR were obtained from Jackson Laboratories. GFP$^+$ RAG1$^-$ B^W TRP-1 TCR reporter mice were generated by crossing RAG1$^-$ B^W TRP-1 TCR mice with UBC-GFP mice. Offspring of RAG1$^-$ B^W TRP-1 TCR and GFP$^+$ RAG1$^-$ B^W TRP-1 TCR mice was routinely screened by labelling lymphocytes with CD45.2 and Vβ14 antibodies. T cell receptor transgenic Pmel-1 TCR mice were obtained from Jackson

Laboratories. Venus⁺ Pmel-1 TCR mice were generated by crossing Pmel-1 TCR mice with CAG-Venus mice (kindly provided by Wolfgang Kastenmüller, Würzburg). Offspring of Pmel-1 TCR and Venus⁺ Pmel-1 TCR mice was routinely screened by labelling lymphocytes with CD90.1 and Vβ13 antibodies. CD11c-Venus mice were kindly provided by Andreas Müller (IMKI, Magdeburg).

3.2.9 Tumour transplantation experiments

Melanoma cells were harvested during the exponential growth phase with 70-80% confluency. Cell culture medium was removed and cells were washed with 10 ml DPBS. 1 ml of Trypsin-EDTA (Gibco) was distributed onto the cells and incubated for 2-3 minutes at 37 °C. After the cells detached from the tissue culture surface, enzyme activity was stopped by adding 10 ml of complete RPMI medium. The cell suspension was washed twice in DPBS and counted with a Neubauer chamber. Cells were kept on ice until shortly before the injection. Intracutaneous injection of 2×10^5 cells was performed in 50 µl PBS on the shaved right flank of the mice. For melanoma cell transplantation in intravital imaging experiments, mice were anaesthetized with 100 mg/kg ketamine and 10 mg/kg xylazine, injected i.p., prior to intracutaneous injection of 2×10^5 melanoma cells, diluted in 20 µl PBS in both hind legs. Vidisic® eye gel was applied to moisture the eyes during anaesthesia.

Animal welfare was monitored daily, tumour size was measured three times per week and presented as mean diameter. Animals were sacrificed either when the experimentally determined endpoint was reached, when the mean tumour diameter exceeded 15 mm or when the mice showed symptoms of sickness, in accordance with the local ethical regulations.

3.2.10 Adoptive cell therapy immunotherapy

When transplanted tumours reached 3-5 mm diameter, mice were chemotherapeutically preconditioned by a single intraperitoneal injection of 2 mg Cyclophosphamide (Endoxan, Baxter), diluted in 100 µl PBS. One day later, spleens of T cell receptor transgenic donor mice were collected in DPBS and meshed with a 5 ml syringe plunger through a 70 µm cell strainer. The strainer was washed twice with 10 ml DPBS. The single cell suspension was centrifuged at 350x g for 5 minutes and the supernatant was discarded. Cells were

resuspended in 1x red blood cell lysis buffer (Biolegend) and incubated for 2 minutes. Cells were washed twice in 10 ml DPBS and counted using a Neubauer chamber in a 1:1 mixture with Trypan Blue. After the second wash, cells were resuspended accordingly to reach 5×10^5 antigen-specific CD4$^+$ T cells and/or CD8$^+$ T cells in 100 µl DPBS. In preparation for the injection, mice were sedated by short-term isoflurane inhalation anaesthesia. Intravenous injections of the T cells were carried out intravenously with 1 ml Omnifix-F Luer Solo syringes (B.Braun) and 30 G Microlance needles (0.3 x 13 mm; BD). Adoptively transferred T cells were activated with a single i.p. injection of 2.5×10^7 focus forming units (FFU) Ad-PT adenoviruses in 100 µl PBS. Injections of 50 µg polyinosinic:polycytidylic acid (polyI:C) and 50 µg Cytosine-phosphatidyl-Guanosine (CpG) 1826 DNA (MWG Biotech) in 100 µl water were administered peritumourally on days 3, 6 and 9 after the adoptive cell transfer.

3.2.11 Supplementary *in vivo* treatments

Depleting *in vivo* antibodies were all diluted in 100 µl diluent pH 7.0 (BioXCell) and administered into the intraperitoneal cavity of the animals. For NK cell depletion, a single i.p. injection of 200 µg anti-NK1.1 (PK137, BioXCell) was performed one day before tumour transplantation. For MHC-II-blockade, a single i.v. injection of 500 µg anti-I-E/I-A (Y3P, BioXCell) was performed directly before intravital imaging. For IFNγ-blockade, a single i.p. injection of 500 µg anti-IFNγ (XMG1.2, BioXCell) was performed four days after CD4 ACT. For inhibition of iNOS via L-NIL, daily i.p. injections of 200 µg L-NIL, diluted in 100 µl DPBS, were administered starting at day 2 after CD4 ACT and over a duration of 10 days total.

3.2.12 Intravital 2-photon microscopy of mouse melanoma

Mice were anaesthetized with 100 mg/kg ketamine and 10 mg/kg xylazine i.p., complemented by 3 mg/kg acepromazine s.c. after reaching unconsciousness. The mice were transferred and fixed on a preheated slide. Vidisic® eye gel is applied to moisture the eyes during narcosis. The hind leg was fixed in an elevated position and the skin at the melanoma side was carefully operated open using surgical precision tools. One drop of the transparent Vidisic® gel was used on the wound as mounting medium. Then, two component STD carbomer putty (3M ESPE) was prepared and placed next to the wound.

In order to create a level surface, a 24 x 60 mm cover slip was gently pressed on the putty and the wound until polymerization of the putty fixed the setup. The fixed mice were transferred on a 37° C heating plate under the 2-photon microscope.

Imaging was performed using distilled water or transparent Vidisic® carbomer gel as immersion liquid with a W Plan-Apochromat 20x/1.0 DIC VIS-IR objective mounted to a Zeiss LSM 700 upright microscope with the ZEN software environment (Version 2.1, Zeiss), or a LaVision TrimScope mounted to an Olympus BX50WI fluorescence microscope stand and a XLUMPlanFl 20x/0.95 objective. Excitation on the LSM700 setup was performed with Mai Tai DeepSee (tuned to 800 nm) and Insight X3 (tuned to 980 nm) Ti:Sa oscillators (both from Spectra-Physics), dsRed, Venus, SHG, tagBFP and eGFP fluorescence were read out on a detector cascade with 555nm with 565-610 nm BP (transmitted, 980 nm excitation), 520 nm dichroic with 534/30 nm BP (transmitted, 980 nm excitation), 445 nm dichroic (deflected, 800 nm excitation), and 490 nm dichroic with 485 nm SP (deflected, 800 nm excitation) and 525/50 nm BP for transmitted fluorescence, respectively (Figure 3.1a). Excitation on the TrimScope setup was performed with a Chamaeleon Ultra II Ti:Sa oscillator tuned to 880 nm with a double split detector array with a 495 nm main dichroic and a 445 nm and 520 nm secondary dichroics for SHG, tagBFP filtered with a 494/20 BP, eGFP filtered with a 514/30 nm BP, and Venus filtered with a 542/27 nm BP filter, respectively (Figure 3.1b). Non-descanned PMT (for SHG, Venus, and eGFP in the TrimScope Setup) and high sensitivity detectors (for tagBFP and eGFP in the Zeiss setup) were used for signal collection. Typically, three to four representative fields of view of 353 µm^2 size in x- and y- and a z-range of 48 to 60 µm with 4 µm step size were chosen for data acquisition. Z-stacks were captured in 60-90 second intervals and individual movie length was 15-30 minutes.
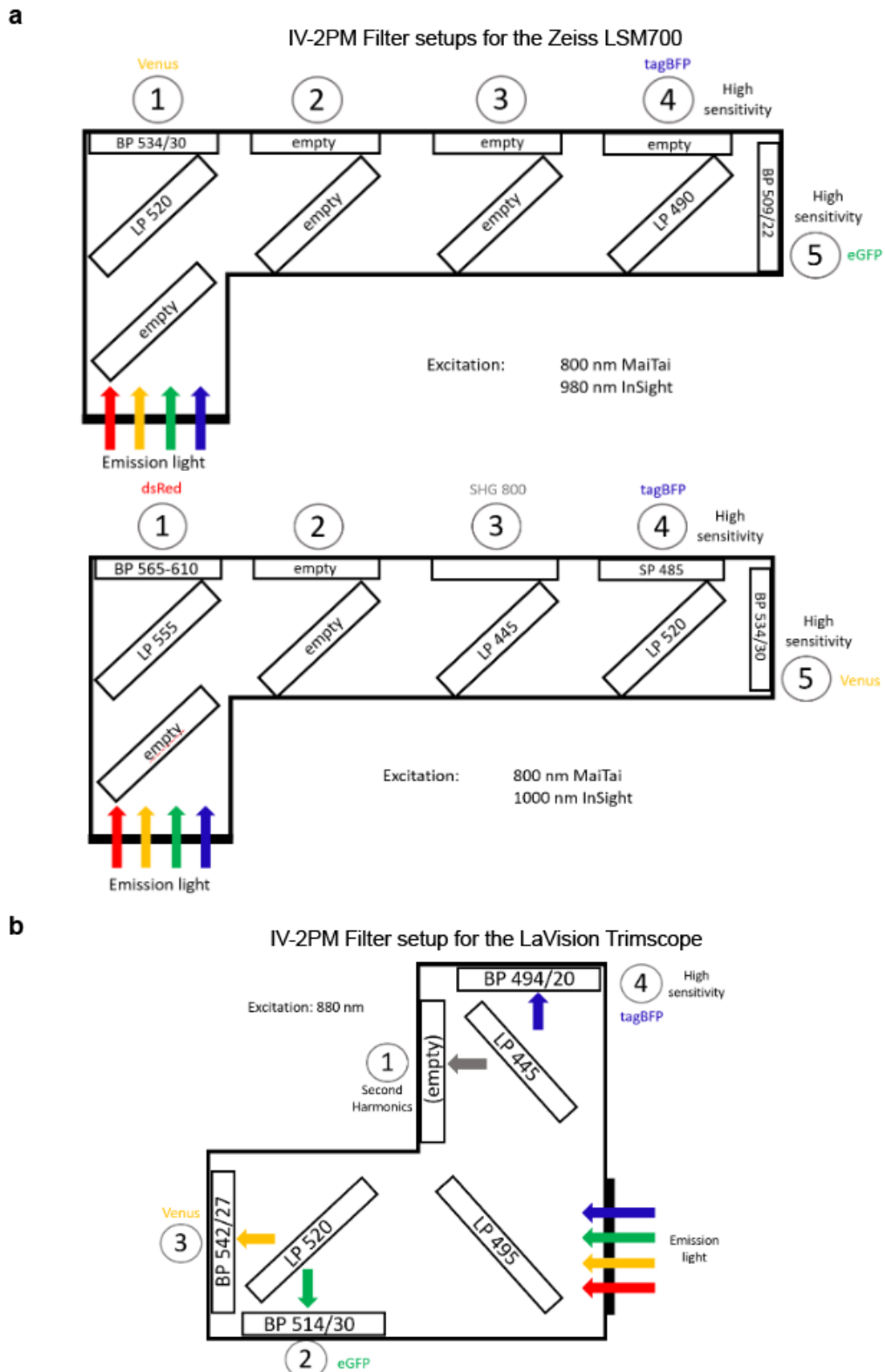
Figure 3.1: IV-2PM filter setups. **a,** Filter setups for the Zeiss LSM 700 microscope for intravital imaging of mouse melanoma tissue with the fluorophore combinations Venus/eGFP/tagBFP (top) or dsRed/Venus/tagBFP (bottom). The circled numbers indicate the individual detectors. **b,** Filter setup for the LaVision TrimScope microscope for intravital imaging of mouse melanoma tissue with the fluorophore combinations Venus/eGFP/tagBFP. The circled numbers indicate the individual detectors.

The analysis of intravital 2-photon microscopy data was performed using IMARIS Software (Bitplane, v9.3.1 - 9.7). As a first measure, translational tissue drift was corrected by choosing a stationary object as reference. Next, the post-processing tool median filter was applied to all images to reduce background signals. The tumour parenchyma was defined with low detail surface detection of the tumour cells, allowing to subsequently distinguish cells inside and outside the defined tumour parenchyma area by enabling the option "Object-to-object statistics" in the detection wizard. T cells were analysed using spot detection with an estimated cell diameter of 8-10 µm. CD11c-Venus detection was performed via high detail surface detection. Cell motility was directly calculated by IMARIS and cell-to-cell contact was derived from the object-to-object distance. These values were exported to MS Excel, where cells were considered in contact when the distance of the centre of mass of a T cell was < 8 µm to the closest CD11c-Venus surface. Representative videos and images were generated in IMARIS or ImageJ (v1.52i).

3.2.13 Fixation, embedding and cryosectioning

Tumour tissue was excised and fixed in 4% PFA for 24 hours at 4 °C followed by dehydration with 20% sucrose in PBS for at least 24 hours at 4 °C and until the tissue sinked to the bottom of the tube. Then, tissues were placed in a cassette (Sakura Finetek) and the cassettes were filled with the OCT compound TissueTek (Sakura Finetek). The cassettes were placed in a cup filled with ice-cold 2-methylbutane for approximately 1 minute until the TissueTek turned white and then immediately transferred to a -80 °C freezer. Cryosections were cut by technicians of the Tüting laboratory with a CM305S cryostat (Leica), adhered to Superfrost Plus slides (VWR) and stored at -20 °C until further use. Up to 3 sections of 6 to 12 µm thickness were placed on each slide.

3.2.14 Immunofluorescence

Cryosections were thawed for 30 minutes at RT and washed in DPBS three times for 5 minutes. Then, slides were either fixed with ice-cold acetone and stained with rat anti-mouse I-A/I-E (1:50) and anti-rat IgG-Alexa Fluor 594 (1:100) or directly mounted using Vectashield® Antifade Mounting Medium and a 24 x 60 mm cover slip (Menzel-Gläser). Samples were closed with commercially available nail polish. Immunofluorescence

images were taken with an Axio Imager.M2 with a Colibri 7 LED illumination system (Zeiss).

3.2.15 Flow cytometry

Blood samples were collected from the right *Vena facialis*, using a Solofix microlancette (B. Braun) and a microvette (Sarstedt). Erythrocytes were lysed using 1x RBC lysis buffer (Biolegend) twice for 10 minutes at room temperature and cells were washed in FACS buffer (1% FCS, 2 mM EDTA in PBS). Surface staining was performed with fluorochrome-conjugated antibodies for mouse antigens according to standard protocols. Details of all used antibodies are listed in the materials section. Tumour, spleen and lymph node tissues were excised after sacrificing the mice and meshed with a 5 ml syringe plunger through a 70 µm cell strainer to create single cell suspensions. Spleen samples were resuspended in 1x red blood cell lysis for 2 minutes before centrifugation at 350 g for 5 minutes. Tumour, spleen and lymph node single cell suspensions were washed in FACS buffer once. Blocking of of IgG Fc receptors was performed with TruStain anti-CD16/CD32 antibodies (Biolegend) for 10 minutes. Then, cell surface staining was performed with fluorochrome-conjugated antibodies according to standard protocols. For intracellular target molecules, cells were fixed using a PFA-based fixation buffer (Biolegend) and permeabilized with 1x Permeabilization buffer (Biolegend). Intracellular antibody staining was performed according to standard protocols. After cell staining, cells were washed twice and resuspended in an appropriate volume of FACS buffer for data acquisition with the Attune NxT acoustic focusing flow cytometer. Analysis was performed with FlowJo (TreeStar, v10.5 – 10.8). For the generation of dimensionality reduced t-SNE plots, 2,000 cells of interest per biological sample were concatenated to a single FCS file. Then, the FlowJo-integrated opt-SNE learning configuration with the vantage-point tree KNN and Barnes-Hut gradient algorithm was used[95], set to 1000 iterations, 30 perplexity and 840 learning rate. Immune cell populations were annotated manually based on the expression of characteristic marker combinations, depicted in the respective figures.

To calculate absolute immune cell counts in the tumour tissue, tumours were excised with tweezers and scissors and weighed using the Entris 224-1S analytical balance (Sartorius). Creation of single cell suspensions and immunostaining was performed as described above. After immunostaining, cells were suspended in a defined volume and analysed on

the Attune NxT acoustic focusing flow cytometer that uses a unique volumetric sample and sheath fluid delivery system allowing for accurate measurements of the number of cells analysed in a defined sample volume. The total number of viable CD45$^+$ immune cells in an individual tumour were calculated by multiplying the number of CD45$^+$ immune cells counted in a defined sample volume with the total volume of the respective single cell suspension. Division of this number by the total weight of the tumour yielded the absolute immune cell count per mg tumour weight.

3.2.16 Single cell RNA-sequencing

Three individual tumours per experimental group were harvested and processed into single suspensions. CD45$^+$ immune cells were enriched using CD45 microbeads (Miltenyi). Next, individual samples were hashtagged with unique TotalSeq-B antibodies B0301-B0310 (Biolegend) and subsequently stained with fluorescently labelled antibodies. CD45$^+$CD11b$^+$Ly6G$^-$ cells were sorted with an Aria III fluorescence-activated cell sorter (BD Biosciences). Isolated cells were transported to the Helmholtz-Centre for Infection Research (HZI) in Braunschweig, where the laboratory of Dr. Robert Geffers loaded the cells onto one lane of a 10x Chromium microfluidics controller. cDNA of hashtag and gene expression libraries were amplified, and indices added via PCR. Sequencing was performed on an Illumina Novaseq on two lanes of a S1 cartridge with 150 bp read length in paired end mode. Reading depth was calculated to obtain ~50,000 reads/cell for the gene expression library and 5,000 reads/cell for the hashtag library.

The scRNA-seq data generated via 10X Genomics Chromium technology were analysed with the help of Andreas Braun. First, the data were aligned and quantified using the Cell Ranger Single-Cell Software Suite against the mm10 mouse reference genome. The raw, unfiltered data generated from Cell Ranger were used for downstream analyses. Quality control was performed on cells based on the three metrics: total UMI (Unique Molecular Identifier) count, number of detected genes and proportion of mitochondrial gene count per cell. Specifically, cells with less than 1000 UMIs, 1000 detected genes, and more than 25% mitochondrial UMIs were filtered out. To remove potential doublets, cells with UMI count above 40,000 were removed. Then, the samples were demultiplexed and tagged with distinct hashtag-oligonucleotides using Solo[96]. After quality control, the raw counts were normalised by their size factors using scran and subsequently performed log2

transformation[97]. The logarithmised and normalised count matrix was used for the downstream analyses.

Analyses of normalised data were performed using the scanpy Python package[98]. Initially, the 4,000 most highly-variable genes were selected for subsequent analysis using scanpy.pp.highly_variable_genes with the parameter "n_top_genes=4000". Next, a principal component analysis (PCA) was performed with 50 components using scanpy.tl.pca with the parameters "n_comps=50, use_highly_variable=True, svd_solver='arpack'". Subsequently, dimensionality reduction was performed using Uniform Manifold Approximation and Projection (UMAP) with scanpy.tl.umap. Single cells were automatically assigned using R package SingleR, with transcriptomes from the Immunological Genome Project as a reference[99]. Clustering of single cells by their expression profiles was conducted employing the Leiden-algorithm using scanpy.tl.leiden with the parameter "resolution=1.0". Clusters with fewer than 20 cells were removed from further analysis. Differential gene expression was performed between cells classified as macrophages and monocytes from non-treated and CD4 ACT-treated mice using a hurdle model implemented in the R package MAST. Subsequent gene set enrichment analysis was performed using GSEA in preranked mode using the log2 fold change as a ranking metric. The interferon score was determined by calculating a z-score for all genes from the MSigDB gene set "HALLMARK_INTERFERON_GAMMA_RESPONSE" for each cell.

For RNA velocity, count matrices of spliced and unspliced RNA abundances were generated using the velocyto workflow for 10x chromium samples, with the genome annotation file supplied by 10x Genomics for the mm10 genome and a repeat annotation file retrieved from the UCSC genome browser. Subsequent analyses were performed using scVelo[100]. The count matrices were loaded into the scanpy environment, merged with the previously generated anndata objects and normalised using scvelo.pp.filter_and_normalize. Next, moments for velocity estimation were calculated, gene-specific velocities were estimated, and the velocity graphs were computed. Furthermore, a partition-based graph abstraction was generated with velocity-directed edges.

3.2.17 Statistical analysis

Mann-Whitney U-tests, unpaired two-tailed t-tests, one-way ANOVA with Tukey post-hoc and log-rank tests were performed using the GraphPad Prism (v8.0.1) software and the specific tests used for each statistic are indicated in the figure legends. Statistical significance was assessed based on p-values and depicted as follows: $*p<0.05$, $**p<0.01$, $***p<0.001$, $****p<0.0001$.

4. Results

4.1 A small population of CD4^{+} T cells can eradicate immune-evasive melanomas

Early successes in T cell immunotherapy for melanoma patients were achieved by ACTs of *ex vivo* expanded tumour-infiltrating lymphocytes[101,102]. More recently, a major clinical breakthrough was the discovery and therapeutic targeting of immunoregulatory checkpoints expressed on T cells, mainly PD1 and CTLA4[5]. These therapies and most currently investigated approaches to improve immunotherapy put their main focus on reinvigorating and unleashing cytotoxic effector functions of CD8^{+} T cells, which recognise tumour cells in the form of processed peptide epitopes presented by MHC-I molecules on the tumour cell surface. While ICB can lead to long-lasting therapy responses in some patients, CD8^{+} T cell functions are antagonised by the emergence of immune-evasive, MHC-deficient and IFN-unresponsive tumour cells.

CD4^{+} T cells have been shown to exert a variety of anti-tumour effector functions beyond their role as helpers and regulators of CD8^{+} T cells[103–105]. A subset of CD4^{+} T cells is able to develop cytolytic effector functions against MHC-II expressing tumour cells, analogous to CD8^{+} T cells[65,106–108]. Moreover, CD4^{+} T cells can also eradicate tumours independent of direct tumour cell recognition and thus have the potential to target immune-evasive tumours[66,69,70,72,74,109]. However, the therapeutic potential of CD4^{+} T cells and the contribution of the various CD4^{+} T cell-mediated effector mechanisms are incompletely understood. The aim of the first results section of this thesis was to develop an experimental model to directly compare CD4^{+} and CD8^{+} T cell anti-tumour effector functions in the context of an adoptive cell therapy.

To directly compare anti-tumour effector functions of CD4^{+} and CD8^{+} T cells, TRP-1 mice harbouring TCRtg CD4^{+} T cells[77] and Pmel-1 mice harbouring TCRtg CD8^{+} T cells[75] were crossed with B6-GFP mice and CAG-Venus mice, respectively, and used for ACT immunotherapies. The adenoviral vaccine Ad-PT encoding a fusion protein of Pmel/gp100 and TRP-1 was used to simultaneously activate and directly compare the efficacy and mechanism of Pmel-1 CD8^{+} and TRP-1 CD4^{+} T cells under identical experimental conditions (Figure 4.1a). The complete ACT therapy protocol included a preconditioning dose of cyclophosphamide (C), Ad-PT vaccination (V) to prime the naïve, adoptively

transferred Pmel-1-specific CD8$^+$ and/or TRP-1-specific CD4$^+$ T cells (T) and three intra-tumoural injections of innate immune stimulation (I) with the nucleic acids polyI:C and CpG 3, 6 and 9 days after ACT, as published previously by the Tüting laboratory (Figure 4.1b)[6]. Initial flow cytometric analyses on the peripheral blood, inguinal lymph nodes and spleens of mice 7 days after ACT with both TRP-1 CD4$^+$ and Pmel-1 CD8$^+$ T cells revealed that TRP-1 CD4$^+$ T cell expand much less efficiently when compared to Pmel-1 CD8$^+$ T cells, irrespective of the amount of transferred cells (Figure 4.1 c,d). Since the peak of CD8$^+$ T cell expansion was reached using 5x10^5 transferred cells (Figure 4.1 d), all subsequent experiments in this thesis were performed using 5x10^5 transferred TCRtg T cells.
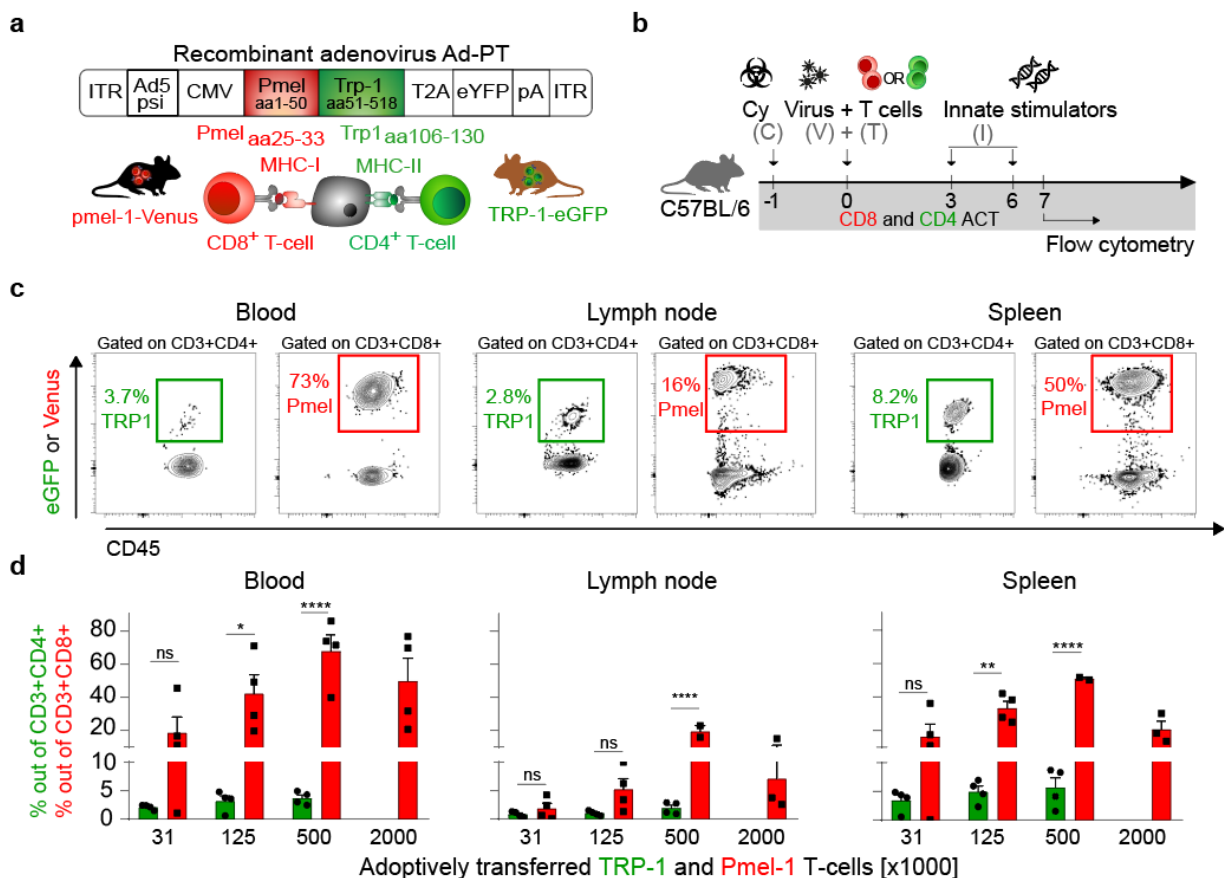
Figure 4.1: Establishment of an experimentally tractable adoptive cell transfer model to compare CD4$^+$ and CD8$^+$ T cells.
a, Structure of recombinant adenovirus designed to simultaneously stimulate Pmel-1 CD8$^+$ and TRP-1 CD4$^+$ TCRtg T cells (Ad-PT). **b,** Experimental protocol for the ACT immunotherapy of established tumours in mice (Cy, C, cyclophosphamide; V, Ad-PT; T, TCRtg Pmel-1 CD8$^+$ or TRP-1 CD4$^+$ T cells; I, innate stimuli, polyI:C and CpG) and time point for flow cytometric analyses. **c,** Representative flow cytometric contour plots with 5 x 10^5 transferred cells each (top) and **d,** quantitation of Pmel-1 CD8$^+$ and TRP-1 CD4$^+$ TCRtg T cell expansion in peripheral blood, lymph nodes and spleen 7 days after ACT (mean ± SEM). Means between groups were statistically compared using one-way ANOVA with Tukey's post-hoc test, *p<0.05, **p<0.01, ****p<0.0001.

To compare the therapeutic efficacy of TRP-1 CD4^{+} T cells and Pmel-1 CD8^{+} T cells, the transplantable mouse melanoma cell line HCmel12, derived from a serially transplanted, DMBA-induced melanoma of an Hgf-Cdk4[R24C] mouse, was used[76]. HCmel12 cells, that were transfected with an empty CRISPR/Cas9 plasmid (pX330) and termed CRISPR-ctrl, showed a low baseline expression of both MHC-I and MHC-II molecules, which was inducible via IFNγ, thus enabling direct tumour cell recognition by CD4^{+} and CD8^{+} T cells (Figure 4.2 a). HCmel12 CRISPR-ctrl cells were injected onto the flanks of wild type mice and treated with the complete CD4 or CD8 ACT when the tumours reached 3 to 5 mm mean diameter (Figure 4.2 b). Despite the relatively poor *in vivo* expansion of TRP-1 CD4^{+} T cells, mice receiving adoptively transferred TRP-1 CD4^{+} T cells were able to eradicate HCmel12 tumours as efficiently as Pmel-1 CD8^{+} T cells (Figure 4.1 c,d).

Previously, it has been shown that adoptively transferred CD4^{+} T cell can eradicate B16 melanomas via direct MHC-II-dependent recognition and cytolytic destruction[62,63]. However, the majority of human melanomas do not express MHC-II molecules[65]. Moreover, a frequent mechanism of therapy resistance is the emergence of MHC-deficiency or IFN-unresponsiveness[110,111]. To investigate whether CD4^{+} T cells are able to target MHC-deficient, IFN-unresponsive melanomas, CRISPR/Cas9-engineered knockout cells for the *Jak1* gene, previously established in the Tüting laboratory, were used. HCmel12 Jak1-KO cells were confirmed to be IFN-unresponsive and thus deficient in their expression of MHC-I and MHC-II molecules (Figure 4.2 e). Of note, previous work in the laboratory revealed that robust *in vivo* growth of HCmel12 Jak1-KO cells required antibody-mediated depletion of NK cells, likely due to their low MHC-I expression (Figure 4.2 f, manuscript in preparation). Strikingly, two thirds of HCmel12 Jak1-KO tumours treated with TRP-1 CD4^{+} T cells were eradicated, whereas Pmel-1 CD8^{+} T cells failed to control tumours in all mice (Figure 4.2 g,h), indicating an indirect CD4^{+} T cell-mediated effector mechanism that was independent of both cytolytic NK and CD8^{+} T cells.
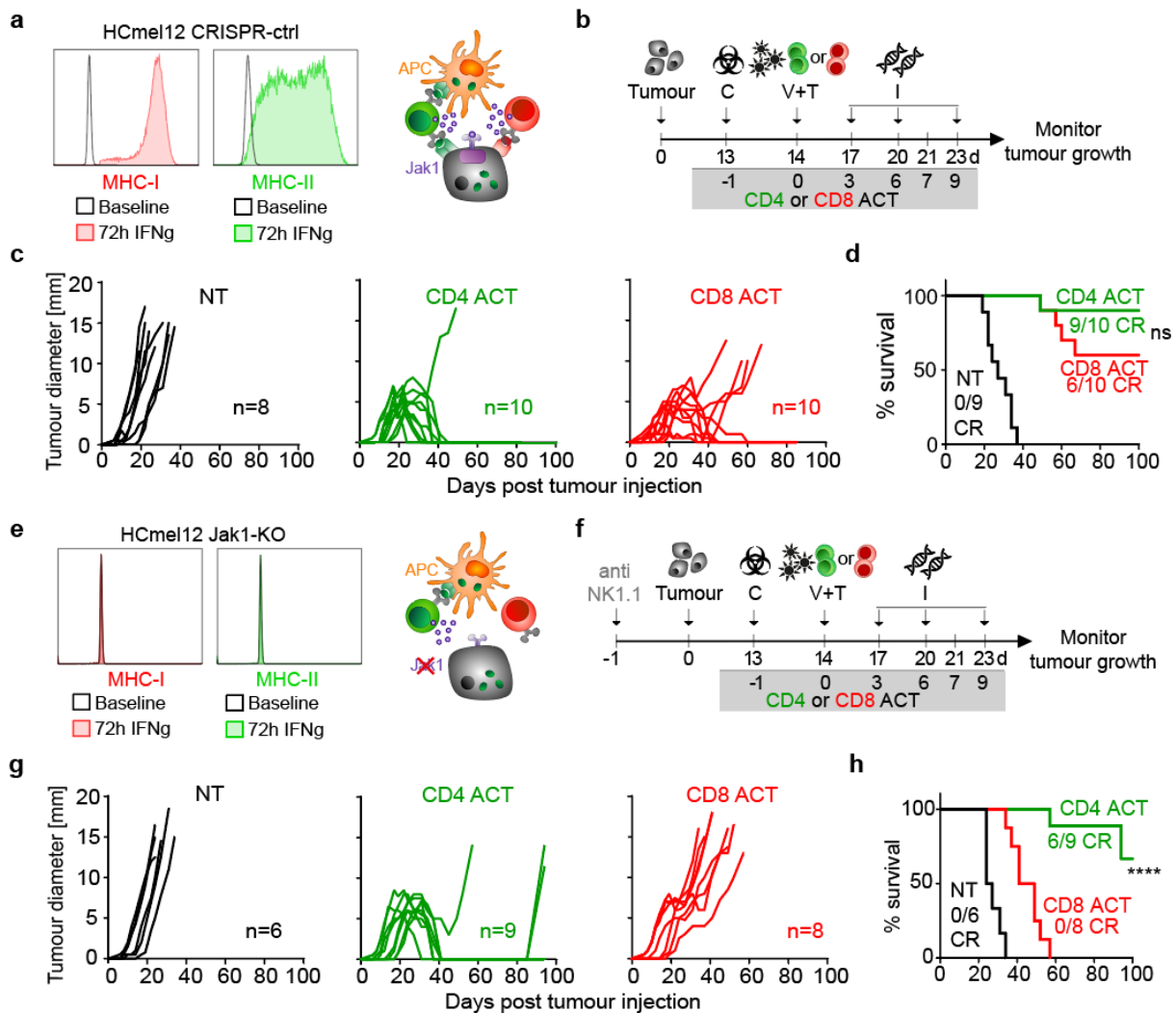
Figure 4.2: CD4+ T cells eradicate IFN-unresponsive, MHC-deficient HCmel12 Jak1-KO tumours that evade CD8+ T cell therapy.

a, Representative flow cytometric histograms for MHC-I and MHC-II expression on HCmel12 CRISPR-ctrl cells cultivated in the presence or absence of IFNγ (left) and illustration of the interaction phenotype of HCmel12 CRISPR-ctrl cells with CD4+ and CD8+ T cells (right). **b,** Experimental protocol to assess therapy efficacy of adoptive cell therapy with CD4+ or CD8+ T cells. **c,** Individual tumour growth curves of mice bearing established HCmel12 CRISPR-ctrl melanomas and treated as indicated. **d,** Kaplan-Meier survival curves of mice bearing establish HCmel12 CRISPR-ctrl tumours and treated as indicated. NT, non-treated. CR, complete responders. **e,** Representative flow cytometric histograms for MHC-I and MHC-II expression on HCmel12 Jak1-KO cells cultivated in the presence or absence of IFNγ (left) and illustration of the interaction phenotype of HCmel12 Jak1-KO cells with CD4+ and CD8+ T cells (right). **f,** Experimental protocol to assess therapy efficacy of adoptive cell therapy with CD4+ or CD8+ T cells. **g,** Individual tumour growth curves of mice bearing established HCmel12 Jak1-KO melanomas and treated as indicated. **h,** Kaplan-Meier survival curves of mice bearing establish HCmel12 Jak1-KO tumours and treated as indicated. NT, non-treated. CR, complete responders. Survival was statistically compared using log-rank Mantel-Cox test, ****p<0.0001.

To understand how CD4$^+$ and CD8$^+$ T cells differ in altering the tumour immune landscape, the immune infiltrate of CRISPR-ctrl and Jak1-KO tumours was analysed via flow cytometry 7 days after CD4 or CD8 ACT (Figure 4.3 a). Analysis using the t-SNE (t-Distributed Stochastic Neighbor Embedding) algorithm allowed an abstraction of multiparametric data in a two-dimensional space (Figure 4.3 b). In accordance with the systemic expansion data (see Figure 4.1), Pmel-1 CD8$^+$ T cells infiltrated the TME in large numbers, irrespective of the tumour genotype and thus independent of therapy efficacy. Only around 1% of the tumour-infiltrating immune cells were TRP-1 CD4$^+$ T cells in both HCmel12 CRISPR-ctrl and Jak1-KO tumours (Figure 4.3 c). Quantification of cells per milligram tumour weight revealed that treatment-naïve HCmel12 CRISPR-ctrl tumours featured an immune-infiltrated phenotype. Importantly, this infiltrated immune phenotype was lost in the Jak1-KO tumour variant (Figure 4.3 d). Regardless of the HCmel12 genotype, both CD4 and CD8 ACT induced the recruitment of myeloid cells, most notably monocyte-derived cells, to the TME.

Taken together, this results section revealed that adoptively transferred CD4$^+$ T cells expand and infiltrate melanomas much less efficiently when compared to CD8$^+$ T cells, which is independent of the amount of transferred cells. Nevertheless, these few CD4$^+$ T cells were able to eradicate established HCmel12 melanomas as efficiently as CD8$^+$ T cells. Most notably, IFN-unresponsive and MHC-deficient HCmel12 Jak1-KO tumours, that resist CD8 ACT therapy, were able to be controlled by adoptively transferred CD4$^+$ T cells, indicative of an indirect effector mechanisms that is not only fundamentally different to CD8$^+$ T cell-mediated tumour control, but also independent of cytolytic CD8$^+$ T cell and NK cell populations. Flow cytometric analyses revealed that the most remarkable change upon ACT therapies within the TME was a strong infiltration of myeloid cells, most notably monocyte-derived cells.
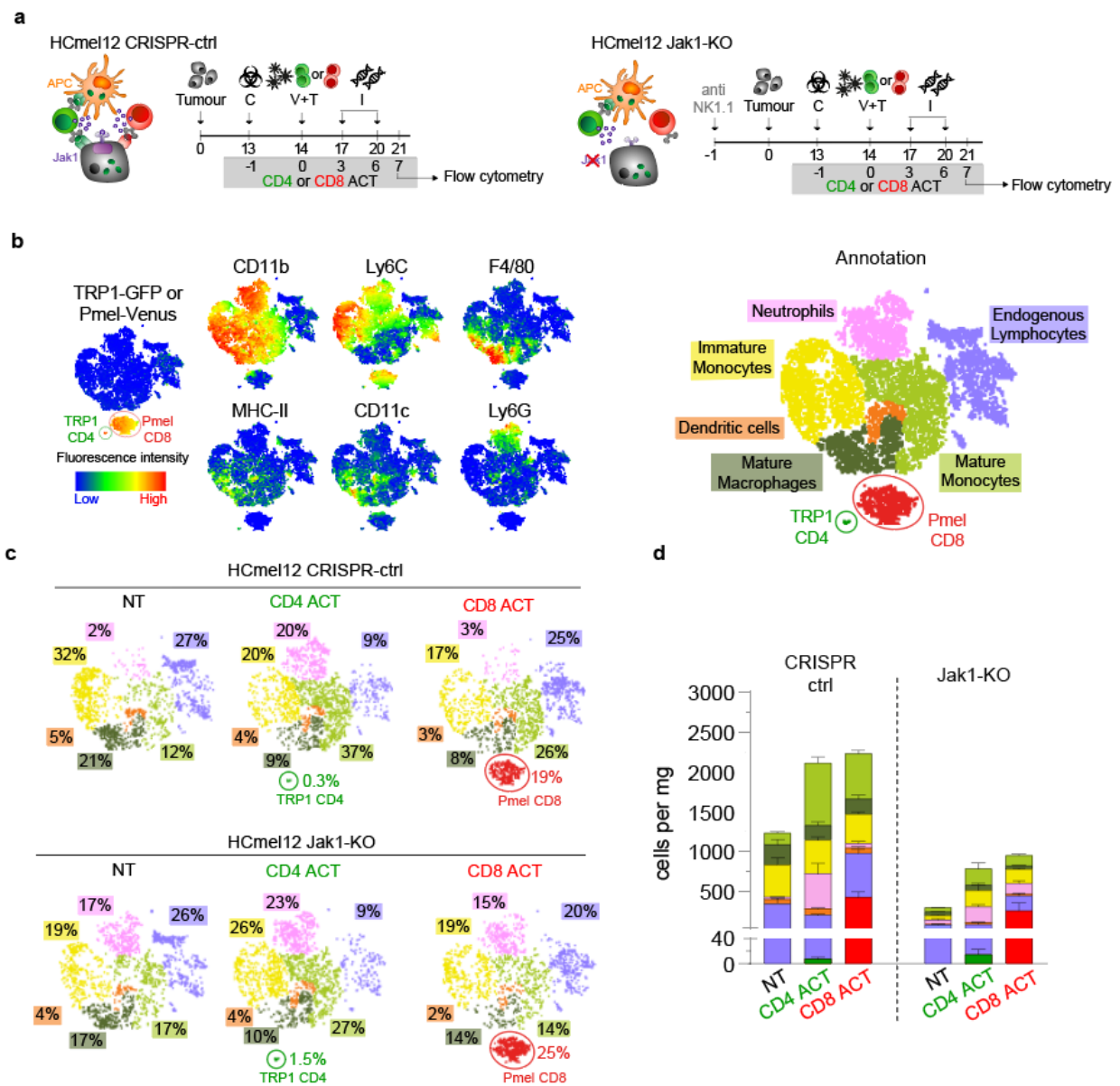
Figure 4.3: Comparative evaluation of CD4+ and CD8+ T cell effector functions against IFN-unresponsive, MHC-deficient tumours.

a, Experimental protocol to assess the immune infiltrate of HCmel12 CRISPR-ctrl and Jak1-KO tumours. **b,** t-SNE heatmaps of indicated cell surface markers and corresponding annotation of cell types: Immature monocytes (CD11b+ Ly6Chi), mature macrophages (CD11b+ F4/80+), mature monocytes (CD11b+ Ly6Clo), TRP-1 CD4 (GFP+), Pmel CD8 (Venus+), dendritic cells (MHC-II+ CD11c+ F4/80-), endogenous lymphocytes (CD11b- CD11c-), neutrophils (CD11b+ Ly6G+). **c,** Immune cell composition HCmel12 CRISPR-ctrl (top) and Jak1-KO (bottom) melanomas treated as indicated and **d,** corresponding cell density (cells per mg tumour weight)

4.2 Effector CD4⁺ T cells show a different spatial distribution and temporal interaction dynamics in tumour tissues when compared to CD8⁺ T cells

The first results section highlighted the potential of adoptively transferred CD4⁺ T cells, despite their low abundance, to eradicate IFN-unresponsive, MHC-deficient tumours that evade CD8⁺ T cell therapy. While the data suggested an indirect CD4⁺ T cell-mediated effector mechanism, it was not elucidated which interactions anti-tumour CD4⁺ T cells require within the TME. The aim of the second results section was to unravel the spatiotemporal dynamics of CD4⁺ T cells in direct comparison to CD8⁺ T cells and to unmask the key cellular interactions of TRP-1 CD4⁺ T cells within the TME of HCmel12 melanomas.

To investigate spatial and temporal properties of intratumoural T cells, amelanotic HCmel12 cells were generated in order to visualise melanomas intravitally. To this end, HCmel12 CRISPR-ctrl and Jak1-KO cells were transfected with a pX458-CRISPR/Cas9 plasmid harbouring a synthetic guide RNA (sgRNA) to target a unique sequence on the first exon of the tyrosinase gene *Tyr* (Figure 4.4 a). Monoclones were expanded and sequenced to identify frameshift mutations at the target site and three individual monoclones were selected for further use. Those monoclones were retrovirally transduced to constitutively express the fluorophore tagBFP and tested *in vivo* to confirm the gene knock-out by the macroscopically visible amelanotic phenotype of the developing tumour (Figure 4.4 b). These newly generated cell lines were termed HCmel12 CRISPR-ctrl Tyr-KO tagBFP and HCmel12 Jak1-KO Tyr-KO tagBFP.
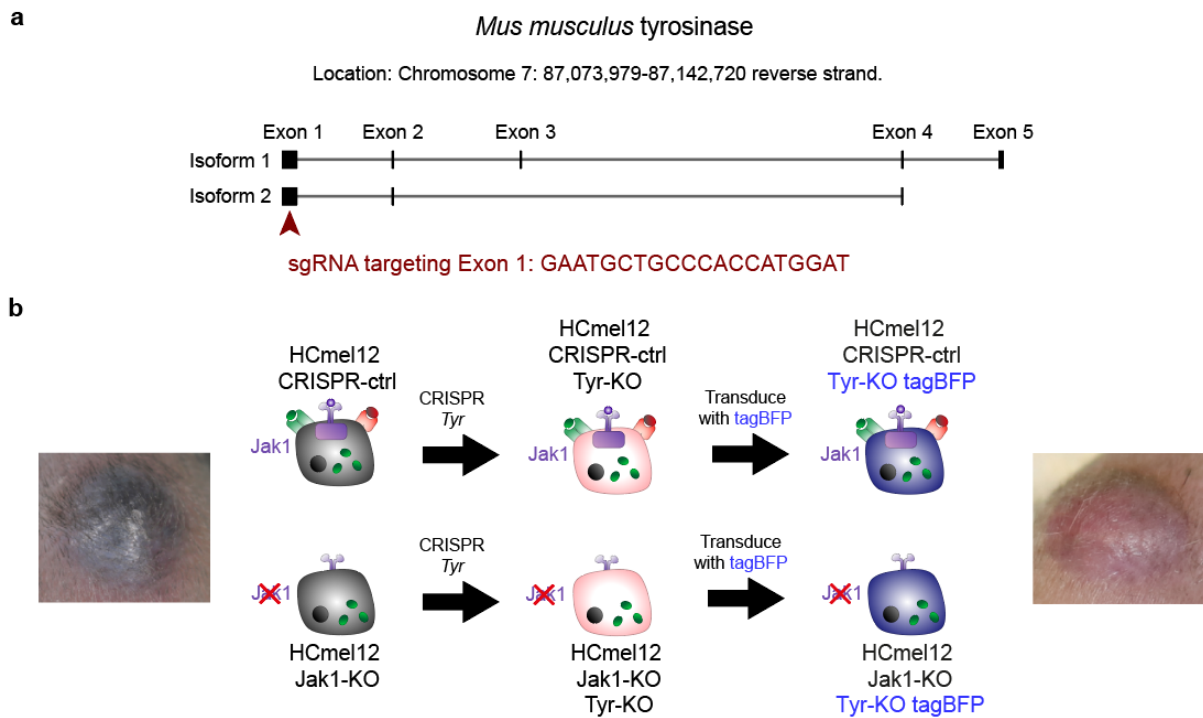
Figure 4.4: Generation of CRISPR/Cas9-engineered amelanotic and fluorescent HCmel12 variants.
a, Illustration of the tyrosinase mouse gene located on chromosome 7 and sgRNA sequence (red) targeting the first exon of the gene. **b,** Representative photographic images of a tyrosinase-expressing HCmel12 tumour (far left) and a tyrosinase knockout tumour (far right) and abstracted illustration of the genetic engineering employed to generate amelanotic and fluorescent tumour variants for immunofluorescence imaging (middle).

To determine the spatial distribution of TRP-1 CD4$^+$ and Pmel-1 CD8$^+$ T cells in the TME, HCmel12 CRISPR-ctrl Tyr-KO tagBFP or Jak1-KO Tyr-KO tagBFP cells were injected onto the hind legs of wild type C57BL/6J mice and treated with a dual ACT using Pmel-1-Venus CD8$^+$ and TRP-1-eGFP CD4$^+$ T cells when the tumours reached a mean diameter of 3 mm (Figure 4.5 a,b). Five days after ACT, tumours were harvested and analysed via immunofluorescence microscopy. The intra-tumoural location of T cells was divided into the invasive margin (IM, tumour border ±100 µm) and tumour centre (TC). Very few CD4$^+$ T cells were found and were spatially restricted to local clusters at the tumour invasive margin in CRISPR-ctrl tumours. In contrast, large numbers of CD8$^+$ T cells briskly infiltrated the invasive margin and the centre of CRISPR-ctrl tumours (Figure 4.5 c,e). In IFN-unresponsive and MHC-deficient Jak1-KO tumours, few CD4$^+$ T cells also clustered at the invasive margin, whereas CD8$^+$ T cells infiltrated the invasive margin, but not the tumour centre (Figure 4.5 d,f). These results showed that infiltration of the tumour centre

by CD8^{+} T cells depended on the expression of MHC-I on the tumour cells, while CD4^{+} T cells maintained their spatial organisation irrespective of the tumour genotype.
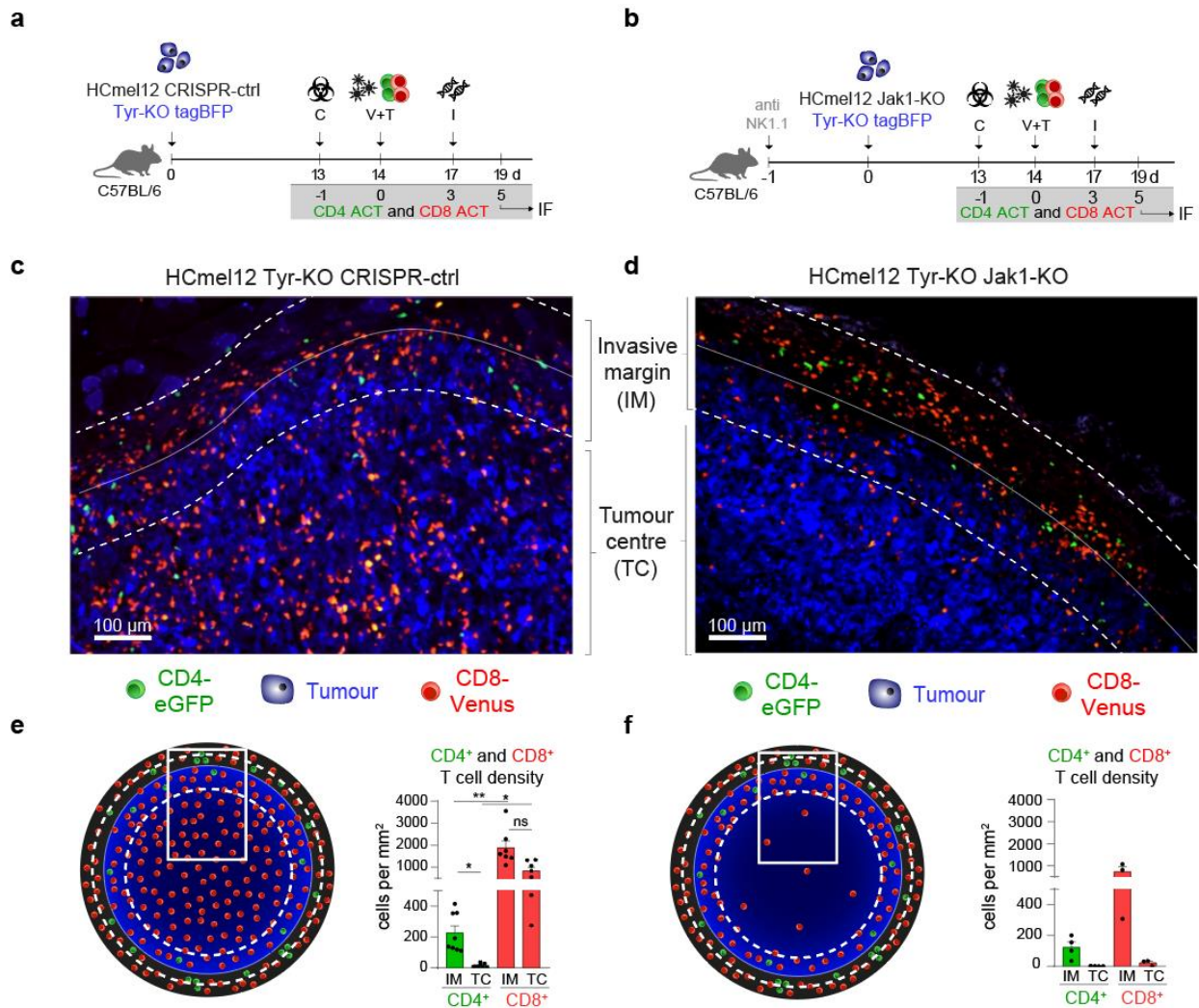
Figure 4.5: CD4^{+} T cells show a different spatial distribution in tumour tissues when compared to CD8^{+} T cells.
a, Experimental protocol to assess the spatial distribution of TRP-1 CD4^{+} and Pmel-1 CD8^{+} T cells in HCmel12 Tyr-KO CRISPR-ctrl tumours. **b**, Experimental protocol to assess the spatial distribution of TRP-1 CD4^{+} and Pmel-1 CD8^{+} T cells in HCmel12 Tyr-KO Jak1-KO tumours. **c,d,** Representative immunofluorescence image of indicated tumours (blue) treated with adoptively transferred TRP-1 CD4^{+} (green) and Pmel-1 CD8^{+} (red) T cells. The solid line indicates the tumour border, the dashed line indicates the invasive margin (= tumour border ± 100 µm) **e,** Graphical illustration (left) and quantified cell density in cells per mm[2] (right) of TRP-1 CD4^{+} and Pmel-1 CD8^{+} T cells in HCmel12 Tyr-KO CRISPR-ctrl tumours. **f,** Graphical illustration (left) and quantified cell density in cells per mm[2] (right) of TRP-1 CD4^{+} and Pmel-1 CD8^{+} T cells in HCmel12 Tyr-KO Jak1-KO tumours. Means between groups were statistically compared using one-way ANOVA with Tukey's post-hoc test, *p<0.05, **p<0.01.

Complementary to the immunofluorescence microscopy, an IV-2PM procedure was established to investigate CD8^{+} and CD4^{+} T cell behaviour dynamically. To this end, mice were injected with a mixture of ketamine and xylazine and after onset of anaesthesia, the tumour-bearing hind leg was fixed in an elevated position. The skin covering the tumour was detached using surgical scissors and forceps. One drop of transparent carbomer gel was used on the exposed site as mounting medium. Two component STD putty (3M ESPE) placed on both sides of the leg was used to create a level surface using a cover slip, which was gently pressed on the putty to make slight contact with the exposed site without exerting pressure on the tumour. After complete polymerisation of the putty, the mice were transferred onto a 37° C heating plate under the 2-photon microscope (Figure 4.6 a,b).
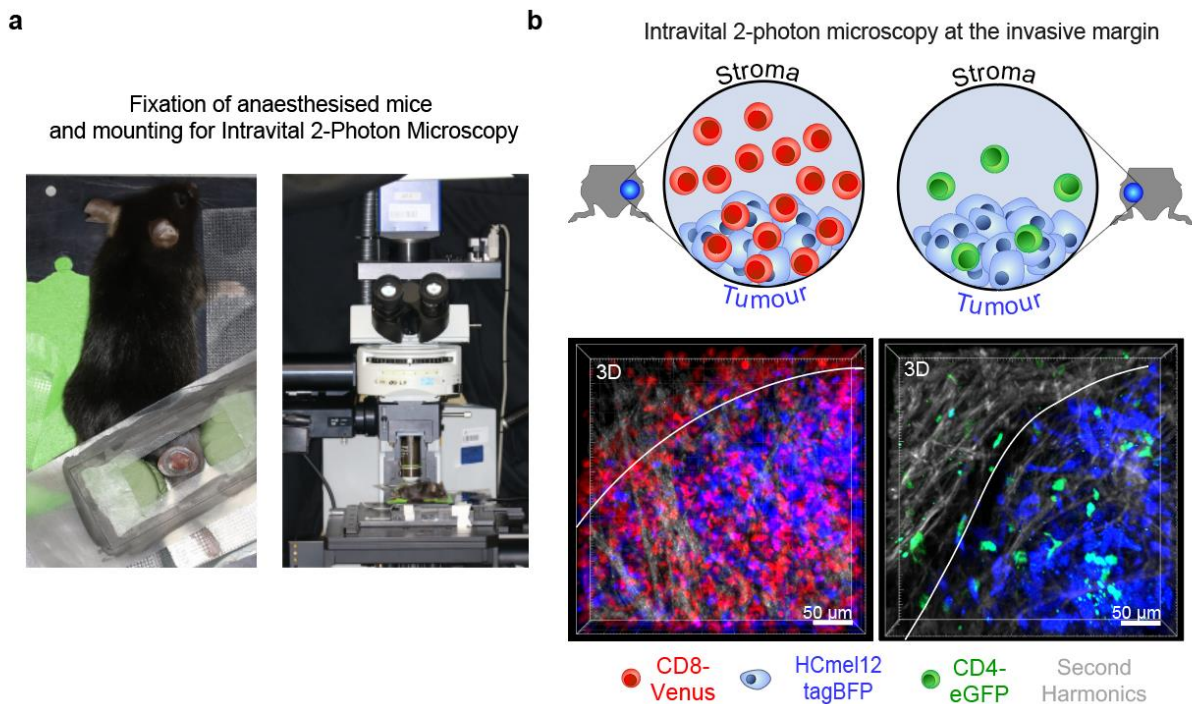
Figure 4.6: Experimental setup for intravital 2-photon microscopy of mouse melanomas.
a, Photographic images of hind leg and tumour tissue fixation of anaesthetised mice (left) and placement of mice under a Zeiss LSM 700 2-photon microscope (right). **b,** Graphical illustration (top) and representative pseudo-3D overview microscopic images (bottom) of tumours treated with adoptively transferred CD8^{+} T cells (red) or CD4^{+} T cells (green).

To compare the migratory behaviour of CD4^{+} and CD8^{+} T cells within the tumour invasive margin, amelanotic CRISPR-ctrl tumours were inoculated on the hind legs of wild type mice and IV-2PM of CD4 or CD8 ACT-treated mice was performed 5 days after T cell

transfer (Figure 4.7 a). To distinguish between T cells in the stroma (S) and tumour (T) compartments of the invasive margin, a tumour border was defined based on the tumour cells tagBFP expression (Figure 4.7 b). In both the stroma and in the tumour compartment of the invasive margin, the majority of TRP-1 CD4$^+$ T cells arrested and harboured similar mean speeds, whereas CD8$^+$ T cells remained highly motile in the stroma and preferentially arrested in association with tumour cells (Figure 4.7 c,d).
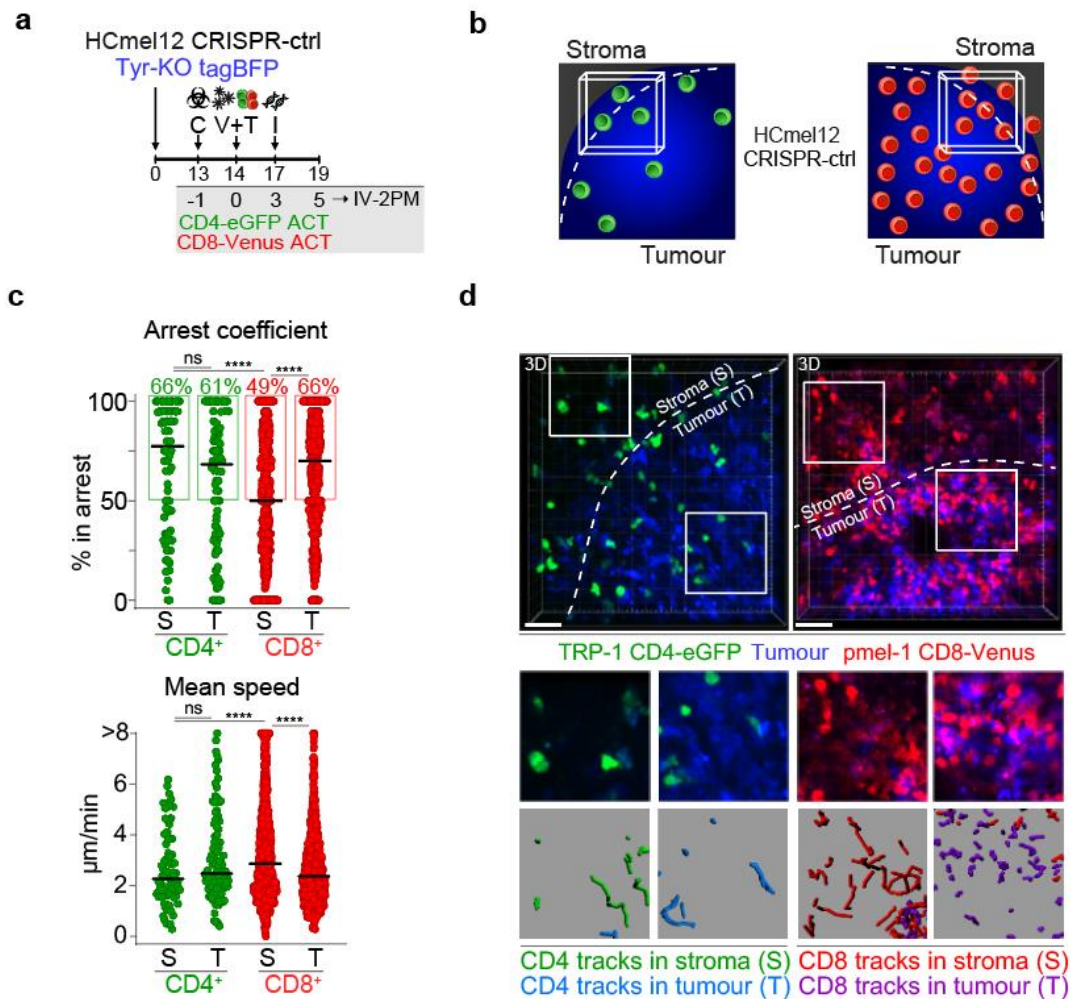
Figure 4.7: CD8$^+$ T cells, but not CD4$^+$ T cells, arrest in association with tumour cells in HCmel12 CRISPR-ctrl tumours.
a, Experimental protocol for intravital 2-photon microscopy (IV-2PM) of ACT treated HCmel12 CRISPR-ctrl Tyr-KO tagBFP tumours. b, Graphics depicting the distribution of adoptively transferred T cells at the invasive tumour margin (Cube, representative field of view; dashed line, tumour border). c, Arrest coefficient and mean speed of adoptively transferred Venus$^+$ Pmel-1 CD8$^+$ (red) and eGFP$^+$ TRP-1 CD4$^+$ T cells (green) in the stromal (S) and tumoural (T) compartment at the invasive margin of CRISPR-ctrl tumours (the bars indicate the median). d, Representative intravital microscopic images (scale bars 100 µm) and insets exemplifying 450 second motion tracks of Venus$^+$ Pmel-1 CD8$^+$ and eGFP$^+$ TRP-1 CD4$^+$ T cells at the stromal (S) and tumoural (T) area of the invasive tumour margin of CRISPR-ctrl tumours. Means between groups were statistically compared using one-way ANOVA with Tukey's post-hoc test, ****p<0.0001.

Next, the motility of TRP-1 CD4$^+$ and Pmel-1 CD8$^+$ T cells was investigated in MHC-deficient HCmel12 Jak1-KO tumours to assess if the observed CD4$^+$ and CD8$^+$ T cell arrest is dependent on MHC expression on the tumour cells. To this end, HCmel12 Jak1-KO tumours were injected in NK cell-depleted wild type mice and treated with CD4 or CD8 ACT (Figure 4.8 a,b). A slight decrease in the cell arrest as well as increase in the mean speed of TRP-1 CD4$^+$ T cells in the tumour (T) compartment compared to the stroma (S) compartment was observed. More strikingly, CD8$^+$ T cells failed to arrest in association with Jak1-KO tumour cells and instead remained highly motile, irrespective of their intra-tumoural location (Figure 4.8 c,d). Together, these observations indicate CD8$^+$ T cells require MHC-I-dependent antigen recognition specifically on the tumour cell surface, while CD4$^+$ T cells did not rely on MHC-II expression on tumour cells to decelerate.
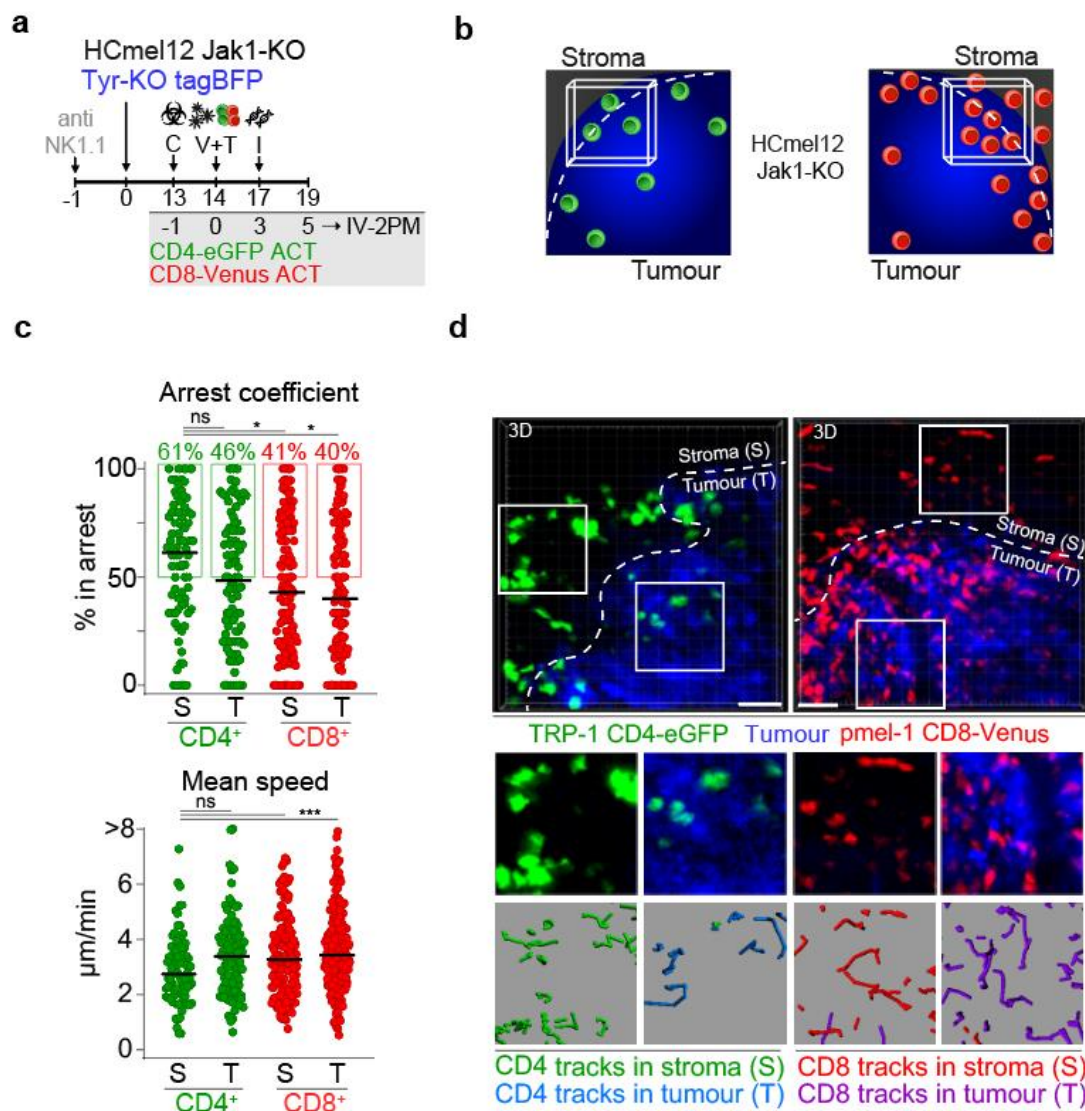
Figure 4.8: CD8⁺ T cells fail to arrest in association with IFN-unresponsive and MHC-deficient HCmel12 Jak1-KO tumours.
a, Experimental protocol for intravital 2-photon microscopy (IV-2PM) of ACT treated HCmel12 Jak1-KO Tyr-KO tagBFP tumours. **b,** Graphics depicting the distribution of adoptively transferred T cells at the invasive tumour margin (Cube, representative field of view; dashed line, tumour border). **c,** Arrest coefficient and mean speed of adoptively transferred Venus⁺ Pmel-1 CD8⁺ (red) and eGFP⁺ TRP-1 CD4⁺ T cells (green) in the stromal (S) and tumoural (T) compartment at the invasive margin of Jak1-KO tumours (the bars indicate the median). **d,** Representative intravital microscopic images (scale bars 100 µm) and insets exemplifying 450 second motion tracks of Venus⁺ Pmel-1 CD8⁺ and eGFP⁺ TRP-1 CD4⁺ T cells at the stromal (S) and tumoural (T) area of the invasive tumour margin of Jak1-KO tumours. Means between groups were statistically compared using one-way ANOVA with Tukey's post-hoc test, *p<0.05, ***p<0.001.

To validate the previously shown findings of this thesis with a second T cell model, an ovalbumin (OVA) expressing variant of HCmel12 Jak1-KO Tyr-KO was generated (Figure 4.9 a). An adenoviral vaccine expressing OVA was used to prime Venus$^+$ OT-I CD8$^+$ and dsRed$^+$ OT-II CD4$^+$ T cells, which recognise the epitopes OVA$_{aa257-264}$ and OVA$_{aa323-339}$, respectively (Figure 4.9 b). Firstly, the ability of OT-I and OT-II to eradicate HCmel12 Jak1-KO Tyr-KO OVA-tagBFP tumours was assessed. To enable robust and synchronous tumour growth, NK cell depleting antibodies were administered before tumour inoculation (Figure 4.9 c). In accordance with the melanocyte-specific Pmel-1 and TRP-1 T cell models, OT-I CD8$^+$ T cells failed to control the established melanomas, whereas the majority of mice treated with OT-II CD4$^+$ T cells were able to eradicate the tumours (Figure 4.9 d). Next, the spatial distribution of OT-I and OT-II cells in IFN-unresponsive, MHC-deficient tumours were investigated. Very few OT-II cells were found at the invasive tumour margin and none could be detected in the tumour centre of OVA-expressing Jak1-KO tumours. In contrast, OT-I cells infiltrated the invasive margin in large numbers, but were absent from the tumour centre (Figure 4.9 e). Intravital 2-photon microscopy revealed that OT-II cells arrested both in the stroma (S) and the tumour (T) compartment of the invasive margin, whereas OT-I cells were motile regardless of tumour cell proximity (Figure 4.9 f). In summary, these data using the OVA antigen model were consistent with the findings of the Pmel-1 and TRP-1 T cell models in that CD4$^+$ T cells eradicate IFN-unresponsive, MHC-deficient tumours and differ fundamentally in their spatial organisation and dynamics within the TME when compared to CD8$^+$ T cells.
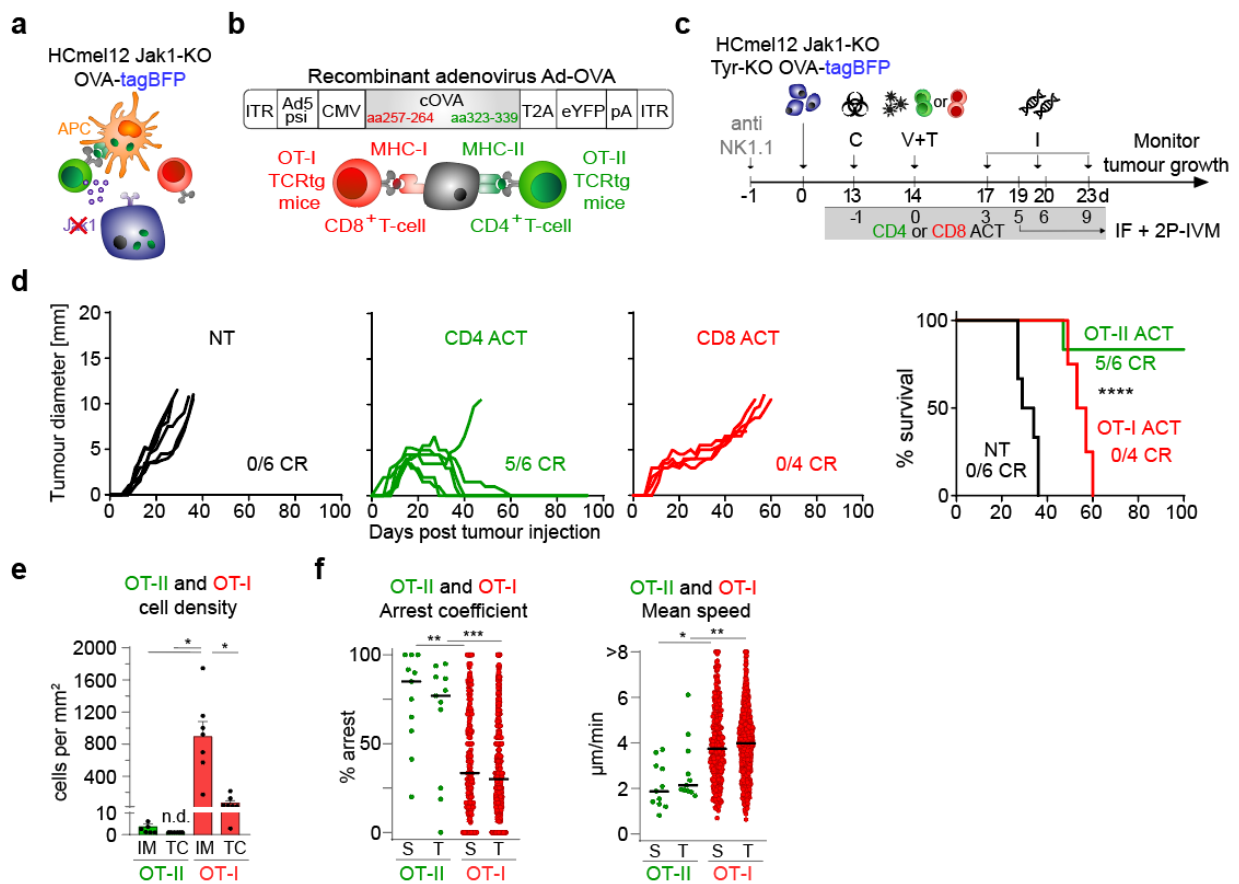
Figure 4.9: OVA-specific OT-II CD4+ T cells eradicate OVA-expressing IFN-unresponsive, MHC-deficient tumours that resist OT-I CD8+ T cell therapy.
a, Interaction phenotype of HCmel12 Jak1-KO Tyr-KO OVA-tagBFP cells. **b,** Structure of recombinant Ad-OVA vaccine used to prime OT-I CD8+ and OT-II CD4+ T cells. **c,** Experimental protocol to investigate therapy efficacy and spatiotemporal dynamics of OVA-specific OT-II CD4+ and OT-I CD8+ T cells. **d,** Individual tumour growth curves (left) and Kaplan-Meier survival graphs (right) of mice bearing HCmel12 Jak1-KO Tyr-KO OVA-tagBFP melanomas. Survival was statistically compared using log-rank Mantel-Cox test, ****$p<0.0001$. **e,** Cell density of OT-II CD4+ (green) and OT-I CD8+ (red) T cells in the invasive margin (IM) and tumour centre (TC) of HCmel12 Jak1-KO Tyr-KO OVA-tagBFP tumours, generated via immunofluorescence (IF) microscopy of cryosections. **f,** Arrest coefficient and mean speed of OT-II CD4+ (green) and OT-I CD8+ (red) T cells in the stroma (S) and tumour (T) compartment of the invasive margin of HCmel12 Jak1-KO Tyr-KO OVA-tagBFP tumours, generated via IV-2PM. Means between groups were statistically compared using one-way ANOVA with Tukey's post-hoc test, *$p<0.05$, **$p<0.01$, ***$p<0.001$.

4.3 Effector CD4⁺ T cells locally cluster with MHC-II-expressing immune cells at the tumour invasive margins in an antigen-dependent manner

As many CD4⁺ effector T cells arrested independent of MHC-II expression on tumour cells, professional APC were a likely interaction partner to present the MHC-II-bound antigen to the CD4⁺ T cells within the invasive tumour margin. A well described type of APC to stimulate CD4⁺ T cell responses are dendritic cells, due to their ability to efficiently ingest and process tumour antigens for MHC-II-dependent antigen presentation[59,60,112]. To visualise antigen-specific interactions of TRP-1 CD4⁺ T cells and dendritic cells, an amelanotic (Tyr-KO) variant of the previously established HCmel12 Trp1-KO cell line, which specifically lacks the antigen for the TCRtg TRP-1 CD4⁺ T cells, was generated via CRISPR/Cas9 and termed HCmel12 Trp1-KO Tyr-KO tagBFP (Figure 4.10 a). CRISPR-ctrl and Trp1-KO cells were injected into opposite hind legs of CD11c-Venus mice that harbour fluorescent dendritic cells[113] and treated with adoptively transferred eGFP⁺ TRP-1 CD4⁺ T cells (Figure 4.10 b). Immunofluorescence microscopy revealed local accumulations of eGFP⁺ adoptively transferred CD4⁺ T cells in the invasive tumour margin only in CRISPR-ctrl, but not in Trp1-KO tumours (Figure 4.10 c,d,e). In addition, surrounding tumour cells upregulated the expression of MHC-II only in CRISPR-ctrl, but not in Trp1-KO tumours (Figure 4.10 c,d), likely caused by local IFNγ-secretion by activated TRP-1 CD4⁺ T cells. Cell-to-cell contacts of adoptively transferred CD4⁺ T cells with MHC-II⁺ CD11c-Venus cells, as well as MHC-II⁺ tumour cells could be observed in CRISPR-ctrl tumours (Figure 4.10 c, insets). Overall, TRP-1 CD4⁺ T cell abundance was lower in Trp1-KO tumours when compared to CRISPR-ctrl tumours (Figure 4.10 f), suggesting that either infiltration or perseverance of CD4⁺ T cells is dependent on antigen expression.
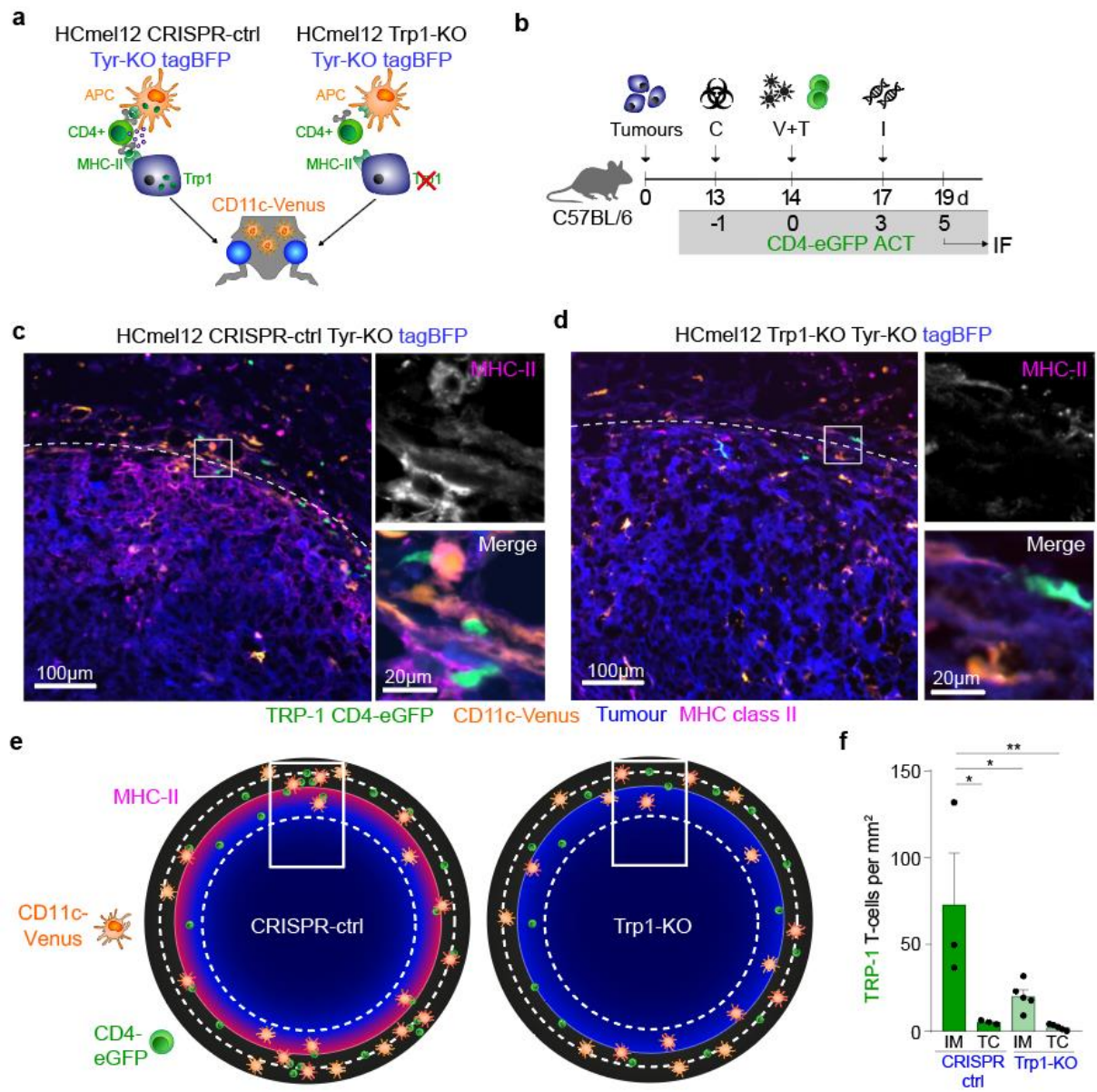
Figure 4.10: CD4+ T cells form local clusters with MHC-II-expressing CD11c-Venus+ immune cells within the invasive tumour margin.

a, Interaction phenotype of indicated HCmel12 variants and experimental setup of tumour injection on contralateral hind legs. **b,** Experimental protocol to investigate antigen-specific interactions of TRP-1 CD4+ T cells and MHC-II expressing CD11c+ immune cells. **c,** Representative immunofluorescence image of an HCmel12 CRISPR-ctrl Tyr-KO tagBFP tumour stained against MHC-II and example of an interactions hotspot of CD4+ T cells and MHC-II expressing CD11c-Venus+ cells (insets). **d,** Representative immunofluorescence image of an HCmel12 Trp1-KO Tyr-KO tagBFP tumour stained against MHC-II and example of a CD4+ T cell not in contact to MHC-expressing CD11c-Venus+ immune cells (insets). **e,** Graphical illustration of the differences in MHC-II expression and CD4+ T cell to CD11c-Venus+ cell interactions in CRISPR-ctrl and Trp1-KO tumours upon CD4 ACT. **f,** Cell density of TRP-1 CD4+ T cells in CRISPR-ctrl and Trp1-KO tumours 5 days after ACT, divided into the invasive margin (IM) and tumour centre (TC). Means between groups were statistically compared using one-way ANOVA with Tukey's post-hoc test, *$p<0.05$, **$p<0.01$.

To next investigate if the migratory behaviour of CD4$^+$ T cells is associated with CD11c-Venus$^+$ immune cells, CD11c-Venus mice were inoculated with both HCmel12 Tyr-KO tagBFP tumour cells that cannot express the CD4$^+$ T cell-specific antigen Trp1 (Trp1-KO) and CRISPR-ctrl tumour cells (Figure 4.11 a). To this end, in addition to the arrest coefficient and the mean speed, the contact duration of adoptively transferred CD4$^+$ T cells to the closest Venus$^+$ CD11c cell surface was determined and tracked over time (Figure 4.11 b). When the distance between the centre of mass of a CD4$^+$ T cells to the closest CD11c-Venus$^+$ surface was <8 µm, the cells were considered in contact (Figure 4.11 c). IV-2PM data demonstrated that CD4$^+$ T cells arrested and showed long-lasting interactions with Venus$^+$ CD11c-expressing cells only in CRISPR-ctrl, but not in antigen-negative Trp1-KO tumours (Figure 4.11 d,e). These data profoundly illustrate the antigen-dependent arrest of tumour-specific CD4$^+$ T cells in contact to CD11c-expressing APCs in the TME.
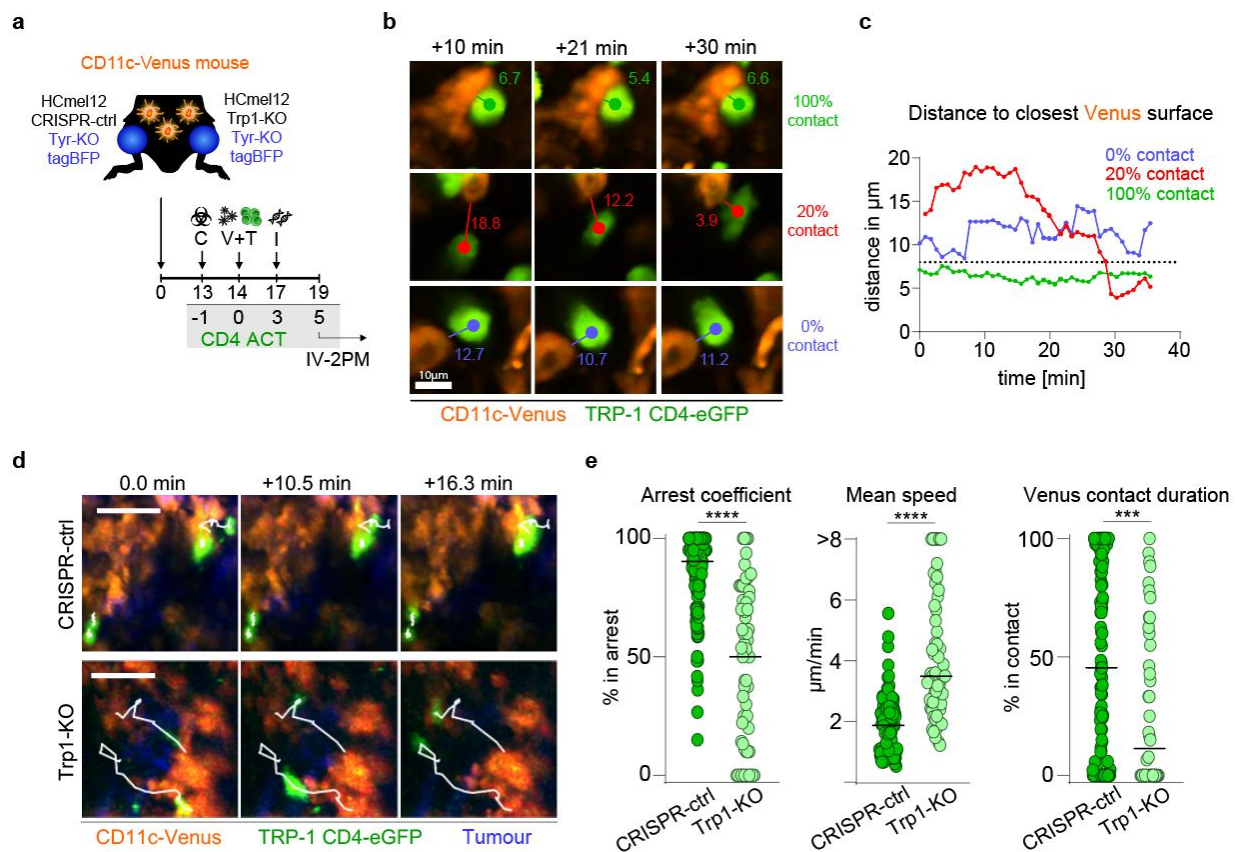
Figure 4.11: CD4+ T cells interact with CD11c-Venus+ immune cells at the invasive margin in an antigen-dependent manner.
a, Experimental protocol to study antigen-specific interactions between eGFP+ TRP-1 CD4+ T cells and CD11c+ cells in CD11c-Venus mice. **b,** Intravital 2P-microscopy images of three exemplary eGFP+ TRP-1 CD4+ T cells and their distance (in µm) to CD11c-Venus cells and **(c)** graphed over time. **d,** Representative motion tracks of eGFP+ TRP-1 CD4+ T cells interacting with CD11c-Venus+ cells in CRISPR-ctrl (top) and Trp1-KO (bottom) melanomas (scale bars 20 µm). **e,** Arrest coefficient, mean speed, and relative contact duration between eGFP+ TRP-1 CD4+ T cells and CD11c-Venus+ cells (the bars indicate the median). Means between groups were statistically compared using one-way ANOVA with Tukey's post-hoc test, ***p<0.001, ****p<0.0001.

To assess if the antigen-dependent arrest of CD4+ T cells with CD11c-Venus cells is dependent on MHC-II, HCmel12 CRISPR-ctrl Tyr-KO tagBFP tumours were inoculated into the hind legs of CD11c-Venus mice and treated with CD4 ACT. Directly before IV-2PM, the mice were i.v. administered with either MHC-II-blocking antibodies, or isotype antibodies (Figure 4.12 a). Motion tracking of adoptively transferred CD4+ T cells showed that the arrest of CD4+ T cells was decreased and the speed increased in mice that received MHC-II-blockade (Figure 4.12 b,c). Moreover, the contact duration of CD4+ T cells to CD11c-Venus+ cells was considerably lowered upon MHC-II-blockade (Figure 4.12 d). These data showed that antigen-dependent interactions of CD4+ T cells with CD11c-

Venus⁺ cells were dependent on MHC-II expression on the CD11c-Venus⁺ cells.
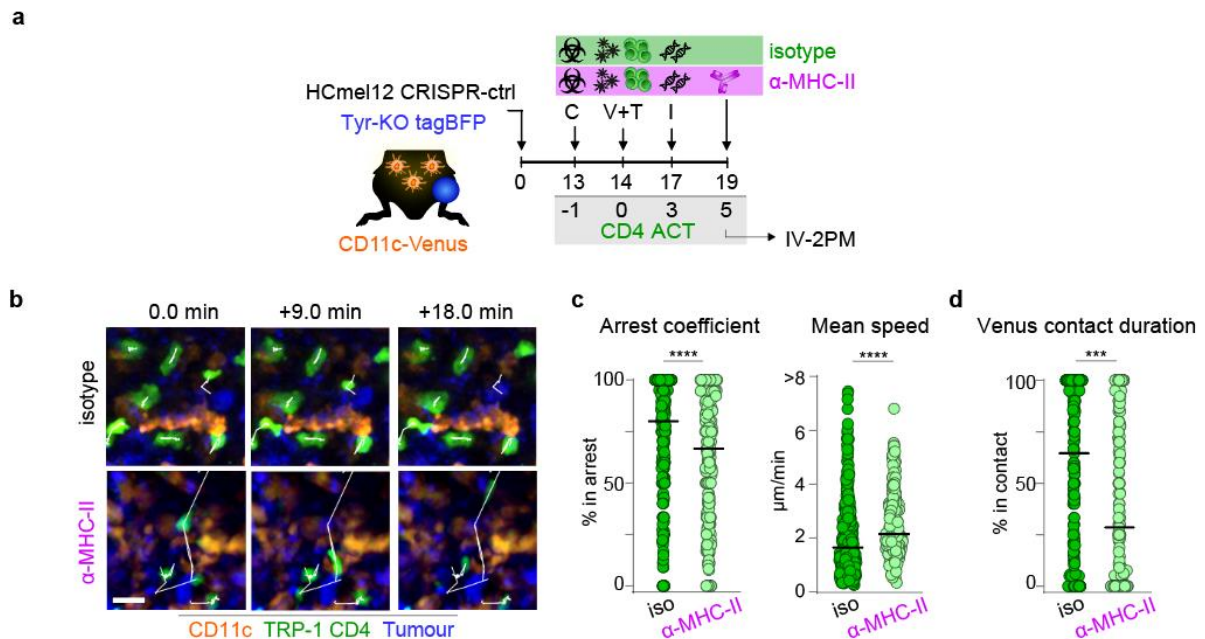
Figure 4.12: MHC-II-blockade abrogates interactions of CD4⁺ T cells with CD11c-Venus⁺ immune cells at the invasive tumour margin.
a, Experimental protocol to study MHC-II-dependent interactions between eGFP⁺ TRP-1 CD4⁺ T cells and CD11c⁺ cells in CD11c-Venus mice. **b,** Representative motion tracks of eGFP⁺ TRP-1 CD4⁺ T cells interacting with CD11c-Venus⁺ cells in CRISPR-ctrl melanomas injected with anti-MHC-II or isotype control antibodies (scale bars 20 μm). **c,d,** Arrest coefficient, mean speed, and relative contact duration between eGFP⁺ TRP-1 CD4⁺ T cells and CD11c-Venus⁺ cells (the bars indicate the median). Means between groups were statistically compared using one-way ANOVA with Tukey's post-hoc test, ***p<0.001, ****p<0.0001.

In summary, the second results section of this work displayed the establishment a 2-photon microscopy technique to visualise intra-tumoural location and migration patterns of T cells in transplantable melanomas. The data demonstrated that CD4⁺ effector T cells fundamentally differed in their spatial organisation and migratory behaviour in the TME when compared to CD8⁺ T cells. While CD8⁺ T cells briskly infiltrated the tumour centre of MHC-competent tumours and decelerated in association with tumour cells, CD4⁺ T cell preferentially clustered at the invasive tumour margin and formed long-lasting interactions with CD11c-expressing immune cells, irrespective of the tumour MHC-II expression phenotype. These cellular interactions were dependent on tumour-derived antigen and MHC-II. The findings suggest that CD4⁺ effector T cells differ in their mode of action against cancer cells when compared to CD8⁺ T cells, as they were able to remotely control the tumours.

4.4 Effector CD4⁺ T cells reprogram the tumour-infiltrating myeloid cell network to indirectly and remotely eradicate immune-evasive tumours

The second results section revealed that CD4⁺ effector T cells harbour different spatial and temporal properties when compared to CD8⁺ T cells and form long-lasting, antigen- and MHC-II dependent interactions with CD11c-expressing immune cells in the tumour. However, as 2-photon microscopy is limited to only a few fluorescent probes, it remained elusive which exact cell types the adoptively transferred CD4⁺ T cells were interacting with, and how the tumour immune compartment as a whole was affected by them. In this third results chapter, a comprehensive phenotyping of the myeloid immune compartment of the TME was conducted to understand the impact of adoptively transferred CD4⁺ effector T cells on its phenotype. Furthermore, a specific focus was put on inflammatory effector molecules to encompass the underlying effector mechanisms of how adoptively transferred CD4⁺ effector T cells control immune-evasive tumours.

In the first results section, it was shown that the majority of tumour-infiltrating immune cells upon CD4 ACT were of monocytic origin (see Figure 4.3 c,d). The second chapter highlighted that antigen-dependent interactions of CD4⁺ T cells and myeloid cells take place and are likely to influence therapy success. To characterise those myeloid cells more holistically, single-cell RNA-sequencing of viable CD11b⁺Ly6G⁻ immune cells in HCmel12 CRISPR-ctrl tumours, either 5 days after CD4 ACT or left non-treated (NT), was performed (Figure 4.13 a). After data processing, demultiplexing and quality control (see method section), a total of 2251 CD4 ACT-treated and 1543 non-treated cells were found to be eligible for analysis. Initially, the Leiden algorithm was used to cluster CD4 ACT-treated cells against the non-treated control cells. The majority of CD4 ACT-treated cells clustered distinctly from the non-treated cells (Figure 4.13 b). Consistent with previous data of this work, SingleR cell type assignment[99] showed that the majority of analysed cells were monocytes (Figure 4.13 c). The pivotal determining factor for this distinct clustering was found to be a strong IFN signature in cells from CD4 ACT treated tumours (Figure 4.13 d) and consequentially, the most differentially expressed genes were many IFN-stimulated genes such as *Stat1*, *Isg15* or *Ifi47* as well as genes involved in antigen presentation (*H2-D1*, *B2m*, *H2-K1*, Figure 4.13 e). Gene set enrichment analyses for

"response to type I IFN" and "IFNγ-mediated signalling pathway" confirmed this notion (Figure 4.13 f).
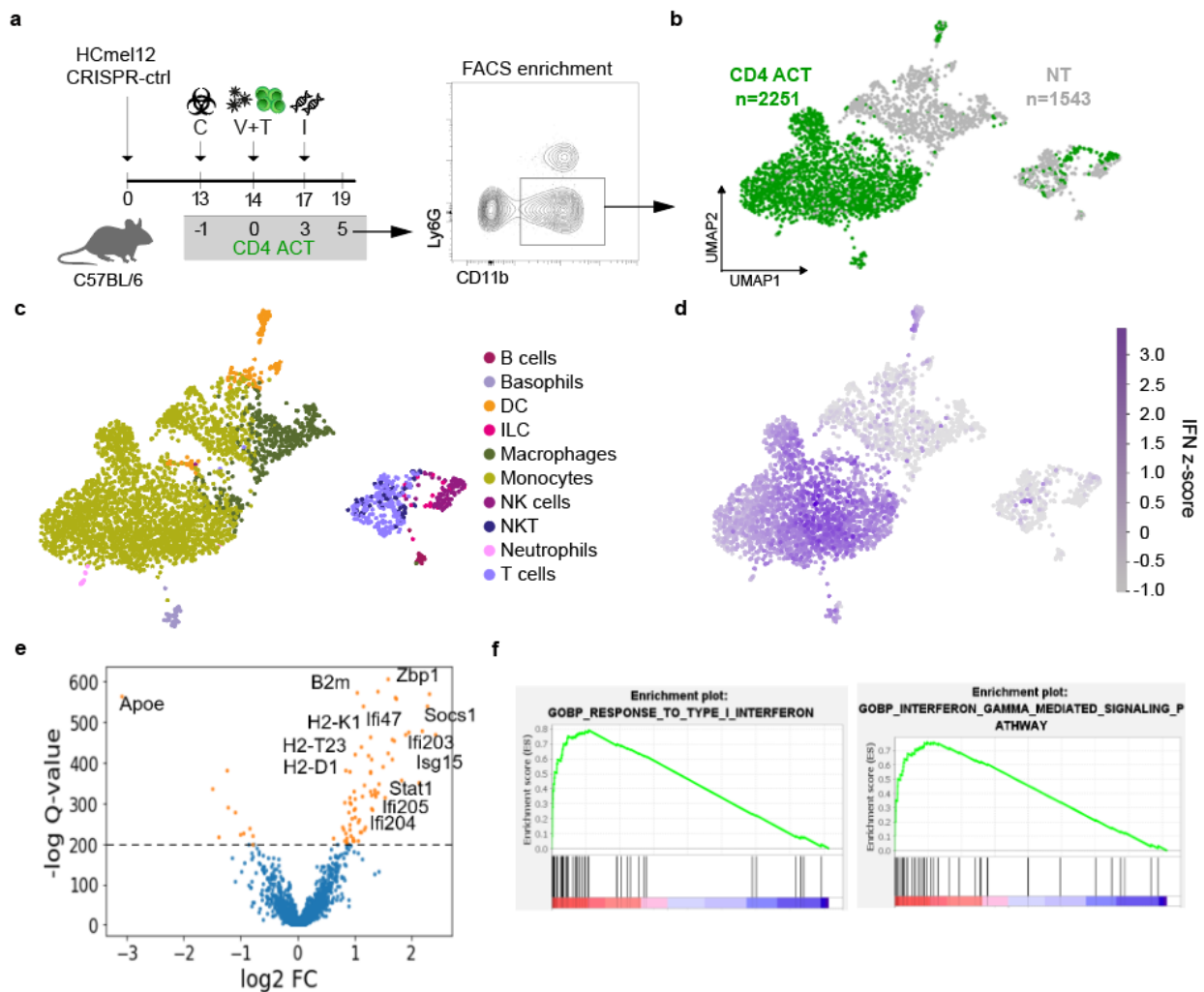
Figure 4.13: Tumour-infiltrating inflammatory monocytes acquire IFN-activated effector phenotypes upon CD4 ACT.
A, Experimental protocol for single cell RNA-seq analysis of FACS-enriched tumour-infiltrating CD11b⁺ Ly6G⁻ cells 5 days after CD4 ACT. **B,** Visualisation and dimensionality reduction of scRNA-seq data UMAP comparing samples from CD4 ACT-treated and non-treated (NT) mice. **c,** UMAP plots showing automatically assigned cell types using SingleR[99]. **d,** Z-score for all genes from the MSigDB gene set "HALLMARK_INTERFERON_GAMMA_RESPONSE" for each cell. **e,** Differentially expressed genes comparing samples from CD4 ACT-treated versus non-treated (NT) mice. Genes with –log Q-values >200 are shown in orange. **f,** Gene set enrichment analysis for the "GOBP RESPONSE TO TYPE I INTERFERON" (left) and "GOBP INTERFERON-GAMMA MEDIATED SIGNALING PATHWAY" (right) gene sets.

To investigate the dynamics of tumour-infiltrating monocyte-derived cells in depth, unsupervised Leiden clustering of all cells that were assigned to be a monocyte or a macrophage by SingleR was performed and disclosed 4 and 7 subclusters in the non-

treated and CD4 ACT-treated cells, respectively (Figure 4.14 a). Each cluster was defined based on the expression profile of 18 selected genes, assigned to lineage or phenotypic categories (Figure 4.14 b). Next, pseudotime inference and partition-based graph abstraction (PAGA) analysis was used to investigate the cells trajectories. The ACT0 cluster was identified as the origin and two distinct differentiation pathways based on the RNA velocity were discovered (Figure 4.14 c). Those pathways were termed "monocyte-to-macrophage effector path" and "monocyte maturation path", based on the expression of classical marker genes for their respective phenotypes. A more comprehensive breakdown of selected markers of the monocyte-to-macrophage effector path highlighted that tumour-infiltrating monocytes acquired different functional phenotypes in the tumour that included antigen presentation (ACT1) and potentially tumouricidal effector functions, particularly *Nos2* and *Arg1* (ACT2b and ACT2c) (Figure 4.14 b,d).
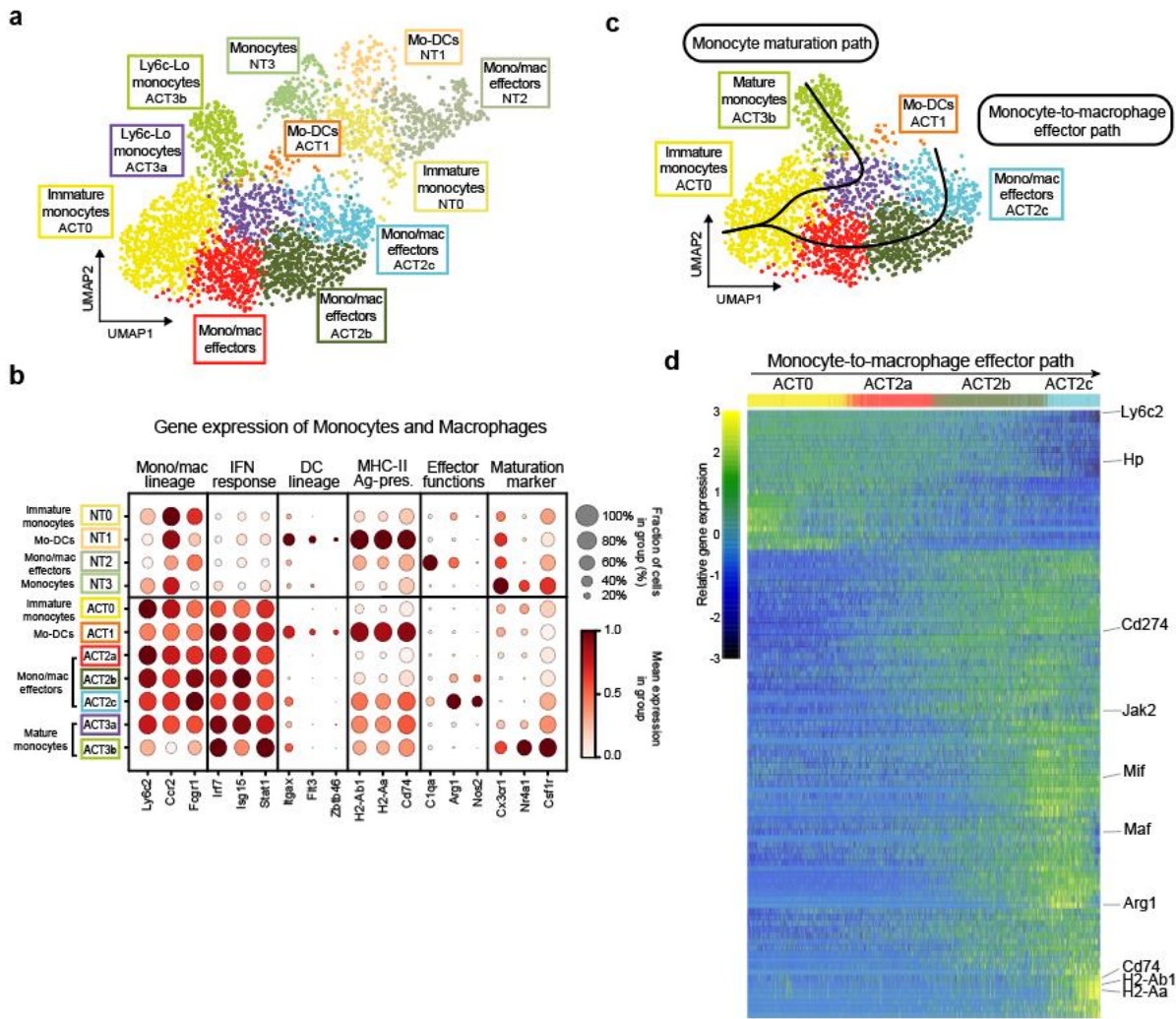
Figure 4.14: CD4 ACT induces distinct differentiation pathways of inflammatory monocytes towards antigen-presenting and tumouricidal effector phenotypes.
a, Graph-based UMAP clustering of tumour-infiltrating FACS-enriched CD11b⁺Ly6G⁻ monocytes and macrophages, assigned automatically by SingleR, using the Leiden algorithm. **b,** Expression levels and expressing cell fractions of selected signature genes, divided into 6 expression categories (Mono/mac lineage, IFN response, DC lineage, MHC-II antigen-presentation, effector functions and maturation marker) for the individual Leiden clusters. **c,** Pseudotime inference using velocyto and graph abstraction using PAGA for monocytes and macrophages of CD4 ACT-treated melanomas. **d,** Heatmap of differentially expressed genes along the pseudotime trajectory of the indicated Leiden clusters.

Prompted by the single-cell RNA-sequencing data, the potential of monocyte-derived cells to not only serve as antigen-presenting cells, but also as tumouricidal effector cells, was investigated next. To this end, the expression of inducible nitric oxide synthase (iNOS) in tumour-infiltrating myeloid cells was assessed, as the iNOS-encoding gene *Nos2* was induced upon CD4 ACT (see Figure 4.14 b) and is well described to induce inflammatory cell death in infection and cancer[114,115]. To recapitulate the dynamic acquisition of effector phenotypes on a protein level, tumour-infiltrating myeloid cells were analysed via flow cytometry 2,5 or 8 days after CD4 ACT or in non-treated control mice (Figure 4.15 a). For data analysis, the t-SNE algorithm was used to provide a holistic view on the tumour immune infiltrate (Figure 4.15 b,c). The data showed that starting 5 days after CD4 ACT, large numbers of $CD11b^+Ly6C^{hi}Ly6G^-$ inflammatory monocytes infiltrated into the tumours. Moreover, a notable fraction of these $Ly6C^{hi}$ cells expressed iNOS (Figure 4.15 d,e). Interestingly, neutrophil infiltration into the tumours was observed with slower kinetics, peaking at day 8 after ACT (Figure 4.15 e). Overall, the data was consistent with the previously observed myeloid cell infiltration in CD4 ACT-treated tumours (see Figure 4.3 c,d) and additionally revealed differential dynamics of the recruited myeloid cell subsets within the TME.
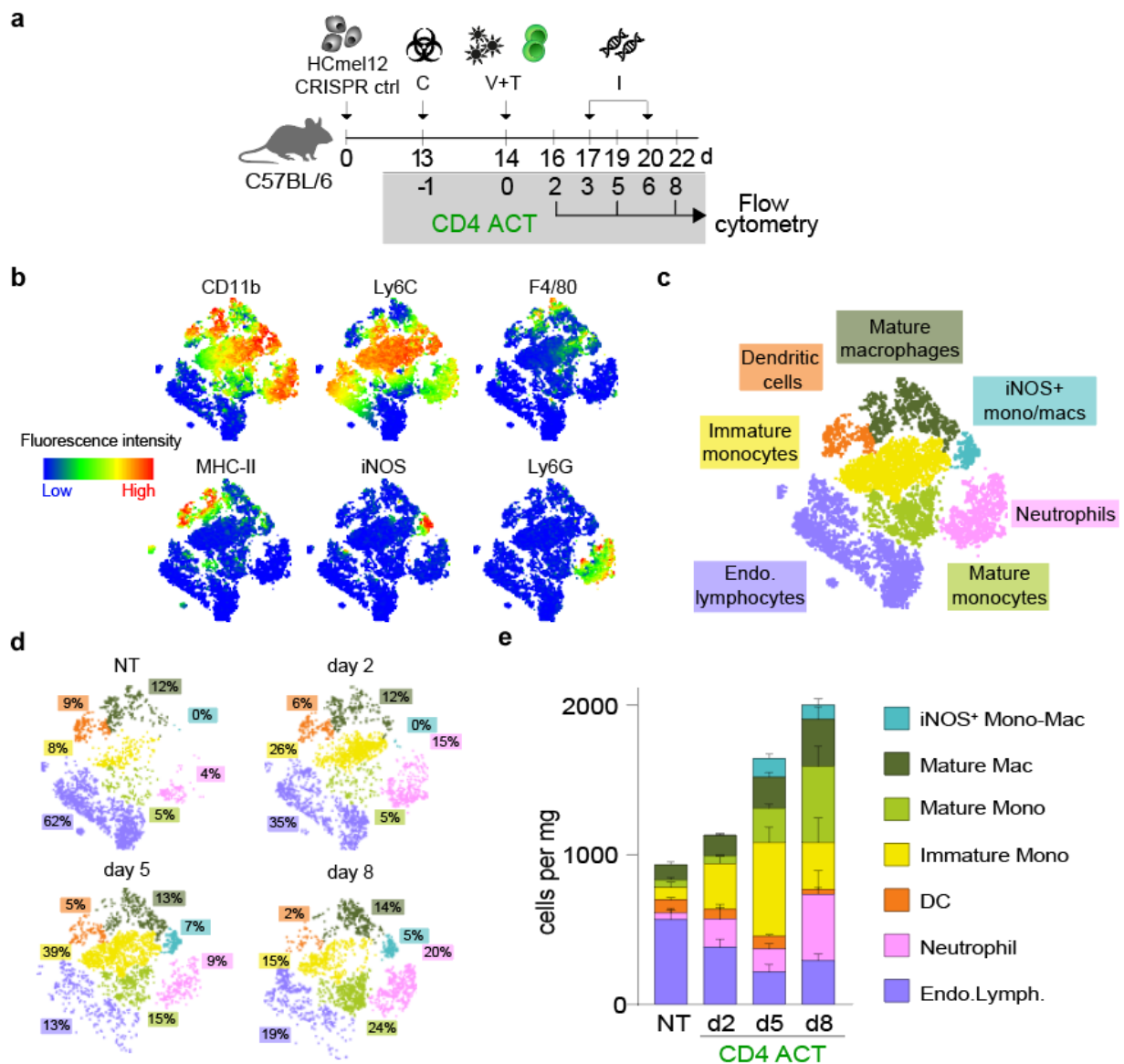
Figure 4.15: CD4 ACT induces nitric oxide production in tumour-infiltrating myeloid cells.
a, Experimental protocol to study CD4 ACT-mediated myeloid cell dynamics in HCmel12 tumours on a protein level. **b,c,** t-SNE heatmaps and corresponding annotation of tumour-infiltrating immune cell types: Immature monocytes (CD11b⁺Ly6Cʰⁱ), iNOS⁺ Mono-Mac (CD11b⁺iNOS⁺), mature macrophages (CD11b⁺F4/80⁺), mature monocytes (CD11b⁺Ly6Cˡᵒ), dendritic cells (MHC-II⁺CD11c⁺F4/80⁻), endogenous lymphocytes (CD11b⁻CD11c⁻), neutrophils (CD11b⁺ Ly6G⁺). **d,** Immune cell composition of tumours at indicated timepoints. **e,** Cells per mg tumour weight of indicated immune cell populations and at the indicated timepoints after CD4 ACT (NT, non-treated).

The expression of iNOS in myeloid cells has been shown to be dependent on IFNγ in various cancer models[73,109,115,116]. To test whether the release of IFNγ was responsible for the CD4⁺ T cell-mediated increase of iNOS-expressing myeloid cells, HCmel12 CRISPR-ctrl bearing mice received CD4 ACT therapy with or without IFNγ-blocking antibodies and tumours were analysed via flow cytometry one day after antibody administration and 5

days after ACT (Figure 4.16 a). Neutrophils were less abundant in the TME when compared to inflammatory monocytes and both population abundancies remained unchanged upon IFNγ-blockade (Figure 4.16 b). Conversely, the frequency of iNOS-expressing monocytes was swiftly reduced upon IFNγ-blockade (Figure 4.16 c). While the frequency of iNOS-expressing neutrophils induced by CD4 ACT was lower when compared to inflammatory monocytes, a decrease in iNOS$^+$ neutrophils was observed upon IFNγ-blockade (Figure 4.16 e). These data suggest that the induction of potentially tumouricidal, nitric oxide-producing myeloid cells was critically dependent on IFNγ release that was induced by adoptively transferred CD4$^+$ T cells.
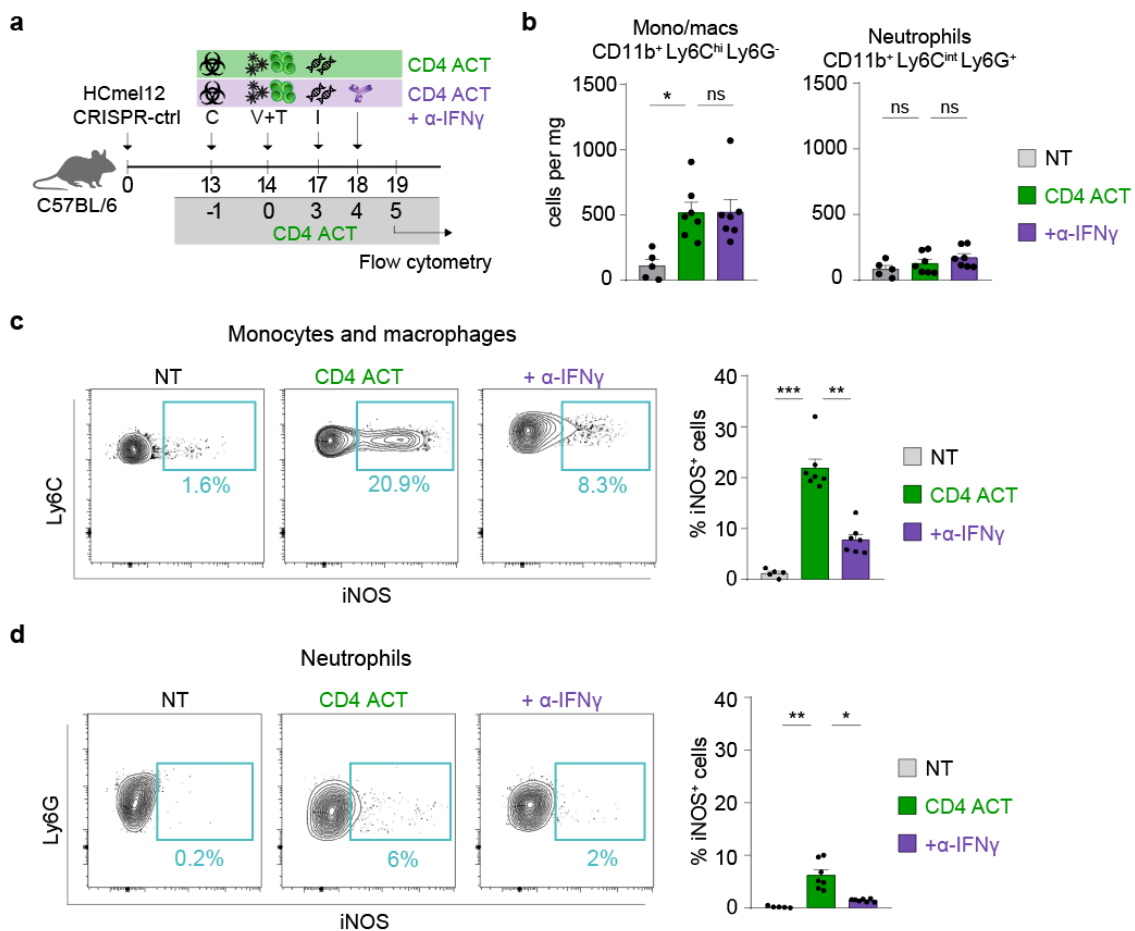
Figure 4.16: Nitric oxide production in tumour-infiltrating myeloid cells are dependent on IFNγ.
a, Experimental protocol to address the impact of IFNγ on iNOS expression in tumour-infiltrating myeloid cells. **b,** Cell density of monocytes and macrophages and neutrophils (in cells per mg) in tumours treated as indicated. **c,** Representative contour plots (left) and bar graph (right) showing the frequency of iNOS$^+$ monocytes and macrophages (CD11b$^+$Ly6C^{hi}Ly6G$^-$) in tumours treated as indicated. **d,** Representative contour plots (left) and bar graph (right) showing the frequency of iNOS$^+$ monocytes and macrophages (CD11b$^+$Ly6C^{int}Ly6G$^+$) in tumours treated as indicated. Means between groups were statistically compared using one-way ANOVA with Tukey's post-hoc test, *p<0.05, **p<0.01, ***p<0.001.

Previous work in the Tüting laboratory showed that the release of IFNγ is essential for CD4^{+} T cell-mediated tumour control[117]. Therefore, the question was raised if IFNγ-dependent nitric oxide production from myeloid cells is also required to control HCmel12 melanomas. It was furthermore hypothesised that IFNγ-dependent nitric oxide release is essential specifically when the tumour itself was deficient in IFNγ-signalling. Hence, the IFN-responsive HCmel12 Ciita-KO cell line was used in direct comparison to the IFN-unresponsive HCmel12 Jak1-KO cell line. Both cell lines were MHC-II-deficient and thus could not be recognised directly by CD4^{+} T cells (Figure 4.17 a). Wild type mice were depleted of NK cells before inoculation with either HCmel12 Ciita-KO or Jak1-KO cells. When tumours reached 3 to 5 mm in diameter, CD4 ACT was performed with one cohort of mice receiving additional injections of the highly specific iNOS-inhibitor N6-(1-iminoethyl)-L-lysine (L-NIL) for 10 consecutive days (Figure 4.17 b). In HCmel12 Ciita-KO tumours, inhibition of iNOS via L-NIL did not alter the therapy efficacy of CD4 ACT (Figure 4.17 c). In HCmel12 Jak1-KO tumours however, iNOS-inhibition prevented CD4^{+} T cell-mediated tumour eradication, ultimately leading to tumour escape and a significantly reduced survival (Figure 4.17 d). These data showed that specifically in an IFN-unresponsive tumour, IFNγ-induced nitric oxide production was required for consistent tumour eradication.

Taken together, in the third results section of this work, a mechanistic link between CD4 ACT-induced IFNγ and the expression of iNOS in tumour-infiltrating myeloid cells, which were predominantly inflammatory monocytes, was elucidated. In particular, CD4 ACT induced the emergence of IFN-activated monocyte-derived cells that underwent distinct differentiation paths towards antigen-presenting and tumouricidal effector cells. On the molecular level, the nitric oxide producing enzyme iNOS was identified as a potential anti-tumoural mediator that was not found in non-treated tumours, but significantly induced upon CD4 ACT. The production of nitric oxide by inflammatory monocytes was found to be dependent on IFNγ. Lastly, nitric oxide production via iNOS was essential for CD4^{+} T cell-mediated tumour control specifically against IFN-unresponsive tumours, but not against IFN-responsive tumours, suggesting that IFNγ acts as a key molecule that can exert anti-tumour functions by directly targeting tumour cells or indirectly by activating myeloid cells in the TME.
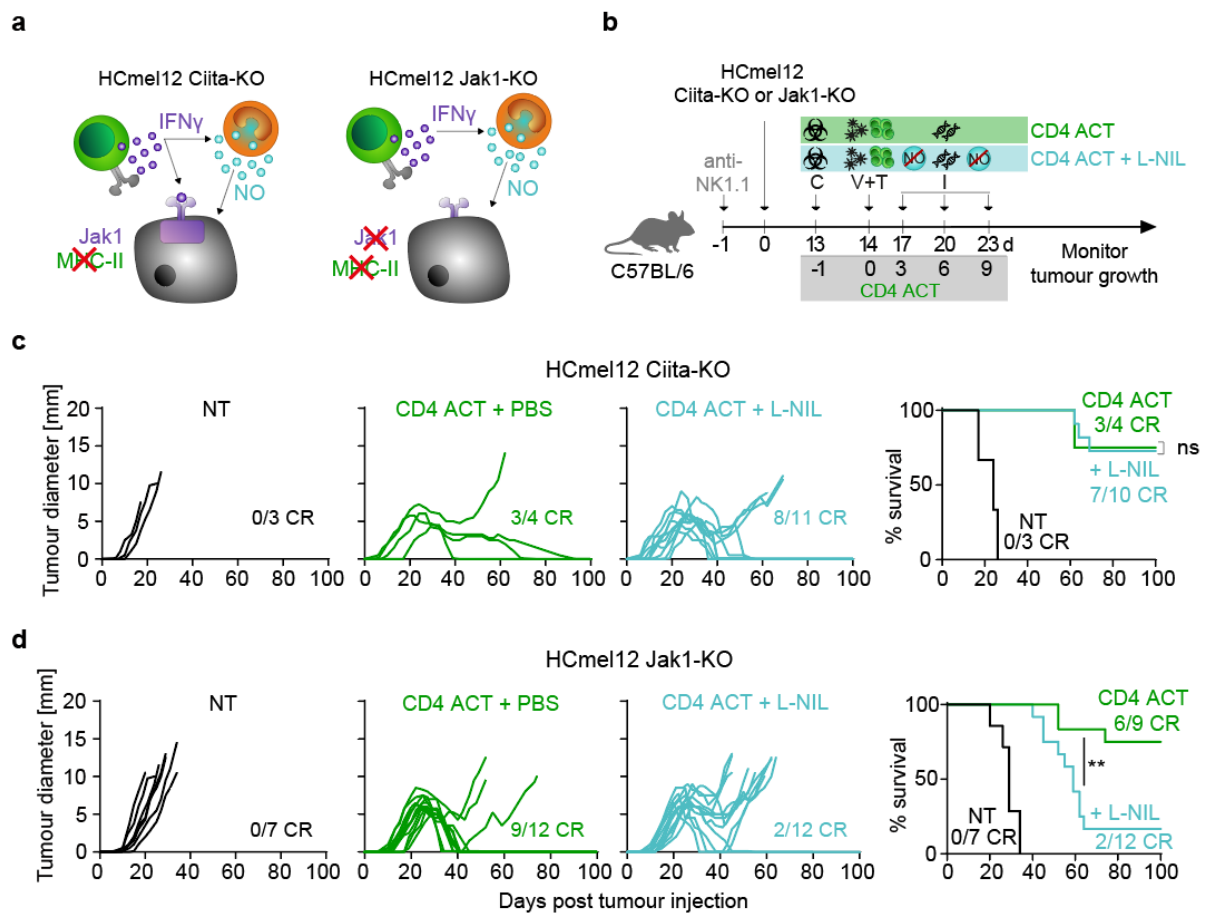
Figure 4.17: IFNγ-induced nitric oxide production by myeloid cells is essential for the CD4⁺ T cell-mediated eradication of IFN-unresponsive melanomas.
a, Diagrammatic representation of the HCmel12 Ciita-KO and HCmel12 Jak1-KO cell lines and their interaction phenotype with effector CD4⁺ T cells (green) and IFN-activated myeloid cells (orange). **b,** Experimental protocol to address the impact of an iNOS-inhibitor (L-NIL) on CD4 ACT-mediated tumour control. **c,** Individual tumour growth curves and Kaplan-Meier survival graphs (right) of established HCmel12 Ciita-KO melanomas treated as indicated**. d,** Individual tumour growth curves and Kaplan-Meier survival graphs (right) of established HCmel12 Jak1-KO melanomas treated as indicated. NO, nitric oxide; NT, non-treated; CR, complete responders. Survival was statistically compared using log-rank Mantel-Cox test, **p<0.01.

5. Discussion

This thesis presents experimental data for a mechanism whereby very few effector CD4+ T cells are sufficient to eradicate MHC-deficient, IFN-unresponsive melanomas that evade CD8+ T cell control. The spatiotemporal organisation of anti-tumour CD8+ and CD4+ T cells were found to differ fundamentally. While CD8+ T cells require direct MHC-I contact to strongly infiltrate the tumour centre in large numbers, CD4+ T cells preferentially cluster at the invasive margins, where they interact with CD11c+ antigen-presenting cells. In cooperation with innate immune stimulation, CD4+ T cells activate the tumour-associated myeloid network towards IFN-activated antigen-presenting and iNOS-expressing tumouricidal effector phenotypes. Together, CD4+ T cells and tumour-infiltrating myeloid cells orchestrate the induction of inflammatory cell death that eradicates MHC-deficient and IFN-unresponsive tumours.

5.1 Adoptively transferred CD4+ T cells eradicate immune-evasive tumours

Historically, conventional effector CD4+ T cells were thought to primarily act as helper cells for the activation of CD8+ T cells, which target tumour cells directly through recognition of MHC-I-bound antigens[58]. In the last decade, unleashing CD8+ T cells via immune checkpoint blockade has been developed to be the standard care for many cancer entities[118]. More recently, evidence of an analogous direct cytotoxic tumour cell killing performed by CD4+ T cells against MHC-II-positive tumour cells accumulated[62,63,106,119]. However, tumours can acquire resistance to direct CD8+ and CD4+ T cell-targeting by downregulation of MHC molecules[111] or loss of IFN-responsiveness[30,31]. The development of successful therapies to treat immunotherapy resistant tumours represents one of the major challenges in the field of cancer research.

In this work, an ACT protocol consisting of melanocyte differentiation antigen-specific TCRtg TRP-1[77] CD4+ and TCRtg Pmel-1[75] CD8+ T cells was used to uncover fundamental differences in the mode of action between anti-tumour CD4+ and CD8+ T cells. Naïve TCRtg T cells were transferred into mice and primed *in vivo* using the previously generated adenoviral vaccine Ad-PT that allowed direct side-by-side comparison of CD4+ and CD8+ T cells[78]. The complete ACT included chemotherapeutic preconditioning with cyclophosphamide, which is also used clinically[102], and innate immune stimulation via

intra-tumoural injections of TLR3 and TLR9 agonistic oligonucleotides polyI:C and CpG, respectively, as published previously for Pmel-1 CD8^{+} T cell ACT[6,53]. While current clinical ACT protocols use IL-2 as an adjuvant to boost T cell responses, TLR agonists show promise to improve therapy outcome and are being explored in early clinical trials[120,121].

This thesis showed that an ACT utilising tumour-specific CD4^{+} T cells were equally efficient as tumour-specific CD8^{+} T cells in eradicating large established melanomas. Similar results have been shown before in an experimental ACT model against transplanted carcinomas and endotheliomas[72]. In this study by Perez-Diez and colleagues, CD4^{+} T cell-mediated tumour control was found to be independent of cytotoxic CD8^{+} T cells, but instead depended on cooperation with NK cells. Here, IFN-unresponsive HCmel12 Jak1-KO cells deficient in MHC-I and MHC-II were utilised as a model for a therapy-resistant tumour. NK cell depletion was essential in order to enable uniform and synchronous Jak1-KO tumour growth. Importantly, while CD8^{+} T cells completely failed to control Jak1-KO tumours, CD4^{+} T cells were able to control the majority of Jak1-KO tumours. NK cell depletion, MHC-deficiency and the lack of CD8 ACT efficacy against Jak1-KO tumours implicated a CD4^{+} T cell-mediated effector mechanism that is largely independent of cytotoxic effector functions by NK, CD4^{+} and CD8^{+} T cell populations as well as IFN-signalling in the tumour cells.

The potential of adoptively transferred CD4^{+} T cells to control tumours independent of cytotoxic CD8^{+} T cells was already appreciated almost 30 years ago by Greenberg and colleagues[122]. Later, this notion was complemented by multiple reports of CD4^{+} T cell-mediated control of MHC-II-negative tumours in experimental fibrosarcoma[70,116], plasmacytoma[74] and pancreatic beta cell[69] tumour models. A common denominator of these studies was the recognition of IFNγ as the essential effector molecule to enable therapy success. However, the key target cells for the CD4^{+} T cell-derived IFNγ were found to be different, as IFNγ-induced tumour cell senescence[69], inhibition of angiogenesis[70] or activation of macrophages[74] were among the specified effector mechanisms. These findings outline the pleiotropic and model-dependent effects of CD4^{+} T cell-derived tumour control that could be partially comprehended with the results of this present study, in which a dual role of CD4^{+} T cell-driven IFNγ on tumour cells and myeloid cells was found. Additionally, while the control of IFNγR-deficient tumours by CD4^{+} T cells

was reported[70,116], this is the first study to show the eradication of tumours that are type I IFN and type II IFN-unresponsive. Therefore, this thesis revives and adds significantly to the notion that exploiting indirect CD4+ T cell effector mechanisms could advance cancer immunotherapies, specifically in the context of targeting immune-evasive tumours.

5.2 The behaviour of effector CD4+ T cells in tumour tissues differs fundamentally when compared to that of cytotoxic CD8+ T cells

The ability of tumours to evade immune cell destruction has been presented as an emerging hallmark of cancer by Weinberg and Hanahan[123]. Conceptually, the tumour immune landscape can be categorised into three immune phenotypes: (1) deserted, (2) excluded or (3) inflamed[37]. While this framework cannot encompass the complexity and uniqueness of each individual tumour, it is widely accepted that an inflamed phenotype, in particular tumour infiltration of CD8+ CTL and NK cells, correlates with a favourable prognosis across multiple cancer entities[56,123,124]. In contrast, there are conflicting reports regarding the effect CD4+ T cells on tumour development. While Tregs are well known to suppress anti-tumour T cell responses[42,43], there are conflicting reports regarding the role of Th2 and Th17 cells in tumours[56]. The subset of Th1 CD4+ T cells is the only one consistently associated with a good prognosis[56]. Nevertheless, it has also been proposed that suppressive TME can convert effector CD4+ T cells into Tregs[125,126]. The phenotypic multiplicity and plasticity of CD4+ T cells in the TME make it a challenging task to understand the contribution of a specific CD4+ T cell subset towards tumour development as well as their spatial organisation.

In this thesis, the unique ACT model and the specified aim to compare adoptively transferred CD4+ and CD8+ T cells enabled the comprehensive investigation of the spatial organisation and migratory behaviour of anti-tumour CD4+ T cells. It was shown that adoptively transferred TRP-1 CD4+ T cells expanded to a much lesser extent systemically when compared to adoptively transferred Pmel-1 CD8+ T cells, which was also reflected by a considerably lower number of tumour-infiltrating CD4+ T cells upon ACT. It is well established that CD4+ and CD8+ T cells harbour intrinsically different proliferative capacities, specifically that CD8+ T cells need less time of antigen exposure to start proliferating and perform cell division at a faster rate when compared to CD4+ T cells[127,128].

Immunofluorescence microscopy showed that the spatial organisation of CD4$^+$ T cells and CD8$^+$ T cells fundamentally differed. CD8$^+$ T cells briskly infiltrated the invasive margin and the tumour centre of HCmel12 CRISPR-ctrl tumours and arrested in association with tumour cells, indicating stable interactions that lead to tumour destruction. In IFN-unresponsive and MHC-deficient Jak1-KO tumours however, CD8$^+$ T cells failed to infiltrate the tumour centre and lost their capability to interact with tumour cells. These findings are supported by a number of intravital microscopy studies showing that intra-tumoural CD8$^+$ T cells decelerate dependent on antigen[129] and in association with tumour cells[130–132]. Together, these data suggest that CD8$^+$ T cell effector functions depended on the infiltration and perseverance of CD8$^+$ T cells in the tumour centre, where they directly interacted with MHC-I$^+$ tumour cells to induce cell death.

In stark contrast, CD4$^+$ T cells almost exclusively infiltrated the invasive margin and decelerated mostly independent of tumour cell proximity, irrespective of the capability of the tumour cells to express MHC-II. An in depth comparison of tumour-infiltrating CD4$^+$ and CD8$^+$ T cell spatial organisation and *in vivo* dynamics in the TME provided in this work is reported for the first time. It is important to note that there are limited data available on intra-tumoural CD4$^+$ T cell dynamics and this evident gap in the literature can be explained by a multitude of factors. The numeric scarcity of clonally expanded CD4$^+$ T cells coupled with their phenotypic multiplicity in tumours renders the acquisition of interpretable and statistically tenable data a major challenge. In addition, the successes of CD8$^+$ T cell-focused immunotherapies repressed the general interest in investigating anti-tumour CD4$^+$ T cells in the past decade.

Together, these data make it evident that the localisation and migratory behaviour of CD4$^+$ and CD8$^+$ T cells are inherently different, which is likely linked to their different effector mechanisms to control tumours. Looking forward, the spatial organisation of immune cells within the TME could have the potential to anticipate therapy outcome and dictate therapeutic strategies.

5.3 CD4^{+} T cells require indirect antigen presentation by MHC-II^{+} immune cells in the tumour microenvironment to exert their indirect effector functions

While the requirements for successful CD4^{+} T cell activation during the T cell priming are well established and to a large degree uniform among disease models[55], the conditions for optimal CD4^{+} T cell activation at the effector site of the immune response, more specifically the TME, is still unclear. Although expression of MHC-II on tumour cells correlate with an inflamed phenotype and better prognosis for patients, the vast majority of human tumours are MHC-II negative[57,133]. In these MHC-II negative tumours, MHC-II expression on stromal cells is critical for CD4^{+} T cell-mediated anti-tumour immunity. While a fraction of non-hematopoietic cells are able to express MHC-II[134], the most likely interaction partners of a CD4^{+} T cell in the tumour tissue are professional antigen-presenting cells, such as conventional dendritic cells[59], macrophages[135] or B cells[136,137]. In support of this notion, secretory antigens have been found to be more efficient in activating CD4^{+} T cells than intracellular antigens[135,138]. However, the critical interactions needed for a successful CD4^{+} T cell activation in the TME remains incompletely understood.

This work addresses how an indirect antigen recognition by CD4^{+} T cells is linked to the spatial organisation of CD4^{+} T cells and how this could provide a therapeutic advantage to control immune-evasive tumours. The use of the CD11c-Venus reporter mouse captured a substantial margin of potential MHC-II[+] interaction partners, as CD11c is not only expressed on conventional dendritic cells[113], but also subsets of macrophages and monocyte-derived cells[139]. Indeed, flow cytometry revealed that upon CD4 ACT around 60% of reported CD11c-Venus were tumour-infiltrating monocytes (data not shown). Immunofluorescence microscopy demonstrated the formation of CD4^{+} T cell interaction hotspots at the tumour invasive margin with CD11c-Venus cells, which was dependent on tumour-derived antigen. IV-2PM exhibited that CD4^{+} T cells decelerated and formed stable interactions with CD11c-Venus cells in CRISPR-ctrl tumours. Importantly, in contralateral tumours, which lacked the Trp1 antigen that the CD4^{+} T cells are specific for, these cell-to-cell contacts were significantly diminished, clearly demonstrating an antigen-dependent interactions. Moreover, the use of MHC-II-blocking antibodies in mice bearing CRISPR-

ctrl tumours confirmed that the long-lasting contacts of CD4⁺ T cells and CD11c-Venus cells were dependent on availability of MHC-II on the CD11c-Venus cell's surfaces.

These findings are supported by a previous report in which CD4⁺ T cells decelerated in an antigen-dependent manner at the infection site of a *Leishmania major* infection model[140]. Moreover, Marangoni and colleagues utilised an NFAT reporter system to show that CD4⁺ T helper cells required stable interactions with conventional dendritic cells for optimal activation in the TME[141]. While CD4⁺ T cell activation through NFAT signalling could not be formally tested in this thesis due to the lack of an appropriate reporter system, CD4⁺ T cells were found to form interaction clusters with CD11c-Venus cells at the tumour invasive margin in an antigen-dependent manner. In proximity to the CD4⁺ T cell clusters, tumour cells upregulated MHC-II, indicating an IFNγ-induced state and suggesting that IFNγ was produced by the transferred CD4⁺ T cells (see Figure 4.10).

Overall, these data suggest an essential role of antigen-presenting, CD11c⁺ cells for CD4⁺ T cell activation in the invasive margin of CD4 ACT-treated tumours, which has the potential to initiate a cooperative inflammatory response of CD4⁺ T cells and myeloid cells to control MHC-negative tumours.

5.4 CD4⁺ T cell effector functions against immune-evasive tumours rely on IFN-dependent reprogramming of the tumour-infiltrating myeloid cell network

IFNγ is known to be a key effector molecule for Th1 CD4⁺ T cell-mediated immune responses. The inflammatory capacity of IFNγ is not limited to infected and malignant cells, but it is also able to help other cells within the microenvironment. As such, IFNγ is described to activate innate immune cells in the TME to induce anti-tumour activities[71,74], by favouring a macrophage polarisation towards an M1-like, pro-inflammatory phenotype[46,142]. Among the IFNγ-induced effector molecules in myeloid cells is nitric oxide, which is produced by the enzyme inducible nitric oxide synthase (iNOS). Already 25 years ago, the concept of tumour control by CD4⁺ T cell-mediated nitric oxide production by macrophages was published[73] and more recently revisited in a plasmacytoma model[115]. However, mouse macrophages were identified solely by F4/80 expression, a marker that is fairly specific but alone does not clearly differentiate between monocytes, monocyte-derived macrophages and tissue-resident macrophages. The

relatively infrequent reporting of iNOS-dependent tumour control in the literature additionally raises the question of under what requirements nitric oxide emerges as a key effector molecule.

Here, single cell RNA sequencing on tumour-infiltrating myeloid cells was performed to understand the underlying effector mechanism of adoptively transferred CD4^{+} T cells. It was shown that CD4 ACT induces a strong recruitment of inflammatory monocytes that dynamically acquire IFN-activated phenotypes in the TME. Analysing the RNA velocity allowed the discrimination of distinct monocyte maturation pathways that led on one hand to mature non-classical monocytes and on the other hand to antigen-presenting and tumouricidal effector cells. This acquisition of IFN-activated phenotypes was confirmed on protein level with flow cytometric analyses over the early course of the CD4 ACT therapy, highlighting particularly the IFN-induced iNOS-expression in myeloid cells starting from day 5 after ACT. Strikingly, nitric oxide production was not required for the eradication of IFN-sensitive Ciita-KO tumours, indicating a direct effect of IFNγ on the tumour cells. However, in IFN-unresponsive Jak1-KO tumours, inhibition of iNOS significantly impaired CD4^{+} T cell-mediated tumour control, demonstrating that IFNγ-induced nitric oxide is required for the destruction of IFN-unresponsive tumours.

The high abundance and functionally distinct monocyte subsets that were revealed in the single cell RNA-sequencing data suggest that CD4 ACT causes an inflammation-induced emergency monopoiesis, as described by Guilliams and colleagues[143], a mechanism that is primarily associated with immune responses against bacterial infections. Moreover, CD4^{+} T cells are known to activate *L. major* infected monocytes to express iNOS as a defence mechanism[114]. Throughout the more recent history, tumour immunotherapy was inspired by anti-microbial immune defence mechanisms and aims to redirect these mechanisms against malignant cells. The concept to mimic a viral infection, and thus induce an inflammatory and cytotoxic immune response directed against a tumour, is the basis of many cancer immunotherapies[144]. This thesis' data suggests that recruiting and activating inflammatory monocytes to a TME is a promising addition to this concept that so far did not gain a lot of attention. Of note, nitric oxide can both benefit and hinder tumour progression by enabling angiogenesis and proliferation or inducing apoptosis and DNA damage, respectively[145,146]. Despite its bifurcating role, utilising nitric oxide as an effector

molecule to target cancer has been suggested a few times with either macrophages or neutrophils described as the main cellular source[73,115,147]. In particular, Hirschhorn and colleagues recently showed that iNOS-expressing neutrophils are essential for the control of tumour antigen escape variants[147]. However, data showing that an iNOS-dependent mechanism is only required against IFN-unresponsive tumours, but not IFN-responsive tumours, are reported here for the first time. One explanation for this lack of information could be that MHC expression of tumour cells is often linked to IFN-signalling. Hence, tumours lacking MHC-I are not exposed to CD8^{+} T cell-derived IFNγ, as activation of CD8^{+} T cells fails in the first place. Furthermore, in a CAR CD4^{+} ACT model, Boulch et al. recently showed remote IFNγ-dependent killing of B cell lymphomas independent of myeloid cells, that critically depended on tumour-intrinsic IFNγ-signalling[148]. Utilising high avidity anti-tumour CD4^{+} T cells, which are able to efficiently recognise tumour antigens through professional APCs, this study was able to unravel that CD4^{+} T cell-derived IFNγ does not only affect the tumour cells directly, but also activates tumour-infiltrating monocytes and macrophages to produce nitric oxide in the context of a CD4 ACT-mediated tumour eradication.

Taken together, this thesis highlights that very few adoptively transferred CD4^{+} T cells cooperate with highly abundant tumour-infiltrating myeloid cells to control MHC-deficient, IFN-unresponsive tumours. Exploiting this cellular axis could complement current clinically applied immunotherapies and potentially diminish events of tumour recurrence.

5.5 Limitations

The results of this thesis show that very few CD4^{+} T cells can remotely destroy immune-evasive tumours from the tumour invasive margin through cooperation with IFN-activated myeloid cells. However, some results must be interpreted with caution and require further investigation. For one, the role of the many different CD4^{+} T cell subsets has not been formally assessed. In particular, Tregs have been shown to have a crucial pro-tumoural effect in HCmel12 melanomas[149]. In this study, naïve CD4^{+} T cells were transferred and activated *in vivo* using the adenoviral vaccine Ad-PT. Further experiments within this project, but beyond the scopes of this thesis, revealed that transferred CD4^{+} T cells were indeed expressing the Th1 transcription factor T-bet, but not FoxP3[117]. Interestingly, complete CD4 ACT also resulted in a vanishing of endogenous Tregs, which likely adds benefit to the CD4^{+} T cell therapy.

Another limitation of this study is that the molecular mechanism leading to inflammatory tumour cell death upon nitric oxide release is not fully addressed in this work. Especially TNFα, a cytokine produced by both T cells and macrophages, which is known to induce inflammatory cell death, was not addressed in this thesis. However, a series of *in vitro* experiments were carried out to find that inflammatory cell death can be mediated by a synergistic effect of IFNγ and TNFα in IFN-responsive mouse and human melanoma cell lines[117]. In IFN-unresponsive tumours, the combination of nitric oxide and TNFα achieved similar efficacy. These findings however require a further and more detailed evaluation *in vivo* to understand the individual contribution of each inflammatory mediator.

Being able to translate experimental mouse work to a clinical setting is often a challenging task in biomedical research, because of limited availability of human samples, few methods to generate functionally relevant data or organisational challenges to successfully bridge experimental research and clinical daily routine. While adoptively transferred CD4^{+} T cells have been shown to contribute to complete responses in a few patients[150,151], larger scale clinical studies using adoptively transferred CD4^{+} T cells are required to understand their full potential. This thesis' findings are exclusively based on experimental *in vitro* and mouse *in vivo* results. However, in cooperation with clinicians in Magdeburg and Leuven, we were able to find similar spatial landscapes of CD8^{+} and CD4^{+} T cells in human histology samples and showed that downregulation oh MHC on tumour

70

cells is a relative frequent event that correlates with immune evasion[117]. Nevertheless, other translational challenges remain unsolved, such as that the ACT protocol used in our work incorporates intra-tumoural injection of the TLR3 and TLR9 agonists polyI:C and CpG, which is an administration route that is not suitable for patients with distant metastases. Clinical studies for TLR agonists in combination with ICB are currently being employed and first promising results have been presented in a recent clinical trial using an intra-tumoural CpG administration[120]. This enhanced efficacy could be due to packaging of CpG in virus-like particles, which results in an enhanced systemic therapy efficacy when compared to administration of naked CpG in mice[152].

Lastly, it should be noted that considerable differences have been reported regarding the metabolic response of mouse and human macrophages to TLR agonists[153]. Particularly the expression of high levels of iNOS by macrophages is not highly conserved between vertebrate species[154,155] and thus data from mouse models require a careful evaluation of the translatability of the experimental findings. To this end, humanised mice, such as a transgenic mouse model expressing the human NOS2 gene on a mouse NOS2 knockout background[156], could be used to study the species-dependent regulation of nitric oxide production.

5.6 Conclusion and outlook

For many years, effector CD4$^+$ T cells in cancer have been appreciated mostly as helper cells for the activation of cytotoxic CD8$^+$ T cells. The emergence of MHC-deficient and IFN-unresponsive tumours however demonstrate a common immune evasion mechanism. Hence, the development of novel strategies expanding on the successes of ICB is necessary. Here, an ACT protocol combining adoptively transferred CD4$^+$ T cells with innate immune stimuli was used to eradicate immune-evasive HCmel12 Jak1-KO tumours. CD4$^+$ T cells differed fundamentally in their spatial and dynamic organisation with tumours when compared to CD8$^+$ T cells. Specifically, CD4$^+$ T cells did not rely on direct tumour cell recognition to eradicate tumours. Instead, indirect recognition of tumour-derived antigen through interactions with antigen-presenting myeloid cells was required for CD4$^+$ T cell-mediated tumour control. These interactions resulted in a strong recruitment of tumour-infiltrating monocytes that, based on gene expression analyses, underwent distinct differentiation paths towards antigen-presenting and effector phenotypes. Flow cytometric analyses confirmed a potentially tumouricidal phenotype in recruited myeloid cells through the enzyme iNOS that synthesises the inflammatory mediator nitric oxide in an IFNγ-dependent manner. Inhibition of iNOS via L-NIL notably abrogated CD4 ACT therapy efficacy in IFN-unresponsive Jak1-KO tumours, but did not alter the outcome of CD4 ACT in CRISPR-ctrl tumour-bearing mice. These results suggest a dual role of CD4$^+$ T cell-derived IFNγ in anti-tumour immunity that can act either directly on IFN-responsive tumour cells or indirectly through tumour-infiltrating myeloid cells, which then induce inflammatory tumour cell death involving nitric oxide (Figure 5.1). This thesis and the encompassing publication provide a framework to exacerbate the efforts to utilise anti-tumour CD4$^+$ T cells in pre-clinical and clinical studies, as their effector functions can complement existing therapeutic strategies. In particular, IFN-unresponsive or MHC-deficient tumours that did not initially respond to ICB therapy could benefit from CD4$^+$ T cells activating tumour-infiltrating myeloid cells in an IFN-dependent manner. Nonetheless, the specifics of anti-tumour CD4$^+$ T cell functions need further experimental investigations, such as the contribution of TNFα to CD4$^+$ T cell-mediated tumour control. Additionally, the different molecular mechanisms of tumour cell death have not been assessed in this work and could have an impact on therapeutic strategies. Otherwise, while in this experimental CD4$^+$ T cells are able to eradicate tumours independent of CD8$^+$

T cells, a cooperation between the two T cell types likely assures the most beneficial for complete therapy responses. To this end, it will be of paramount importance to complement currently applied therapeutic strategies with novel approaches tailored to boost anti-tumour CD4+ T cell responses.
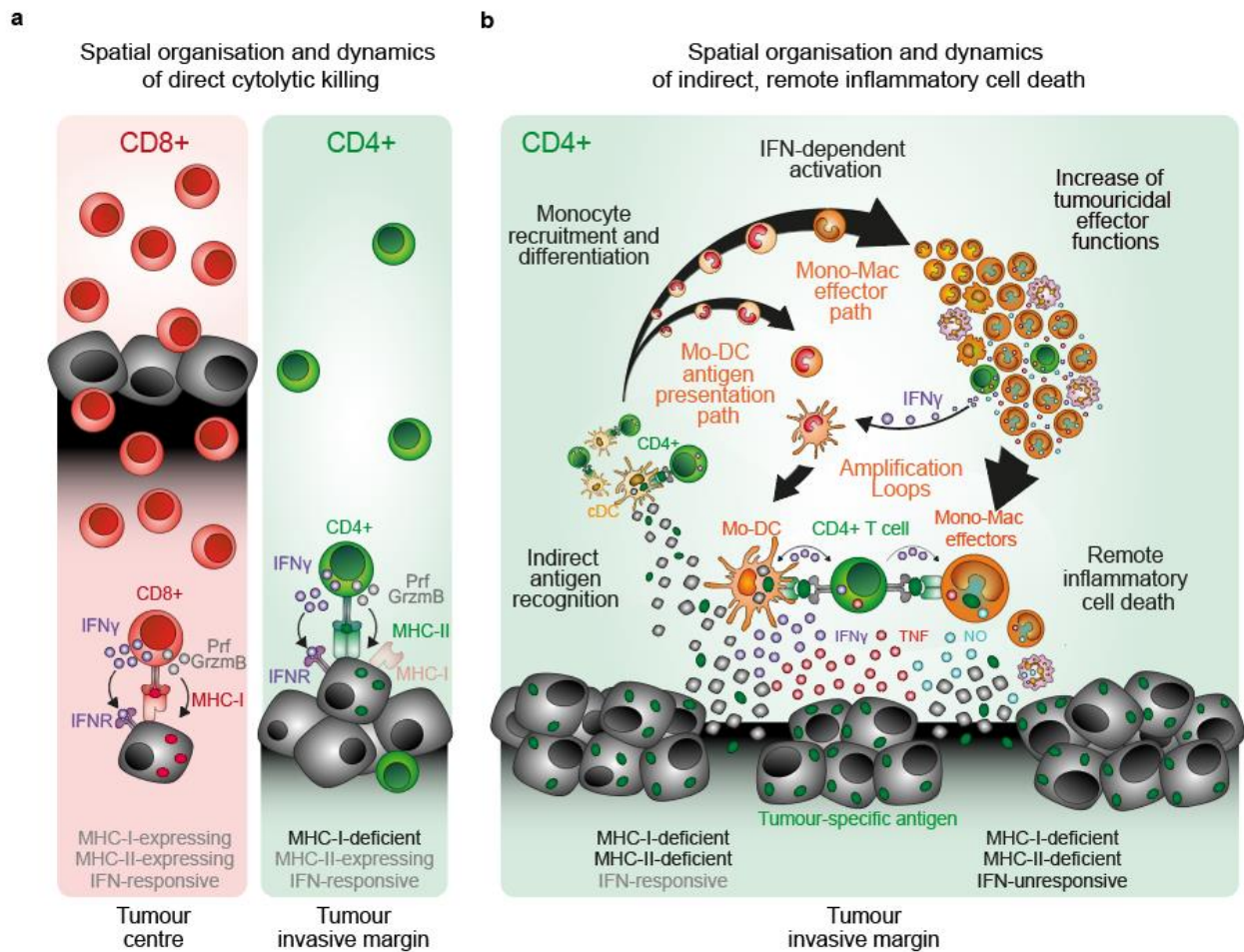
Figure 5.1: Graphical abstract (adapted from Kruse et al.[117])
a, Spatial organisation and dynamics of direct cytolytic killing. CD8+ effector T cells briskly infiltrate tumour tissues where they directly interact with tumour cells (left), while CD4+ effector T cells directly interact with tumour cells mainly near the invasive margin (right). **b,** Spatial organisation and dynamics of inflammatory cell death. CD4+ effector T cells cluster locally at the tumour invasive margin, where they indirectly recognise tumour antigen, presented by dendritic cells. Activated CD4+ T cells secrete IFNγ leading to the recruitment and activation of monocytes into the tumour tissue. Recruited monocytes phenotypically develop along differentiations path towards IFN-activated antigen-presenting (monocyte-derived dendritic cells, Mo-DCs) and tumouricidal phenotypes (monocyte-macrophage effector cells, Mono/Mac effectors). Mo-DCs additionally activate CD4+ T cells and amplify monocyte recruitment, activation and differentiation. CD4+ T cell-derived IFNγ sensitises IFN-responsive melanoma cells for TNF-induced cell death and myeloid cell-derived nitric oxide (NO) contributes to inflammatory cell death of IFN-unresponsive melanoma cells.

List of Abbreviations

Abbreviation	Meaning
ACT	Adoptive cell therapy
APC	Antigen presenting cell
BFP	Blue fluorescent protein
BP	Bandpass
CAR	Chimeric antigen receptor
CpG	Cytosine-phosphatidyl-Guanosine
CRISPR	Clustered Regularly Interspaced Short Palindromic Repeats
CTL	Cytotoxic T lymphocyte
CTLA4	Cytotoxic T-lymphocyte-associated protein 4
DC	Dendritic cell
DMBA	12-dimethylbenz(a)anthracene
DMEM	Dulbecco's modified Eagle medium
DMSO	Dimethyl sulfoxide
DNA	Deoxyribonucleic acid
EDTA	Ethylenediaminetetraacetic acid
FACS	Fluorescence-activated cell sorting
FCS	Fetal calf serum
FDA	Food and drug association (U.S.)
GFP	Green fluorescent protein
HBS	HEPES buffered saline
ICB	Immune checkpoint blockade
IFN	Interferon
IgG	Immunoglobulin G
IL-2	Interleukin 2
iNOS	Inducible nitric oxide synthase
IV-2PM	Intravital 2-photon microscopy
IVC	Individually vented cages
KO	Knockout
LP	Longpass
MAGE	Melanoma-associated antigen
MHC-I	Major histocompatibility complex class I

MHC-II	Major histocompatibility complex class II
MOI	Multiplicity of infection
n.a.	Not available
NCBI	National Center for Biotechnology Information
NGS	Next generation sequencing
NOS2	Nitric oxide synthase 2 (gene; encoding iNOS)
NT	Non-treated
OCT	Optimal cutting temperature
OVA	Ovalbumin
PAGA	Partition-based graph abstraction
PBS	Phosphate buffered saline
PCA	Principal component analysis
PCR	Polymerase chain reaction
PD1	Programmed cell death protein 1
Pmel	Premelanosome protein
PMT	Photomultiplier
polyI:C	Polyinosinic:polycytidylic acid
RBC	Red blood cell
RPMI	Roswell Park Memorial Institute
RNA	Ribonucleic acid
RT	Room temperature
SEM	Standard error of the mean
SHG	Second harmonics generation
t-SNE	t-Distributed Stochastic Neighbour Embedding
TCRtg	T cell receptor transgenic
TIL	Tumour-infiltrating lymphocytes
TLR	Toll-like receptor
TME	Tumour microenvironment
TNFα	Tumour necrosis factor alpha
Tregs	Regulatory T cells
TRP-1	Tyrosinase related protein 1
UMAP	Uniform manifold approximation and projection
UMI	Unique Molecular Identifier

References

1.   McCarthy, E. F. The Toxins of William B. Coley and the Treatment of Bone and Soft-Tissue Sarcomas. *Iowa Orthop J* **26**, 154–158 (2006).

2.   Gresser, I. & Bourali, C. Exogenous interferon and inducers of interferon in the treatment Balb-c mice inoculated with RC19 tumour cells. *Nature* **223**, 844–845 (1969).

3.   Rosenberg, S. A. *et al.* Use of tumor-infiltrating lymphocytes and interleukin-2 in the immunotherapy of patients with metastatic melanoma. A preliminary report. *N Engl J Med* **319**, 1676–1680 (1988).

4.   Rosenberg, S. A. *et al.* Observations on the systemic administration of autologous lymphokine-activated killer cells and recombinant interleukin-2 to patients with metastatic cancer. *N Engl J Med* **313**, 1485–1492 (1985).

5.   Ribas, A. & Wolchok, J. D. Cancer immunotherapy using checkpoint blockade. *Science* **359**, 1350–1355 (2018).

6.   Kohlmeyer, J. *et al.* Complete regression of advanced primary and metastatic mouse melanomas following combination chemoimmunotherapy. *Cancer Res* **69**, 6265–6274 (2009).

7.   Robbins, P. F. *et al.* Tumor regression in patients with metastatic synovial cell sarcoma and melanoma using genetically engineered lymphocytes reactive with NY-ESO-1. *J Clin Oncol* **29**, 917–924 (2011).

8.   Rosenberg, S. A. *et al.* Durable complete responses in heavily pretreated patients with metastatic melanoma using T-cell transfer immunotherapy. *Clin Cancer Res* **17**, 4550–4557 (2011).

9.   van der Bruggen, P. *et al.* A gene encoding an antigen recognized by cytolytic T lymphocytes on a human melanoma. *Science* **254**, 1643–1647 (1991).

10.   Kawakami, Y. *et al.* Identification of a human melanoma antigen recognized by tumor-infiltrating lymphocytes associated with in vivo tumor rejection. *Proc Natl Acad Sci U S A* **91**, 6458–6462 (1994).

11.   Brunet, J. F. *et al.* A new member of the immunoglobulin superfamily--CTLA-4. *Nature* **328**, 267–270 (1987).

12.   Ishida, Y., Agata, Y., Shibahara, K. & Honjo, T. Induced expression of PD-1, a novel member of the immunoglobulin gene superfamily, upon programmed cell death. *EMBO J* **11**, 3887–3895 (1992).

13.   Leach, D. R., Krummel, M. F. & Allison, J. P. Enhancement of antitumor immunity by CTLA-4 blockade. *Science* **271**, 1734–1736 (1996).

14.   Dong, H. *et al.* Tumor-associated B7-H1 promotes T-cell apoptosis: a potential mechanism of immune evasion. *Nat Med* **8**, 793–800 (2002).

15.   Iwai, Y. *et al.* Involvement of PD-L1 on tumor cells in the escape from host immune system and tumor immunotherapy by PD-L1 blockade. *Proc Natl Acad Sci U S A* **99**, 12293–12297 (2002).

16.   Sharma, P., Hu-Lieskovan, S., Wargo, J. A. & Ribas, A. Primary, Adaptive, and Acquired Resistance to Cancer Immunotherapy. *Cell* **168**, 707–723 (2017).

17.   Schumacher, T. N. & Schreiber, R. D. Neoantigens in cancer immunotherapy. *Science* **348**, 69–74 (2015).

18.   Hugo, W. *et al.* Genomic and Transcriptomic Features of Response to Anti-PD-1 Therapy in Metastatic Melanoma. *Cell* **165**, 35–44 (2016).

19.   Groom, J. R. & Luster, A. D. CXCR3 in T cell function. *Exp Cell Res* **317**, 620–631 (2011).
20.   Raskov, H., Orhan, A., Christensen, J. P. & Gögenur, I. Cytotoxic CD8+ T cells in cancer and cancer immunotherapy. *Br J Cancer* **124**, 359–367 (2021).
21.   Farhood, B., Najafi, M. & Mortezaee, K. CD8+ cytotoxic T lymphocytes in cancer immunotherapy: A review. *Journal of Cellular Physiology* **234**, 8509–8521 (2019).
22.   Borghaei, H. *et al.* Nivolumab versus Docetaxel in Advanced Nonsquamous Non-Small-Cell Lung Cancer. *N Engl J Med* **373**, 1627–1639 (2015).
23.   Larkin, J. *et al.* Combined Nivolumab and Ipilimumab or Monotherapy in Untreated Melanoma. *N Engl J Med* **373**, 23–34 (2015).
24.   Motzer, R. J. *et al.* Nivolumab versus Everolimus in Advanced Renal-Cell Carcinoma. *N Engl J Med* **373**, 1803–1813 (2015).
25.   Sucker, A. *et al.* Genetic Evolution of T-cell Resistance in the Course of Melanoma Progression. *Clinical Cancer Research* **20**, 6593–6604 (2014).
26.   Gubin, M. M. *et al.* Checkpoint blockade cancer immunotherapy targets tumour-specific mutant antigens. *Nature* **515**, 577–581 (2014).
27.   Spranger, S., Bao, R. & Gajewski, T. F. Melanoma-intrinsic β-catenin signalling prevents anti-tumour immunity. *Nature* **523**, 231–235 (2015).
28.   Sucker, A. *et al.* Acquired IFNγ resistance impairs anti-tumor immunity and gives rise to T-cell-resistant melanoma lesions. *Nat Commun* **8**, 1–15 (2017).
29.   Shin, D. S. *et al.* Primary Resistance to PD-1 Blockade Mediated by JAK1/2 Mutations. *Cancer Discov* **7**, 188–201 (2017).
30.   Zaretsky, J. M. *et al.* Mutations Associated with Acquired Resistance to PD-1 Blockade in Melanoma. *N Engl J Med* **375**, 819–829 (2016).
31.   Gao, J. *et al.* Loss of IFN-γ Pathway Genes in Tumor Cells as a Mechanism of Resistance to Anti-CTLA-4 Therapy. *Cell* **167**, 397-404.e9 (2016).
32.   Benci, J. L. *et al.* Tumor Interferon Signaling Regulates a Multigenic Resistance Program to Immune Checkpoint Blockade. *Cell* **167**, 1540-1554.e12 (2016).
33.   Schreiber, R. D., Old, L. J. & Smyth, M. J. Cancer immunoediting: integrating immunity's roles in cancer suppression and promotion. *Science* **331**, 1565–1570 (2011).
34.   Restifo, N. P. *et al.* Loss of functional beta 2-microglobulin in metastatic melanomas from five patients receiving immunotherapy. *J Natl Cancer Inst* **88**, 100–108 (1996).
35.   Restifo, N. P. *et al.* Identification of human cancers deficient in antigen processing. *J Exp Med* **177**, 265–272 (1993).
36.   Landsberg, J. *et al.* Melanomas resist T-cell therapy through inflammation-induced reversible dedifferentiation. *Nature* **490**, 412–416 (2012).
37.   Chen, D. S. & Mellman, I. Elements of cancer immunity and the cancer–immune set point. *Nature* **541**, 321–330 (2017).
38.   Chaudhary, B. & Elkord, E. Regulatory T Cells in the Tumor Microenvironment and Cancer Progression: Role and Therapeutic Targeting. *Vaccines* **4**, 28 (2016).
39.   Woo, E. Y. *et al.* Cutting Edge: Regulatory T Cells from Lung Cancer Patients Directly Inhibit Autologous T Cell Proliferation1. *The Journal of Immunology* **168**, 4272–4276 (2002).
40.   Ormandy, L. A. *et al.* Increased Populations of Regulatory T Cells in Peripheral Blood of Patients with Hepatocellular Carcinoma. *Cancer Research* **65**, 2457–2464 (2005).

41.   Sakaguchi, S., Yamaguchi, T., Nomura, T. & Ono, M. Regulatory T Cells and Immune Tolerance. *Cell* **133**, 775–787 (2008).

42.   Viehl, C. T. *et al.* Depletion of CD4+CD25+ Regulatory T Cells Promotes a Tumor-Specific Immune Response in Pancreas Cancer–Bearing Mice. *Ann Surg Oncol* **13**, 1252–1258 (2006).

43.   Simpson, T. R. *et al.* Fc-dependent depletion of tumor-infiltrating regulatory T cells co-defines the efficacy of anti–CTLA-4 therapy against melanoma. *Journal of Experimental Medicine* **210**, 1695–1710 (2013).

44.   Mantovani, A., Marchesi, F., Malesci, A., Laghi, L. & Allavena, P. Tumour-associated macrophages as treatment targets in oncology. *Nat Rev Clin Oncol* **14**, 399–416 (2017).

45.   Hu, W. *et al.* Tumor-associated macrophages in cancers. *Clin Transl Oncol* **18**, 251–258 (2016).

46.   Duan, Z. & Luo, Y. Targeting macrophages in cancer immunotherapy. *Sig Transduct Target Ther* **6**, 1–21 (2021).

47.   Wu, X. *et al.* Depletion of M2-Like Tumor-Associated Macrophages Delays Cutaneous T-Cell Lymphoma Development In Vivo. *Journal of Investigative Dermatology* **134**, 2814–2822 (2014).

48.   Luo, Y. *et al.* Targeting tumor-associated macrophages as a novel strategy against breast cancer. *J Clin Invest* **116**, 2132–2141 (2006).

49.   Ries, C. H. *et al.* Targeting Tumor-Associated Macrophages with Anti-CSF-1R Antibody Reveals a Strategy for Cancer Therapy. *Cancer Cell* **25**, 846–859 (2014).

50.   Tham, M. *et al.* Macrophage depletion reduces postsurgical tumor recurrence and metastatic growth in a spontaneous murine model of melanoma. *Oncotarget* **6**, 22857–22868 (2015).

51.   Shen, M. *et al.* Tumor-Associated Neutrophils as a New Prognostic Factor in Cancer: A Systematic Review and Meta-Analysis. *PLOS ONE* **9**, e98259 (2014).

52.   Templeton, A. J. *et al.* Prognostic role of neutrophil-to-lymphocyte ratio in solid tumors: a systematic review and meta-analysis. *J Natl Cancer Inst* **106**, dju124 (2014).

53.   Glodde, N. *et al.* Reactive Neutrophil Responses Dependent on the Receptor Tyrosine Kinase c-MET Limit Cancer Immunotherapy. *Immunity* **47**, 789-802.e9 (2017).

54.   Acharyya, S. *et al.* A CXCL1 paracrine network links cancer chemoresistance and metastasis. *Cell* **150**, 165–178 (2012).

55.   Speiser, D. E., Chijioke, O., Schaeuble, K. & Münz, C. CD4+ T cells in cancer. *Nat Cancer* **4**, 317–329 (2023).

56.   Fridman, W. H., Pagès, F., Sautès-Fridman, C. & Galon, J. The immune contexture in human tumours: impact on clinical outcome. *Nat Rev Cancer* **12**, 298–306 (2012).

57.   Axelrod, M. L., Cook, R. S., Johnson, D. B. & Balko, J. M. Biological Consequences of MHC-II Expression by Tumor Cells in Cancer. *Clin Cancer Res* **25**, 2392–2402 (2019).

58.   Borst, J., Ahrends, T., Bąbała, N., Melief, C. J. M. & Kastenmüller, W. CD4+ T cell help in cancer immunology and immunotherapy. *Nature Reviews Immunology* (2018) doi:10.1038/s41577-018-0044-0.

59.   Binnewies, M. *et al.* Unleashing Type-2 Dendritic Cells to Drive Protective Antitumor CD4+ T Cell Immunity. *Cell* **177**, 556-571.e16 (2019).

60.   Ferris, S. T. *et al.* cDC1 prime and are licensed by CD4 + T cells to induce anti-tumour immunity. *Nature* **584**, 624–629 (2020).
61.   Sackstein, R., Schatton, T. & Barthel, S. R. T-lymphocyte homing: an underappreciated yet critical hurdle for successful cancer immunotherapy. *Lab Invest* **97**, 669–697 (2017).
62.   Xie, Y. *et al.* Naive tumor-specific CD4+ T cells differentiated in vivo eradicate established melanoma. *Journal of Experimental Medicine* **207**, 651–667 (2010).
63.   Quezada, S. A. *et al.* Tumor-reactive CD4 ⁺ T cells develop cytotoxic activity and eradicate large established melanoma after transfer into lymphopenic hosts. *The Journal of Experimental Medicine* **207**, 637–650 (2010).
64.   Malandro, N. *et al.* Clonal Abundance of Tumor-Specific CD4(+) T Cells Potentiates Efficacy and Alters Susceptibility to Exhaustion. *Immunity* **44**, 179–193 (2016).
65.   Oliveira, G. *et al.* Landscape of helper and regulatory antitumour CD4+ T cells in melanoma. *Nature* **605**, 532–538 (2022).
66.   Mumberg, D. *et al.* CD4(+) T cells eliminate MHC class II-negative cancer cells in vivo by indirect effects of IFN-gamma. *Proc Natl Acad Sci U S A* **96**, 8633–8638 (1999).
67.   Schietinger, A., Philip, M., Liu, R. B., Schreiber, K. & Schreiber, H. Bystander killing of cancer requires the cooperation of CD4(+) and CD8(+) T cells during the effector phase. *J Exp Med* **207**, 2469–2477 (2010).
68.   Shklovskaya, E. *et al.* Tumour-specific CD4 T cells eradicate melanoma via indirect recognition of tumour-derived antigen. *Immunol Cell Biol* **94**, 593–603 (2016).
69.   Braumüller, H. *et al.* T-helper-1-cell cytokines drive cancer into senescence. *Nature* **494**, 361–365 (2013).
70.   Qin, Z. & Blankenstein, T. CD4+ T Cell–Mediated Tumor Rejection Involves Inhibition of Angiogenesis that Is Dependent on IFNγ Receptor Expression by Nonhematopoietic Cells. *Immunity* **12**, 677–686 (2000).
71.   Boulch, M. *et al.* A cross-talk between CAR T cell subsets and the tumor microenvironment is essential for sustained cytotoxic activity. *Sci Immunol* **6**, eabd4344 (2021).
72.   Perez-Diez, A. *et al.* CD4 cells can be more efficient at tumor rejection than CD8 cells. *Blood* **109**, 5346–5354 (2007).
73.   Hung, K. *et al.* The central role of CD4(+) T cells in the antitumor immune response. *J Exp Med* **188**, 2357–2368 (1998).
74.   Corthay, A. *et al.* Primary Antitumor Immune Response Mediated by CD4+ T Cells. *Immunity* **22**, 371–383 (2005).
75.   Overwijk, W. W. *et al.* Tumor regression and autoimmunity after reversal of a functionally tolerant state of self-reactive CD8+ T cells. *J Exp Med* **198**, 569–580 (2003).
76.   Bald, T. *et al.* Ultraviolet-radiation-induced inflammation promotes angiotropism and metastasis in melanoma. *Nature* **507**, 109–113 (2014).
77.   Muranski, P. *et al.* Tumor-specific Th17-polarized cells eradicate large established melanoma. *Blood* **112**, 362–373 (2008).
78.   Shridhar, N. Novel vaccination strategies for CD4+ T cell immunotherapy of melanoma. (Universitäts- und Landesbibliothek Bonn, 2019).
79.   Gordon, S. Elie Metchnikoff: Father of natural immunity. *European Journal of Immunology* **38**, 3257–3264 (2008).

80. Secklehner, J., Lo Celso, C. & Carlin, L. M. Intravital microscopy in historic and contemporary immunology. *Immunol Cell Biol* **95**, 506–513 (2017).

81. Kienle, K. & Lämmermann, T. Neutrophil swarming: an essential process of the neutrophil tissue response. *Immunol Rev* **273**, 76–93 (2016).

82. Tan, S.-Y. & Weninger, W. Neutrophil migration in inflammation: intercellular signal relay and crosstalk. *Current Opinion in Immunology* **44**, 34–42 (2017).

83. Mempel, T. R., Henrickson, S. E. & von Andrian, U. H. T-cell priming by dendritic cells in lymph nodes occurs in three distinct phases. *Nature* **427**, 154–159 (2004).

84. Eisenbarth, S. C. Dendritic cell subsets in T cell programming: location dictates function. *Nat Rev Immunol* **19**, 89–103 (2019).

85. Park, S. L. *et al.* Tissue-resident memory CD8+ T cells promote melanoma–immune equilibrium in skin. *Nature* (2018) doi:10.1038/s41586-018-0812-9.

86. Engelhardt, J. J. *et al.* Marginating Dendritic Cells of the Tumor Microenvironment Cross-present Tumor Antigens and Stably Engage Tumor-Specific T cells. *Cancer Cell* **21**, 402–417 (2012).

87. Boulch, M., Grandjean, C. L., Cazaux, M. & Bousso, P. Tumor Immunosurveillance and Immunotherapies: A Fresh Look from Intravital Imaging. *Trends in Immunology* **40**, 1022–1034 (2019).

88. Bousso, P. Diving into the mechanism of action of tumor immunotherapies with intravital imaging*. *Immunological Reviews* **306**, 218–223 (2022).

89. Breart, B., Lemaître, F., Celli, S. & Bousso, P. Two-photon imaging of intratumoral CD8+ T cell cytotoxic activity during adoptive T cell therapy in mice. *J Clin Invest* **118**, 1390–1397 (2008).

90. Thibaut, R. *et al.* Bystander IFN-γ activity promotes widespread and sustained cytokine signaling altering the tumor microenvironment. *Nat Cancer* **1**, 302–314 (2020).

91. Hoekstra, M. E. *et al.* Long-distance modulation of bystander tumor cells by CD8+ T-cell-secreted IFN-γ. *Nat Cancer* **1**, 291–301 (2020).

92. Mempel, T. R. *et al.* Regulatory T Cells Reversibly Suppress Cytotoxic T Cell Function Independent of Effector Differentiation. *Immunity* **25**, 129–141 (2006).

93. Bauer, C. A. *et al.* Dynamic Treg interactions with intratumoral APCs promote local CTL dysfunction. *Journal of Clinical Investigation* **124**, 2425–2440 (2014).

94. JI, S.-B. *et al.* OutKnocker: a web tool for rapid and simple genotyping of designer nuclease edited cell lines. *Genome research* **24**, (2014).

95. Belkina, A. C. *et al.* Automated optimized parameters for T-distributed stochastic neighbor embedding improve visualization and analysis of large datasets. *Nat Commun* **10**, 5415 (2019).

96. Bernstein, N. J. *et al.* Solo: Doublet Identification in Single-Cell RNA-Seq via Semi-Supervised Deep Learning. *Cell Syst* **11**, 95-101.e5 (2020).

97. Lun, A. T. L., McCarthy, D. J. & Marioni, J. C. A step-by-step workflow for low-level analysis of single-cell RNA-seq data with Bioconductor. *F1000Res* **5**, 2122 (2016).

98. Wolf, F. A., Angerer, P. & Theis, F. J. SCANPY: large-scale single-cell gene expression data analysis. *Genome Biol* **19**, 15 (2018).

99. Aran, D. *et al.* Reference-based analysis of lung single-cell sequencing reveals a transitional profibrotic macrophage. *Nat Immunol* **20**, 163–172 (2019).

100. Bergen, V., Lange, M., Peidli, S., Wolf, F. A. & Theis, F. J. Generalizing RNA velocity to transient cell states through dynamical modeling. *Nat Biotechnol* **38**, 1408–1414 (2020).

101. Restifo, N. P., Dudley, M. E. & Rosenberg, S. A. Adoptive immunotherapy for cancer: harnessing the T cell response. *Nat. Rev. Immunol.* **12**, 269–281 (2012).

102. Rosenberg, S. A. & Restifo, N. P. Adoptive cell transfer as personalized immunotherapy for human cancer. *Science* **348**, 62–68 (2015).

103. Ahrends, T. & Borst, J. The opposing roles of CD4+ T cells in anti-tumour immunity. *Immunology* (2018) doi:10.1111/imm.12941.

104. Oh, D. Y. & Fong, L. Cytotoxic CD4+ T cells in cancer: Expanding the immune effector toolbox. *Immunity* **54**, 2701–2711 (2021).

105. Śledzińska, A. *et al.* Regulatory T Cells Restrain Interleukin-2- and Blimp-1-Dependent Acquisition of Cytotoxic Function by CD4+ T Cells. *Immunity* **52**, 151-166.e6 (2020).

106. Oh, D. Y. *et al.* Intratumoral CD4+ T Cells Mediate Anti-tumor Cytotoxicity in Human Bladder Cancer. *Cell* (2020) doi:10.1016/j.cell.2020.05.017.

107. Zheng, L. *et al.* Pan-cancer single-cell landscape of tumor-infiltrating T cells. *Science* **374**, abe6474 (2021).

108. Veatch, J. R. *et al.* Neoantigen-specific CD4+ T cells in human melanoma have diverse differentiation states and correlate with CD8+ T cell, macrophage, and B cell function. *Cancer Cell* **40**, 393-409.e9 (2022).

109. LaCasse, C. J. *et al.* Th-1 lymphocytes induce dendritic cell tumor killing activity by an IFN-γ-dependent mechanism. *J Immunol* **187**, 6310–6317 (2011).

110. Te, K., Kp, B. & Em, V. A. Genomic correlates of response to immune checkpoint blockade. *Nature medicine* **25**, (2019).

111. Khong, H. T. & Restifo, N. P. Natural selection of tumor variants in the generation of 'tumor escape' phenotypes. *Nat Immunol* **3**, 999–1005 (2002).

112. Cabeza-Cabrerizo, M., Cardoso, A., Minutti, C. M., Pereira da Costa, M. & Reis e Sousa, C. Dendritic Cells Revisited. *Annu Rev Immunol* **39**, 131–166 (2021).

113. Lindquist, R. L. *et al.* Visualizing dendritic cell networks in vivo. *Nat Immunol* **5**, 1243–1250 (2004).

114. Müller, A. J. *et al.* Photoconvertible pathogen labeling reveals nitric oxide control of Leishmania major infection in vivo via dampening of parasite metabolism. *Cell Host Microbe* **14**, 460–467 (2013).

115. Fauskanger, M., Haabeth, O. A. W., Skjeldal, F. M., Bogen, B. & Tveita, A. A. Tumor Killing by CD4+ T Cells Is Mediated via Induction of Inducible Nitric Oxide Synthase-Dependent Macrophage Cytotoxicity. *Front. Immunol.* **9**, (2018).

116. Mumberg, D. *et al.* CD4(+) T cells eliminate MHC class II-negative cancer cells in vivo by indirect effects of IFN-gamma. *Proc Natl Acad Sci U S A* **96**, 8633–8638 (1999).

117. Kruse, B. *et al.* CD4+ T cell-induced inflammatory cell death controls immune-evasive tumours. *Nature* **618**, 1033–1040 (2023).

118. Morad, G., Helmink, B. A., Sharma, P. & Wargo, J. A. Hallmarks of response, resistance, and toxicity to immune checkpoint blockade. *Cell* **184**, 5309–5337 (2021).

119. Matsuzaki, J. *et al.* Direct tumor recognition by a human CD4(+) T-cell subset potently mediates tumor growth inhibition and orchestrates anti-tumor immune responses. *Sci Rep* **5**, 14896 (2015).

120.   Ribas, A. *et al.* Overcoming PD-1 Blockade Resistance with CpG-A Toll-Like Receptor 9 Agonist Vidutolimod in Patients with Metastatic Melanoma. *Cancer Discov* **11**, 2998–3007 (2021).

121.   Neoadjuvant Vidutolimod and Nivolumab in High-Risk Resectable Melanoma. https://www.researchsquare.com (2022) doi:10.21203/rs.3.rs-2235839/v1.

122.   Greenberg, P. D., Kern, D. E. & Cheever, M. A. Therapy of disseminated murine leukemia with cyclophosphamide and immune Lyt-1+,2- T cells. Tumor eradication does not require participation of cytotoxic T cells. *J Exp Med* **161**, 1122–1134 (1985).

123.   Hanahan, D. & Weinberg, R. A. Hallmarks of cancer: the next generation. *Cell* **144**, 646–674 (2011).

124.   Joyce, J. A. & Fearon, D. T. T cell exclusion, immune privilege, and the tumor microenvironment. *Science* **348**, 74–80 (2015).

125.   Liu, V. C. *et al.* Tumor Evasion of the Immune System by Converting CD4+CD25− T Cells into CD4+CD25+ T Regulatory Cells: Role of Tumor-Derived TGF-β. *The Journal of Immunology* **178**, 2883–2892 (2007).

126.   Valzasina, B., Piconese, S., Guiducci, C. & Colombo, M. P. Tumor-Induced Expansion of Regulatory T Cells by Conversion of CD4+CD25− Lymphocytes Is Thymus and Proliferation Independent. *Cancer Research* **66**, 4488–4495 (2006).

127.   Foulds, K. E. *et al.* Cutting Edge: CD4 and CD8 T Cells Are Intrinsically Different in Their Proliferative Responses. *The Journal of Immunology* **168**, 1528–1532 (2002).

128.   Seder, R. A. & Ahmed, R. Similarities and differences in CD4+ and CD8+ effector and memory T cell generation. *Nat Immunol* **4**, 835–842 (2003).

129.   Boissonnas, A., Fetler, L., Zeelenberg, I. S., Hugues, S. & Amigorena, S. In vivo imaging of cytotoxic T cell infiltration and elimination of a solid tumor. *Journal of Experimental Medicine* **204**, 345–356 (2007).

130.   Deguine, J., Breart, B., Lemaître, F., Di Santo, J. P. & Bousso, P. Intravital Imaging Reveals Distinct Dynamics for Natural Killer and CD8+ T Cells during Tumor Regression. *Immunity* **33**, 632–644 (2010).

131.   Lau, D. *et al.* Intravital Imaging of Adoptive T-Cell Morphology, Mobility and Trafficking Following Immune Checkpoint Inhibition in a Mouse Melanoma Model. *Front. Immunol.* **11**, (2020).

132.   Qi, S. *et al.* Long-term intravital imaging of the multicolor-coded tumor microenvironment during combination immunotherapy. *eLife* **5**,.

133.   Seliger, B., Kloor, M. & Ferrone, S. HLA class II antigen-processing pathway in tumors: Molecular defects and clinical relevance. *Oncoimmunology* **6**, e1171447 (2017).

134.   Harlé, G. *et al.* Macroautophagy in lymphatic endothelial cells inhibits T cell-mediated autoimmunity. *J Exp Med* **218**, e20201776 (2021).

135.   Haabeth, O. A. W. *et al.* CD4+ T cell-mediated rejection of MHC class II-positive tumor cells is dependent on antigen secretion and indirect presentation on host APCs. *Cancer Research* canres.2426.2017 (2018) doi:10.1158/0008-5472.CAN-17-2426.

136.   McDaniel, J. R. *et al.* Identification of tumor-reactive B cells and systemic IgG in breast cancer based on clonal frequency in the sentinel lymph node. *Cancer Immunol Immunother* **67**, 729–738 (2018).

137.   Jiang, W., Adler, L. N., Macmillan, H. & Mellins, E. D. Synergy between B cell receptor/antigen uptake and MHCII peptide editing relies on HLA-DO tuning. *Sci Rep* **9**, 13877 (2019).

138.   Oosterhuis, K., Aleyd, E., Vrijland, K., Schumacher, T. N. & Haanen, J. B. Rational design of DNA vaccines for the induction of human papillomavirus type 16 E6- and E7-specific cytotoxic T-cell responses. *Hum Gene Ther* **23**, 1301–1312 (2012).

139.   Jiao, J. *et al.* Central Role of Conventional Dendritic Cells in Regulation of Bone Marrow Release and Survival of Neutrophils. *J Immunol* **192**, 3374–3382 (2014).

140.   Filipe-Santos, O. *et al.* A Dynamic Map of Antigen Recognition by CD4 T Cells at the Site of Leishmania major Infection. *Cell Host & Microbe* **6**, 23–33 (2009).

141.   Marangoni, F. *et al.* Expansion of tumor-associated Treg cells upon disruption of a CTLA-4-dependent feedback loop. *Cell* **184**, 3998-4015.e19 (2021).

142.   Mantovani, A., Allavena, P., Marchesi, F. & Garlanda, C. Macrophages as tools and targets in cancer therapy. *Nat Rev Drug Discov* **21**, 799–820 (2022).

143.   Guilliams, M., Mildner, A. & Yona, S. Developmental and Functional Heterogeneity of Monocytes. *Immunity* **49**, 595–613 (2018).

144.   Garg, A. D. & Agostinis, P. Cell death and immunity in cancer: From danger signals to mimicry of pathogen defense responses. *Immunol Rev* **280**, 126–148 (2017).

145.   Mintz, J. *et al.* Current Advances of Nitric Oxide in Cancer and Anticancer Therapeutics. *Vaccines (Basel)* **9**, 94 (2021).

146.   Choudhari, S. K., Chaudhary, M., Bagde, S., Gadbail, A. R. & Joshi, V. Nitric oxide and cancer: a review. *World Journal of Surgical Oncology* **11**, 118 (2013).

147.   Hirschhorn, D. *et al.* T cell immunotherapies engage neutrophils to eliminate tumor antigen escape variants. *Cell* **186**, 1432-1447.e17 (2023).

148.   Boulch, M. *et al.* Tumor-intrinsic sensitivity to the pro-apoptotic effects of IFN-γ is a major determinant of CD4+ CAR T-cell antitumor activity. *Nat Cancer* 1–16 (2023) doi:10.1038/s43018-023-00570-7.

149.   Sektioglu, I. M. *et al.* Basophils Promote Tumor Rejection via Chemotaxis and Infiltration of CD8+ T Cells. *Cancer Res* **77**, 291–302 (2017).

150.   Hunder, N. N. *et al.* Treatment of Metastatic Melanoma with Autologous CD4+ T Cells against NY-ESO-1. *New England Journal of Medicine* **358**, 2698–2703 (2008).

151.   Veatch, J. R. *et al.* Tumor-infiltrating BRAF^{V600E}-specific CD4$^+$ T cells correlated with complete clinical response in melanoma. *J Clin Invest* **128**, 1563–1568 (2018).

152.   Lemke-Miltner, C. D. *et al.* Antibody Opsonization of a TLR9 Agonist-Containing Virus-like Particle Enhances In Situ Immunization. *J Immunol* **204**, 1386–1394 (2020).

153.   Schroder, K. *et al.* Conservation and divergence in Toll-like receptor 4-regulated gene expression in primary human versus mouse macrophages. *Proc Natl Acad Sci U S A* **109**, E944-953 (2012).

154.   Schneemann, M. & Schoedon, G. Species differences in macrophage NO production are important. *Nat Immunol* **3**, 102–102 (2002).

155.   Vijayan, V. *et al.* Human and murine macrophages exhibit differential metabolic responses to lipopolysaccharide - A divergent role for glycolysis. *Redox Biol* **22**, 101147 (2019).

156.   Vitek, M. P. *et al.* Characterization of NO and cytokine production in immune-activated microglia and peritoneal macrophages derived from a mouse model expressing the human NOS2 gene on a mouse NOS2 knockout background. *Antioxid Redox Signal* **8**, 893–901 (2006).

Declaration of Honour

I hereby declare that I prepared this thesis without the impermissible help of third parties and that none other than the aids indicated have been used; all sources of information are clearly marked, including my own publications.

In particular I have not consciously:

• fabricated data or rejected undesirable results,

• misused statistical methods with the aim of drawing other conclusions than those warranted by the available data,

• plagiarized external data or publications,

• presented the results of other researchers in a distorted way.

I am aware that violations of copyright may lead to injunction and damage claims by the author and also to prosecution by the law enforcement authorities.

I hereby agree that the thesis may be electronically reviewed with the aim of identifying plagiarism.

This work has not yet been submitted as a doctoral thesis in the same or a similar form in Germany, nor in any other country. It has not yet been published as a whole.